universität wien

MASTERARBEIT / MASTER'S THESIS

Titel der Masterarbeit / Title of the Master's Thesis

„Dynamics of Associations between Host-Derived MicroRNAs with Human Gut Microbiota"

verfasst von / submitted by

Kayla Jean Flanagan

angestrebter akademischer Grad / in partial fulfilment of the requirements for the degree of

Master of Science (MSc)

Wien, 2023 / Vienna, 2023

Studienkennzahl lt. Studienblatt / degree programme code as it appears on the student record sheet:	UA 066 830
Studienrichtung lt. Studienblatt / degree programme as it appears on the student record sheet:	Master in Molecular Microbiology, Microbial Ecology and Immunobiology
Betreut von / Supervisor:	Univ.-Prof. David Berry, Privatdoz. PhD

Table of Contents

Table of Figures

Table of Tables

Acknowledgements

Firstly, I would like to sincerely thank Univ.-Prof. Dr. David Berry for giving me the opportunity to work as a member of his laboratory group for the duration of my master's project. I would additionally like to extend a very special thank you to Dr. Fatima Pereira for allowing me to work with her on this project and for her outstanding guidance and mentorship over the past years. I have grown and learned so much under her supervision and am extremely grateful for all the time, training, patience, and advice she has granted me. I would additionally like to thank Klara Maritsch, MSc, and other members of the Gut group for assisting me with several of the larger experiments throughout this study. Lastly, I would like to thank the TA team and other personnel at DOME, as well as the Joint Microbiome Facility for all their assistance and support throughout my project.

Many thanks to my family and friends for all their support throughout the duration of my academic career. I am extremely grateful for all I have learned at the University of Vienna and am excited to step into this next stage of life.

Abstract

The human gut harbors a diverse and complex community of microorganisms, known as the gut microbiota, and represents one of the largest, most dynamic interfaces between commensal microbiota, environmental factors and host immunity and metabolism. In addition to better understanding the role of the gut microbiome and its interactions with other host systems, several studies have focused on the mechanisms of regulation and modulation of the gut microbiome. One regulatory molecule of particular interest is MicroRNAs (miRNAs), which are small non-coding regulatory RNAs that have been shown to direct post-transcriptional repression and degradation of messenger RNAs. Previous studies have successfully identified various miRNAs present in the human gut lumen and have additionally revealed an intricate relationship between host miRNAs and gut microbiota. This suggests a potential mechanism for the role of miRNAs in the manipulation of the host microbiome. In this study, we aim to identify the dynamics of this relationship, in the context of hsa-miR-21-5p (miR21), a miRNA with a well-established role in the pathogenesis and development of Inflammatory Bowel Diseases (IBD). Incubations with both live and ethanol-fixed (dead) fecal-sample derived microbial communities were set up with the addition of either miR21 or a miR21 scramble control. Subsequent downstream analysis including total RNA extraction, cDNA synthesis and quantitative PCR (qPCR), was performed to quantify the differential association of miR21 and miR21 scramble across cell-free and cell-rich fractions of the live and dead cell incubations. Our findings revealed an association between microbiota in the human gut and miRNAs that is not sequence specific. Fluorescence-activated cell sorting using either fluorescently labelled miR21 or miR21 scramble revealed that species belonging to the families *Bacteroidaceae*, *Lachnospiraceae*, *Lactobacillaceae*, *Oscillospiraceae*, *Rikenellaceae* and *Veillonellaceae* predominantly associate with miRNAs, but that miRNA sequence has a minimal effect on the composition of the miRNA-associating bacterial community. Lastly, *in vitro* growth studies and transcriptomic analysis on *Bacteroides thetaiotaomicron* (*Bt*) in pure culture with different small RNA molecules elucidated the complex impact that miR21 has on bacterial expression. The transcriptomic analysis revealed that miRNA supplementation significantly represses transcription in *Bt*. However, miR21 interestingly was found to induce overexpression of the gene cluster encoding L-tryptophan biosynthesis. All together, these results provide a comprehensive overview of the complex interactions between miRNAs and host microbiome and gives insight into the underlying mechanisms behind miR21-mediated inflammation and its role in IBD pathogenesis.

Zusammenfassung

Der menschliche Darm beherbergt eine vielfältige und komplexe Gemeinschaft von Mikroorganismen, die als Darmmikrobiota bekannt ist, und stellt eine der größten und dynamischsten Schnittstellen zwischen kommensalen Mikrobiota, Umweltfaktoren sowie der Immunität und dem Stoffwechsel des Wirts dar. Neben einem besseren Verständnis der Rolle des Darmmikrobioms und seiner Wechselwirkungen mit anderen Wirtssystemen, haben sich mehrere Studien auf die Mechanismen der Regulierung und Modulation des Darmmikrobioms konzentriert. Ein regulatorisches Molekül von besonderem Interesse sind MicroRNAs (miRNAs), kleine, nicht-kodierende regulatorische RNAs, die nachweislich die posttranskriptionelle Repression und den Abbau von Boten-RNAs steuern. Frühere Studien haben erfolgreich verschiedene miRNAs im menschlichen Darmlumen identifiziert und darüber hinaus eine komplexe Beziehung zwischen miRNAs des Wirts und der Darmmikrobiota aufgedeckt. Dies deutet auf einen möglichen Mechanismus für die Rolle von miRNAs bei der Manipulation des Wirtsmikrobioms hin. In dieser Studie wollen wir die Dynamik dieser Beziehung im Kontext von hsa-miR-21-5p (miR21) identifizieren. MiR21 ist einer miRNA mit einer bekannten Rolle bei der Pathogenese und Entwicklung entzündlicher Darmerkrankungen (IBD). Inkubationen sowohl mit lebenden als auch mit Ethanol-fixierten (toten) mikrobiellen Gemeinschaften aus Stuhlproben wurden unter Zugabe von entweder miR21 oder einer miR21-Scramble-Kontrolle durchgeführt. Nachfolgende Downstream-Analysen, einschließlich Gesamt-RNA-Extraktion, cDNA-Synthese und quantitativer PCR (qPCR), wurden durchgeführt, um die unterschiedliche Assoziation von miR21 und miR21-Scramble über zellfreie und zellreiche Fraktionen der Inkubationen mit lebenden und toten Zellen zu quantifizieren. Unsere Ergebnisse zeigten einen Zusammenhang zwischen Mikrobiota im menschlichen Darm und miRNAs, der nicht sequenzspezifisch ist. Die fluoreszenzaktivierte Zellsortierung mit entweder fluoreszenzmarkiertem miR21 oder miR21-Scramble ergab, dass Mitglieder der Familien *Bacteroidaceae, Lachnospiraceae, Lactobacillaceae, Oscillospiraceae, Rikenellaceae* und *Veillonellaceae* überwiegend mit miRNAs assoziieren, die miRNA-Sequenz jedoch nur einen minimalen Einfluss auf die Zusammensetzung der miRNA-assoziierenden Bakteriengemeinschaft hat. Schließlich haben In-vitro-Wachstumsstudien und transkriptomische Analysen an *Bacteroides thetaiotaomicron (Bt)* in Reinkultur mit verschiedenen kleinen RNA-Molekülen den komplexen Einfluss von miR21 auf die bakterielle Expression aufgeklärt. Die transkriptomische Analyse ergab, dass eine miRNA-Supplementierung die Transkription in *Bt* signifikant unterdrückt. Interessanterweise wurde jedoch festgestellt, dass miR21 eine Überexpression des Genclusters induziert, der für die L-tryptophan-Biosynthese kodiert. Insgesamt bieten diese Ergebnisse einen umfassenden Überblick über die komplexen Wechselwirkungen zwischen miRNAs und dem Wirtsmikrobiom und geben Einblick in die zugrunde liegenden Mechanismen der miR21-vermittelten Entzündung und ihre Rolle bei der IBD-Pathogenese.

1.0 Introduction

1.1 The Gut Microbiome

Scientific methods and technology are ever evolving, and with them, so too are the research questions scientists are trying to answer. During the last few decades, microbiology has started to shift away from cultivation-dependent methods and towards omics approaches that study the dynamics and interactions of microbial communities. Advancements in metagenomics and DNA sequencing technologies have allowed for complex microbial communities to be better defined and more thoroughly analyzed, leading to scientific research programs such as The Human Microbiome Project (HMP) (Ding & Schloss, 2014; Gevers *et al.*, 2012). The HMP was a collaborative effort that aimed to characterize the complex community profile of the human microbiome and elucidate the relationship between human health and disease and the microbiome. The HMP was only the beginning, and the field of microbiome research has expanded exponentially, fueled by a constant growing library of references and sequence data (Peterson *et al.*, 2009).

1.1.1 Introduction to the Human Gut Microbiome: Community Acquisition and Composition

The average healthy adult is inhabited with trillions of microbes, but the microbiome profiles of these healthy individuals may vary drastically and can be influenced by a myriad of factors ranging from infant feeding method and birthing process to stress, diet, and medications (Cresci & Bawden, 2015; Ding & Schloss, 2014; Huttenhower *et al.*, 2012). Of particular interest has been the gut microbiome, which has drawn attention from several studies highlighting an inextricable relationship between the gut microbiome and host nutrition and metabolism (N. Wu *et al.,* 2021). The human gut alone is home to one of the most complex and diverse communities, hosting over 95% of all human microbes, consisting of approximately 10^{14} bacteria that belong to up to 1000 different species, and the gut microbiome refers to all the genomes of these microorganisms (N. Wu *et al.,* 2021). Acquisition of the gut microbiome begins as early as before birth, and every life cycle stage thereafter plays a significant role in forming an individual's unique microbial profile. For example, the mode of birth- be it vaginal or Cesarean determines which bacterial communities from the mother colonize neonates. This initial colonization can have long term effects on the subsequent development of the pediatric microbiome and concomitant predispositions that may follow (Rosenbaum *et al.*, 2015). A myriad of additional environmental and genetic factors thereafter helps to influence and shape how an individual's microbiome evolves over the course of their lifetime. These factors include geographic location (industrialized societies vs. non-industrialized societies), lifestyle and diet, and even cultural traditions, as these can shape the social structures in a society and therefore influence vertical transmission of microbiota within a population(Valles-Colomer *et al.,* 2023; Yatsunenko *et al.,* 2012).

Although there is a great degree of variability across different individuals, scientists have spent the past few decades trying to define a "core microbiome". This concept would summarize

commonalities across the microbiomes of most humans (Turnbaugh *et al*., 2007). Several publications from the Human Microbiome Consortium and beyond have striven to do this through the exploitation of various models and approaches, but there is still work to be done to comprehensively define such a concept (Li *et al.,* 2013; Sharon *et al.,* 2022). The 5 dominant phyla in the gut are *Firmicutes*, *Bacteroidetes*, *Actinobacteria*, *Proteobacteria*, and *Fusobacteria*, with *Firmicutes* and *Bacteroidetes* being the most dominant, compromising over 90% of the total gut microbiota community (Arumugam *et al.,* 2011). More than 200 genera of *Firmicutes* are present in the gut (Rinninella *et al*., 2019). One well-known Firmicute is *Ruminococcus bromii*, which has been identified as a keystone species for its ability to support other species in the gut through the production of sugars and other metabolites via the degradation of otherwise insoluble starch (Chen *et al*., 2008; Qiu *et al*., 2022). *Bacteroides thetaiotaomicron* (*Bt*) is a member of the *Bacteroidetes* phyla and of the most well studied symbionts in the human gut. *Bt* is a gram-negative anaerobe and prominent gut mutualist that constitutes 6% of all bacteria in the intestine (Zocco *et al.,* 2007). The phylum *Actinobacteria* is significantly less abundant than other phlya in the gut and is dominated mainly by the genus *Bifidobacterium*, which plays an important role in strengthening the intestinal mucosa (Cresci & Bawden, 2015). In recent decades, scientists have been interested in exploring ubiquitous healthy gut microbiota across populations, and one metagenomic study identified a common subset of genera found in most healthy individuals. This subset, based on average abundance, is comprised of *Prevotella*, *Bacteroides*, *Faecalibacterium*, *Ruminococcus*, *Blautia* and *Clostridium* (Piquer-Esteban *et al.,* 2022). Major perturbations in these communities can greatly influence the metabolic capabilities and subsequently the overall health of the host and can lead to a potentially dysbiotic gut (Turnbaugh *et al*., 2009).

1.1.2 Functionalities of the Human Gut Microbiome

The gut microbiome confers several essential functions in the human body. These functions include the fermentation of polysaccharides and otherwise indigestible food substrates such as dietary fibers, the biosynthesis of complex vitamins (i.e., vitamin K and B vitamins), the formation, maturation and strengthening of the intestinal barrier and gut immune system, and the prevention of infection (Heintz-Buschart & Wilmes, 2018; Kamada *et al.,* 2013; LeBlanc *et al.*, 2013). Dietary fibers are an important component of human nutrition. Since they cannot be hydrolyzed by their own digestive enzymes, humans rely on their resident gut microbiota to break down these valuable components into soluble metabolites, such as short-chain fatty acids (SCFAs). These SCFAs can subsequently be absorbed by the host or be used as secondary metabolites for other microbes, and studies have shown that an increased concentration of these gut-derived SCFAs improves overall health and lowers susceptibility to metabolic diseases (Heintz-Buschart & Wilmes, 2018; Myhrstad *et al.,* 2020). With respect to host nutrition, *Bt* can metabolize a variety of dietary polysaccharides that the host would otherwise not be able to break down, and it can additionally utilize host-derived glycans as a crucial energy source (Hooper *et al.,* 2002). Humans are also incapable of synthesizing many essential vitamins and often rely on diet and commercially produced supplements to satisfy their vitamin-intake. The gut is home to many vitamin-producing microorganisms that can also satisfy this

dietary need and can synthesize essential vitamins such as vitamin K, biotin, cobalamin, folates, riboflavin and thiamine (LeBlanc *et al.,* 2013).

Besides nutrient acquisition and metabolism, the gut microbiome also plays an important role in immune development and homeostasis. The gut microbiota has been shown to induce the maturation of the intestinal immune system and lymphoid structures and regulate immune cell differentiation and immune mediators such as cytokines and chemokines (Sommer & Bäckhed, 2013). For example, *Bt* plays a critical role in the development of the gut immune system, and many studies have demonstrated that an overall decrease in abundance of this gut mutualist can lead to the pathogenesis of inflammatory diseases (Pither *et al.,* 2022). The gut microbiota additionally helps to protect the host from infection, be it from exogenous pathogens or from potentially harmful indigenous microorganisms. It does this via direct competition with potential pathogens for nutrients or via indirect regulation of the host immune response (Kamada *et al.,* 2013; Sommer & Bäckhed, 2013). For example, some *Proteobacteria* commensals such as *Escherichia coli* inhibit pathogen colonization by directly competing for pathogens' nutrients supply in the intestine (Kamada *et al.,* 2013).

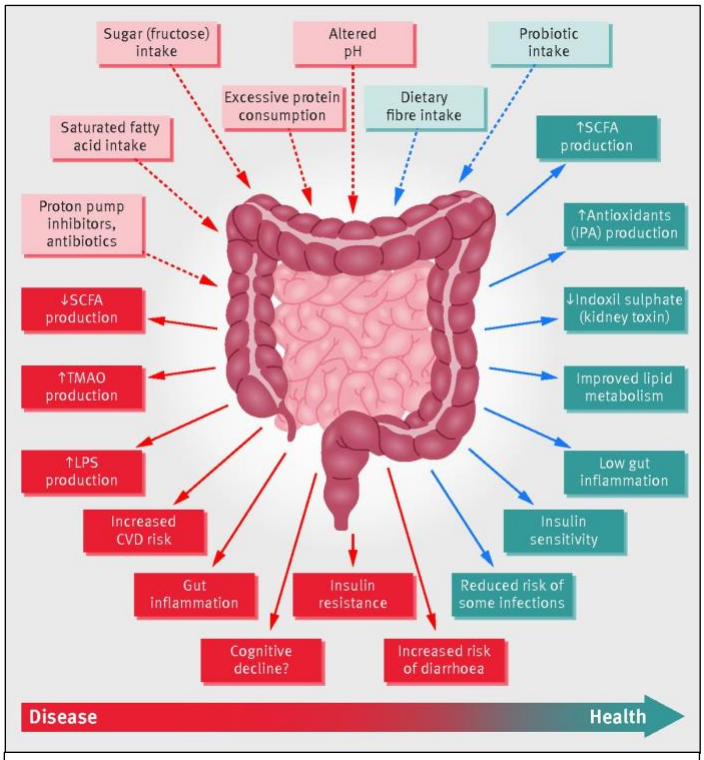

Figure 1: The above graphic summarizes the intricate relationship between the gut microbiome and human health and disease, with examples of various inputs and outputs that can modulate the microbiota (Valdes *et al.,* 2018).

Studies involving germ-free models, in which animal subjects are brought up in a sterile environment with no exposure to any microorganisms, have shown significant immune and non-immune deviations between germ-free and otherwise healthy animal subjects (Smith *et al*., 2007). For example, one study on germ-fee mice determined that the gut microbiota is necessary for the development of lymphoid tissues, which help to fortify the intestinal barrier and protect the host from exogenous pathogens (Kamada *et al.,* 2013). Selective colonization of various intestinal microbiota in germ-free mice has also been done to help pinpoint specific commensals or pathogens that play key roles in host immune. Additional studies with antibiotics have further fortified observations that the indigenous microbiota population plays a critical role in host immunity, as shown by both gnotobiotic and antibiotic-treated mice presenting similar decreased responses of the adaptive and innate immune systems (Kamada *et al.,* 2013).

Many studies in mice have also shown that the gut microbiota has measurable effects on host metabolism and energy homeostasis. In rodents, this importance of the gut microbiota in metabolism has been best illustrated through studies that have used the depletion and subsequent replenishment of the hosts' resident microbiota via probiotic administration (Rosenbaum *et al.,* 2015). Probiotics are live microorganisms that, when prescribed at the proper dosage, can provide the host with an array of health benefits. They support human health by promoting a healthy gut, improving mucosal and intestinal immunity and reducing the risk for gastrointestinal disorders, diabetes and other diseases (Balthazar *et al.,* 2022; Hill *et al*., 2014). Administration of probiotics offers a promising approach for modulating the microbiome in both rodents and humans (Rosenbaum *et al.,* 2015). Today, probiotics are commercially available to everyone, and much research has subsequently gone into developing the ideal consortia of microorganisms to target individual health concerns and optimize probiotic use.

1.1.3 Modulation of the Gut Microbiota

In addition to better understanding the role of the gut microbiome and its dynamics with other host systems, several of these studies have also focused on the mechanisms of regulation and modulation of the gut microbiome (Flanagan *et al*., 2022). For example, probiotics have sparked interest in other supplements that can improve the longevity and amplify the health benefits of probiotics themselves. These include prebiotics, which are polysaccharides that that serve as food for probiotics and stimulate growth of healthy bacteria, and postbiotics, which are beneficial metabolites of bacteria such as short chain fatty acids and essential vitamins (Balthazar *et al*., 2022). Diet is one of the most relevant factors impacting the gut microbiome, and the use of prebiotics, probiotics and postbiotics all additionally contribute to these dietary alterations to the host microbial community (Cresci & Bawden, 2015).

Additional factors that can modify the gut microbiome include physiological stress, pharmaceutical medications and antibiotics, and chronic illness and immune disorders. Antibiotic therapy with broad-spectrum antibiotics has become a norm in modern medical practices, and several studies have highlighted the detrimental effects these medications have on the human gut microbiota (Patangia *et al*., 2022). Not only do antibiotics target harmful pathogenic bacteria, but they also kill healthy microbiota and decrease diversity in the gut. This can leave the host susceptible to opportunistic pathogens or other indigenous microorganisms whose growth is otherwise inhibited by health bacteria (Cresci & Bawden, 2015; Patangia *et al.,* 2022). One example of a pathogen that is favored by antibiotic modification of the gut microbiome is *Clostridioides difficile*. *C. difficile* is the most frequent health care-associated infection in the United States and is responsible for thousands of deaths annually (Feuerstadt *et al.*, 2022; Guh & Kutty, 2018). Although a major cause of the infection, antibiotic treatment is also one of the most widely practiced treatments for *C. difficile*. However, emerging studies have found that additional antibiotic treatments can further destabilize the gut microbial community and that alternative treatments to replenish the patient with healthy microbiota should be followed (Cresci & Bawden, 2015; Guh & Kutty, 2018). For patients with recurring disease, Fecal Microbiota Transplants (FMTs) are recommended, in which a homogenized fecal sample from a clinically healthy donor is administered into the gastrointestinal tract of the

infected patient. The treatment of *C. difficile* with FMTs has motivated many researchers and clinicians to further examine whether FMTs can be used to treat other diseases associated with a dysbiotic gut, such as Inflammatory Bowel Disease (IBD) (Cresci & Bawden, 2015; Wang *et al.,* 2014).

1.2 Inflammatory Bowel Disease

Inflammatory bowel diseases (IBD), which include the conditions Crohn's Disease (CD) and Ulcerative Colitis (UC), are defined by chronic inflammation of the gastrointestinal tract that is typically the result of tissue damage from an overactive immune response (Casado-Bedmar & Viennois, 2022; Cao *et al.*, 2017). In a recent study, nearly 1.3% of Americans were diagnosed with IBD, which estimates a large increase from a previous study in the late 90's reporting that approximately 0.9% of Americans were diagnosed with the disease (Dahlhamer *et al.,* 2015). IBD imposes a significant burden, both financial and physical, on patients, so the significant uptrend in prevalence of IBD diagnoses has motivated several inquiries into the intricacies of the disease. Despite decades of research, the exact etiology of IBD is still not well understood. However, researchers have hypothesized that the interaction of genetic influences, a divergent immune response, environmental factors, and a dysbiosis, or imbalance, of the gut microbiome all contribute to a patient's susceptibility to the disease (Wu, *et al.*, 2021). As a result, several studies have focused on the role of the gut microbiome in different disease models in attempts to not only understand its specific role in pathogenesis of IBD, but also to explore the therapeutic potential of manipulation of the gut microbiome (Liu *et al.,* 2019).

The gut microbiome plays a key role in the development of the host immune system, and evidence has shown that an offset ratio of pro- and anti-inflammatory bacteria contributes to the development and exacerbation of IBD (Wu, *et al.,* 2021). The overall fluctuation of the gut microbiota in healthy patients is lower than in patients suffering from IBD, and some studies have also identified different degrees of dysbiosis across the different subtypes of IBD, further emphasizing the complexity of IBD etiology (Qiu *et al.,* 2022). IBD patients typically present with an unbalanced, less diverse intestinal community with a reduced abundance of species with anti-inflammatory properties (Casado-Bedmar & Viennois, 2022). Specific patterns across the flora of IBD patients highlight a decreased abundance of anaerobic commensals such as *Bacteroidota* and *Firmicutes* and an overall increase in facultative anaerobes such as *Enterobacteriaceae* and *Proteobacteria* (Khan *et al.,* 2019; Kriss *et al.,* 2018). Although it is still not well understood whether a dysbiotic gut microbiota is the etiological cause or a consequence of IBD, much research points to microbiota-targeted therapies as the best approach to ameliorate IBD symptoms and intestinal inflammation (Khan *et al.,* 2019). Examples of such therapies include the administration of functional foods such as synbiotics, which consist of a combination of pre- and probiotics, and FMTs (Bengmark, 2001; Khan *et al.,* 2019).

In the gut, host metabolism and host microbiome are closely interconnected, and the gut microbiome can regulate host intestinal homeostasis and immunity via regulation of host

metabolism. Host metabolism consists of all chemical reactions necessary for host survival and function and includes pathways such as amino acid metabolism, glycolysis, and the breakdown of additional otherwise insoluble compounds (Michaudel C., *et al*., 2023). Because many of these pathways are central for maintaining host health and intestinal homeostasis, their deregulation can lead to disease pathogenesis. For example, gut microbiota plays a key role in the synthesis and metabolism of the essential amino acid tryptophan, and many studies have linked tryptophan metabolism to IBD (Nikolaus *et al*., 2017). Patients suffering from immune diseases such as IBD have been found to have decreased concentrations of tryptophan in serum and increased levels of end-product metabolites produced through the Kynurenine and Indole tryptophan metabolism pathways. The Kynurenine Pathway (KP) is of special interest in the context of inflammatory diseases, as many conditions such as IBD are associated with the activation of KP (Michaudel C., *et al*., 2023; Nikolaus *et al*., 2017). Additional studies investigating the mechanisms of how gut microbiota can regulate these pathways and the role of these metabolites in disease can provide important insight into their subsequent role in IBD and aid in the design of potential therapies.

1.3 MicroRNAs

1.3.1 Introduction to MicroRNAs

One regulatory molecule of particular interest in recent studies is microRNAs (miRNAs). MiRNAs are small non-coding regulatory RNAs typically ranging from 22-25 nucleotides in length that have been shown to direct post-transcriptional repression and degradation of mRNAs (Flanagan *et al*., 2022). MiRNAs were first discovered in the model organism*, Caenorhabditis elegans* (*C. elegans*)*,* in which scientists discovered that developmental genes *lin-4* and *let-7* were producing short (~22 nt) RNAs to aid in the temporal regulation of *C. elegans* development via antisense interactions (Bartel, 2018). These same small RNAs were later subsequently identified in humans and several other animals, showing that this temporal regulation via small regulatory RNAs is not isolated to *C. elegans*. This further sparked scientific curiosity, as scientists began to believe that any mRNA of interest could be regulated by one or several of these miRNAs (Bartel, 2018; Pasquinelli *et al.*, 2000). To date, there are over 1800 annotated human miRNA precursor genes that are processed into more than 2500 miRNAs, and these miRNAs regulate nearly a third of the human genome (Ardekani & Naeini, 2010; Plotnikova *et al.,* 2019). Aside from the miRNAs encoded in the human genome, miRNAs can additionally be uptaken from the environment through diet and can influence the host microbiome (Teng *et al.,* 2018). However, many of the regulatory functions of miRNAs are still not well understood (Peng & Croce, 2016). What is understood, however, is that dysregulation of miRNA synthesis and expression is associated with various human diseases, including cancer and inflammatory diseases such as Inflammatory Bowel Disease (O'Brien *et al.,* 2018; Peng & Croce, 2016).

There are numerous families of miRNAs that have been shown to influence the prevalence of various phenotypes in animals. These regulatory molecules play key roles in a host of

regulatory pathways, such as control of development timing, cell differentiation, apoptosis, and cell replication and division (Lee *et al.,* 2004). Researchers have found that miRNAs not only exist intracellularly, but also that they can be secreted extracellularly, and concentrations of miRNAs have been measured in both the gut lumen and in human and mouse feces (Liu *et al.,* 2019). Additionally, miRNA-deficient mice have been found to suffer from exacerbated colitis, indicating that miRNAs play a role in the pathogenesis of the disease and in influencing the gut microbiota (Liu *et al.*, 2016).

1.3.2 MicroRNAs: Biosynthesis, Modes of Action and Circulation

Due to many structural and mechanistic similarities between the two pathways, scientists believe that the miRNA biogenesis pathway is likely derived from an ancestral RNA interference (RNAi) system. During RNA interference, large double stranded RNA molecules are processed into short interfering RNA (siRNA) molecules, which subsequently trigger the activation of the RNA-induced silencing complex (RISC). The siRNAs then bind to and cleave target RNAs in a complementary, sequence-specific manner (Neumeier, J. & Meister, G., 2021). However, it is necessary to note that significant evolution has occurred since, resulting in many differences between miRNAs and siRNAs (Shabalina & Koonin, 2008). During canonical miRNA biogenesis in eukaryotes, DNA sequences are initially transcribed in the nucleus by RNA Polymerase II (Pol II) to a primary miRNA (pri-miRNA) (Shabalina & Koonin, 2008). Each pri-miRNA contains a hairpin structure, formed by regions of the RNA molecule that fold back onto itself. This structural element is necessary for the interaction between the pri-miRNA molecule with a heterotrimeric protein, known as the Microprocessor, which is made up of the endonuclease Drosha and two molecules of its cofactor protein DGCR8 (Bartel, 2018; Nguyen *et al.,* 2015). The Microprocessor complex cleaves the pri-miRNA hairpin and exports the pre-miRNA complex into the cytoplasm via Exportin 5 and Ran-GTP, where it is subsequently processed by another endonuclease, Dicer. Dicer cuts the pre-miRNA

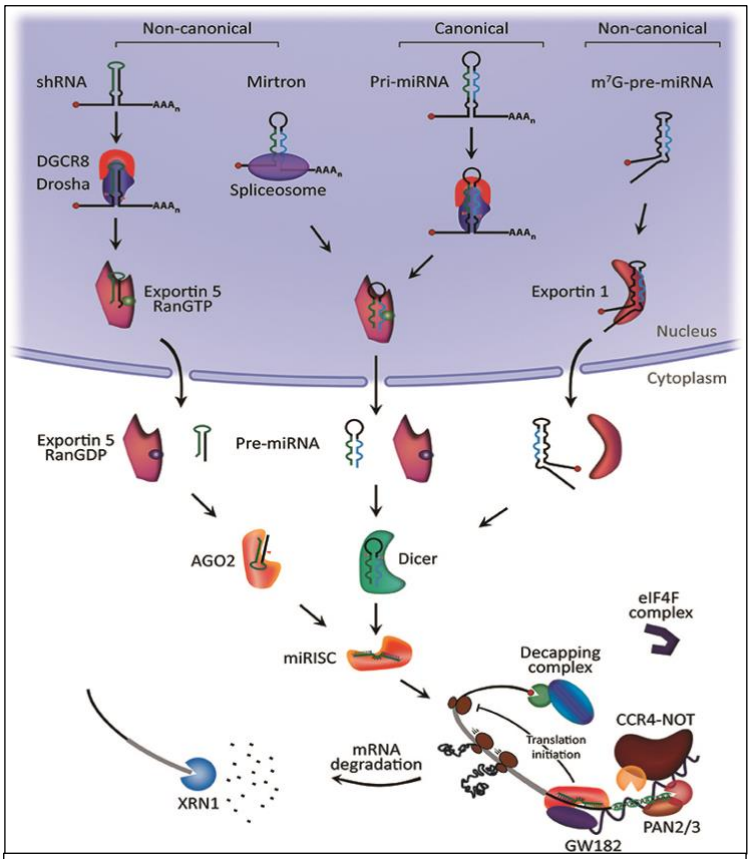

Figure 2: A summary of the different pathways of miRNA biogenesis and mechanisms of action (O'Brien et al., 2018).

hairpin to form the miRNA duplex. The miRNA duplex contains 2 strands- the first being a guide strand, which will eventually become the mature miRNA, and the second a passenger strand, which is also referred to as miRNA* (Shabalina & Koonin, 2008). The miRNA duplex is then loaded onto an Argonaute (AGO) protein to form the miRNA-induced silencing complex (miRISC), and the manner in which the miRNA binds will determine the designation of the guide and passenger strands (Petkovic *et al.*, 2020). One strand of the miRNA is loaded into the guide-strand channel of the AGO protein to form the silencing complex, while the other strand is ejected from the complex and consequently degraded (Bartel, 2018). The non-canonical pathway uses a combination of proteins similar to those in the canonical pathway (Dicer, Drosha, AGO2), but there are some key differences. For instance, rather than beginning with the transcribed pre-miRNA, the non-canonical biogenesis pathway starts with either a small hairpin RNA (shRNA), a mitron, or a 7-methylguanine capped (m^7G)-pre-miRNA. ShRNAs are subsequently cleaved by the Microprocessor complex and exported via Exportin 5 and Ran-GTP into the cytoplasm for AGO-dependent and Dicer-independent processing. In contrast, mitrons and m^7G-pre-miRNAs undergo Dicer-dependent processing but rely on different Exportins for transfer into the nucleus. Despite these differences, both canonical and non-canonical miRNA biogenesis pathways (summarized in Fig. 2) result in the formation of active miRISC complexes, which can directly bind mRNA and inhibit translation (Bartel, 2018; O'Brien *et al.,* 2018).

The majority of available studies have shown that miRNAs bind to specific sequences on target mRNA, referred to as seed sequences (2-8 nt) and induce translational repression (Bartel, 2018; O'Brien *et al.,* 2018). The level of complementarity between miRNAs and their complementary seed segments ultimately determines the mechanism of action for target mRNA degradation or silencing. In the rare case that a fully complementary miRNA:seed sequence complex is formed, the endonuclease activity of the AGO RISC Catalytic Component 2 (AGO2) is activated and slices the target mRNA (Jo *et al.,* 2015). However, in the majority of cases, this miRNA:seed sequence complex is not completely complementary, thus activating alternative modes of mRNA targeting such as translational repression and mRNA degradation via destabilization of the target strand through deadenylation or decapping (Huntzinger & Izaurralde, 2011; Jo et al., 2015). Although less common, miRNAs have also been observed to up-regulate gene expression, showing that they are not exclusively negative regulators of transcription (Truesdell *et al.,* 2012). AGO proteins are a family of nucelases found in both eukaryotes (eAGO) and prokaryotes (pAGO). Whereas eAGOs use small RNA guide strands to recognize target mRNA and regulate gene expression, their prokaryotic homologues have been shown to use small DNA guide strands to find their targets Kuzmenko, A. *et al.*, 2020). While the majority of pAGOs proteins target DNA in a process called DNA interference, some more newly discovered classes have also been shown to process RNA targets (Lisitskaya, L. *et al.*, 2022).

A few short years after their initial discovery in 1993, miRNAs were subsequently found to be circulating extracellularly in blood plasma and serum, as well as in several other body fluids including saliva, urine, and amniotic fluid. For example, several placental miRNAs, including hsa-miR-16 and hsa-miR-141, were discovered in maternal plasma and serum (Dennis Lo *et al*., 1997; Turchinovich *et al.,* 2012). Following this discovery of extracellular miRNAs, researchers

questioned whether this export or secretion of miRNAs was targeted or just the result of cell lysis and death. Although a positive correlation exists between extracellular miRNA concentrations and cell death rates (Turchinovich *et al.,* 2011), several studies have confirmed the former that miRNA secretion is in fact a regulated process that acts as a mode of communication across cells and tissues (Mori *et al.,* 2019; Valadi *et al.,* 2007). In 2007, a group of researchers made the initial discovery that cells were able to actively secrete miRNAs within extracellular vesicles (EVs) and that these vesicle-encapsulated miRNAs could be subsequently taken up by other cells (Valadi *et al.,* 2007). The identification of miRNAs in EVs supports previous notions that miRNAs have an increased stability in extracellular fluids, as these vesicles can effectively protect them from degradation via RNase activity. However, it has since been reported that these vesicle-encapsulated microRNAs are only the minority and that most extracellular miRNAs are membrane-vesicle-free (Turchinovich *et al.,* 2012). These vesicle free miRNAs are less protected from Ribonuclease (RNase) activity, which are hydrolytic enzymes that degrade RNA molecules, but they still remain significantly more stable than their cellular counterparts. Extracellular miRNAs in serum, compared to other cellular RNA molecules, are extremely stable in serum and other fluids and can remain intact for up to 4 days at room temperature and even in harsher conditions (Chen *et al.,* 2008). Given that most extracellular miRNAs are free and not in complex with other proteins or membrane-bound vesicles, their persistent stability likely suggests that these miRNAs are resistant to RNase digestion (Chen *et al.,* 2008).

1.3.3 Fecal MicroRNAs Facilitate the Crosstalk between Intestine and Gut Microbiota

he human intestinal microbiome plays a significant role in shaping host physiology and gaining a better understanding behind the underlying mechanisms that regulate and modify the intestinal microbiome can pave the way for the design and development of novel therapies capable of manipulating the microbiome and improving health (Sarshar *et al*., 2020). This category of host regulatory molecules includes fecal microRNAs, which were first identified in human stool 2008 (Ahmed *et al*., 2009). These fecal miRNAs have been shown to be key regulators of the host intestinal microbial composition and have been identified as possible biomarkers for intestinal dysbiosis or malignancy (Liu *et al*., 2016). In a study comparing the miRNA composition of germ-free versus SPF mice, it was found that germ-free mice had a significantly increased abundance of miRNAs, compared to SPF mice. Additionally, it was also found that that the ileal lumen also contained an increased abundance of miRNAs compared to the more densely colonized colon. Together, these findings bolster the conclusion that there is an inverse relationship between the abundance of microbes and the concomitant abundance of intestinal miRNAs, suggesting that intestinal microbiota may be degrading or associating with these miRNAs (Liu *et al.,* 2016). Much like fecal miRNAs can modify the host gut microbiome, resident intestinal microbes too can shape the host miRNA composition. For example, in previous studies on pigs that investigated the impact of probiotics on host immunity and health, the administration of the probiotic *Enterococcus faecium* resulted in a significant upregulation of ssc-miR-423-5p (Kreuzer-Redmer *et al*., 2016).

In addition to being present in the gut, miRNAs have also been shown to modulate bacterial transcripts and growth (Liu *et al.,* 2016) (Liu, *et al*., 2019). For example, hsa-miR-30d has been shown to regulate the expression of a lactase found in *Akkermansia muciniphila*. Lactase is an enzyme involved in the breakdown of lactose into simpler monosaccharides, galactose and glucose, and it is important for the growth of *A. muciniphila* (Liu *et al.*, 2019). Thus, the upregulation of the gene encoding this lactase promotes *A. muciniphila* growth and allows it to utilize other substrates, subsequently increasing its abundance in the gut (Liu *et al.*, 2019). In another experiment investigating the effects of host miRNAs on the growth of gut bacteria *in vitro*, hsa-miR-515-5p was found to boost the growth of *Fusobacterium nucleatum*, while hsa-miR-1226-5p boosted the growth of *Escherichia coli* (Liu *et al.,* 2016). These effects were additionally found to be sequence-specific, as scrambled controls of the miRNAs did not elicit the same responses. In this study, fluorescently-labelled miRNAs were added to the incubations, additionally demonstrating the ability for bacteria to uptake fluorescently-tagged miRNAs. Important to note, however, that these experiments were performed using pure cultures and that it is still not well understood how these miRNA-microbiota interactions may differ in a complex community.

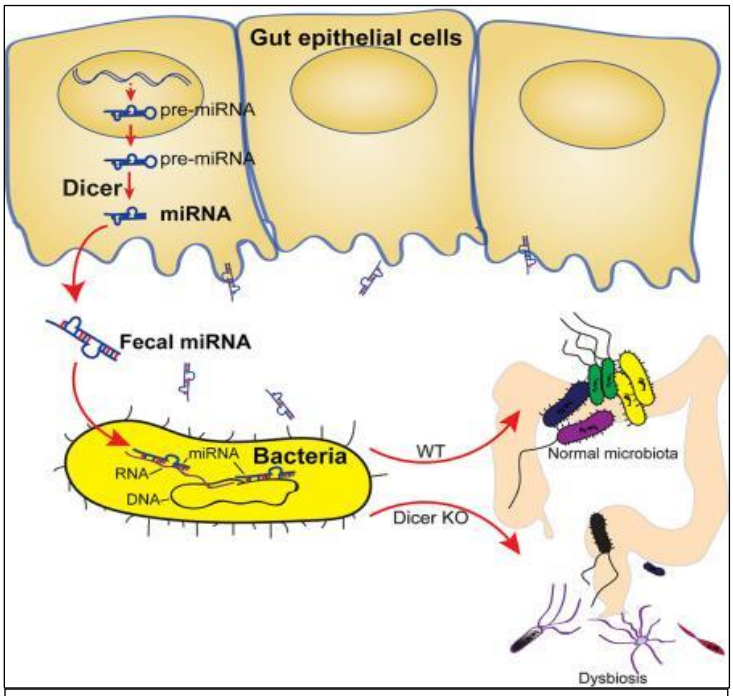

Figure 3: The above figure illustrates the complex interphase between host secreted microRNAs, intestinal microbiota, and host immunity. MicroRNAs are secreted into the gut lumen and can target gut bacteria and regulate bacterial transcripts. MicroRNAs additionally play a critical role in host immunity and protecting the integrity of the intestinal epithelium. In the absence of intestinal microRNAs, an exacerbated pathogenesis of colitis and a dysbiotic microbial community are observed (Liu et al., 2016).

In the gut, intestinal epithelial cells (IECs) are a crucial source for fecal miRNAs. In previous studies, IECs had been observed to secreted exosome-like vesicles, which motivated researchers to better understand if these cells were also capable of secreting vesicle-encapsulated miRNAs (Van Niel *et al.,* 2003). In addition to IECs, researchers identified Hopx (HOP homeobox gene) expressing cells as another major source of miRNAs in the gut (Bi *et al.,* 2020; Liu *et al*., 2016). The intestinal epithelium plays a critical role in host immunity, and IECs are able to regulate host immune responses through the secretion of humoral factors and cytokines (Okumura & Takeda, 2017). Thus, the intestinal epithelium bridges the gap between the resident intestinal microbiota and host immunity, and its role in intestinal miRNA generation provides an additional level of complexity to this interphase. Previous studies have also shown that miRNAs themselves are important regulators of epithelial

barrier function and other immune functions (Bi *et al.,* 2020). Similar experiments were performed on mice to study the effects of targeted elimination of miRNAs in the gut through the design of Dicer1$^{\Delta IEC}$ mutants, in which the mice are defective in IEC-specific miRNAs. Dicer1$^{\Delta IEC}$ mice exhibited uncontrolled, dysbiotic intestinal microbiota and aggravated colitis compared to their wildtype cohort, thus suggesting that miRNAs are critical in maintaining a healthy and balanced gastrointestinal environment (Liu *et al.,* 2016).

1.4 MicroRNAs in Human Diseases

1.4.1 Fecal MicroRNAs and IBD Pathogenesis

In 2008, a group of researchers first identified altered miRNA expression patterns in patients suffering from UC, compared to a cohort of healthy patients (F. Wu *et al.,* 2008). Since then, miRNA, particularly miRNAs circulating in serum, have become the center of attention for a myriad of studies trying to better understand their role in the pathogenesis of IBD (Casado-Bedmar & Viennois, 2022; James *et al.,* 2020). To this date, several studies have drawn a tight correlation between abnormal miRNA expression and dysbiosis of intestinal microbiota, and specific miRNAs can modulate the composition of the intestinal microbiota. For example, hsa-miR-144 and hsa-miR-211 have been shown to be important regulators of the gut microbiota for CD (Rojas-Feria *et al.,* 2018). A better understanding of the underlying mechanisms behind these observations could give better insight into the role that these small RNAs play in the gut microbiome and give insight into potential therapies for chronic gut inflammation and diseases like IBD.

Despite the significant increase in studies surrounding miRNAs and IBD, the exact mechanisms and modes of action through which miRNAs directly impact IBD pathogenesis are still not fully understood. What is known, however, is that miRNAs are key in maintaining intestinal homeostasis and can alter the microbial composition of the intestinal ecosystem and causing a dysbiotic gut (Liu *et al.,* 2016). Researchers have identified several ways through which miRNAs are capable of indirectly altering the host microbial community in the gut (Casado-Bedmar & Viennois, 2022). For example, miRNAs can regulate and modify antimicrobial peptides (AMPs), of which the most abundant in the gut is defensins. Defensins play a critical role in protecting the host intestinal mucosa against infection, and their abnormal expression has been shown in many cases of IBD (Arijs *et al.,* 2009). Additionally, miRNAs can regulate processes that impact and can potentially compromise the integrity of the intestinal epithelial barrier, causing what is referred to as leaky gut. A dysfunctional barrier promotes mucosal inflammation and aberrant host immune response, and it is often the first stage in IBD pathogenesis (Michielan & D'Incà, 2015). Lastly, microbiota-miRNA communication networks allow resident microorganisms in the intestinal ecosystem to interact with these miRNAs and subsequently alter the function of the miRNAs, contributing to either an exacerbated or ameliorated host pathophysiology. For example, the administration of probiotic *Lactobacillus* species has been shown to ameliorate DSS-induced colitis by significantly reducing the expression of miR-155, which subsequently lessens intestinal inflammation and protects intestinal barrier function (Casado-Bedmar &

Viennois, 2022; Singh *et al.,* 2014). Conversely, *Salmonella* has been shown to upregulate miR-155 expression and consequently trigger pro-inflammatory processes and induce macrophage death, which are all indicative of IBD pathogenesis (Ro *et al.,* 2018). Similar to *Salmonella*, several other opportunistic pathogens have evolved mechanisms through which they can manipulate miRNA expression levels and compromise the host immune system, leaving the host more susceptible to infection (Casado-Bedmar & Viennois, 2022).

One of the most studied miRNAs when it comes to its role in the pathogenesis of IBD is hsa-miR-21-5p (miR21) (Casado-Bedmar & Viennois, 2022). In previous studies, miR21 has been shown to be highly expressed in IBD, as well as in experimental models of IBD, such as the Dextran Sodium Sulfate (DSS)- induced colitis model (Johnston *et al.,* 2018; Rojas-Feria *et al*., 2018). Additionally, its overexpression is conserved across both plasma and colonic tissues (Thorlacius-Ussing *et al.,* 2017). In previous studies comparing miRNA expression patterns across serum and intestinal mucosa, researchers failed to identify conserved patterns in any of the selected miRNAs across serum and tissue, thus suggesting that miR21 may play a larger role in IBD pathogenesis compared to others (Iborra *et al.,* 2013). MiR21 is a well-described miRNA with several potential functions for the immune system, including the proliferation of cells, enhancement of cancer invasion and metastasis and altered macrophage polarization. Additionally, miR21 plays an important role in functions of the gut and has been found to regulate intestinal permeability (Bartel, 2018; Zhang *et al.,* 2015). In an experiment investigating the effect of a complete miR21 knockout in mice, scientists determined that miR21 $^{-/-}$ mice were significantly protected from colitis compared to their wildtype counterparts (Johnston *et al.,* 2018). The complete knock-out of miR21 reduced the recruitment of pro-inflammatory cytokines including tumor necrosis factor, reducing tissue injury and inflammation and rendering the mouse better protected from developing colitis (Shi *et al.,* 2013). These miR21 $^{-/-}$ mice were also found to have an altered gut microbiota population, defined by an increased abundance of *Actinobacterium* and several *Firmicutes* genera including *Bifidobacterium, Oscilibacter and Coprococcus,* as well as a decreased abundance of some *Bacteroides* and *Prevotella* species. When transferred into wildtype mice, this unique microbiome profile continued to confer a protective state against colitis. This confirms that the microbiota is responsible for mediating this colitis-associated phenotype of miR21 observed in wildtype mice, highlighting the intricate connection between miR21 and the gut microbiome (Johnston *et al.,* 2018).

1.4.2 Therapeutic and Diagnostic Potential of microRNAs

This discovery of extracellular miRNAs and their accompanying stability has produced many reports aimed at investigating the therapeutic potential of miRNA concentrations in serum. Several studies have associated varying levels of miRNAs with different physiological conditions, indicating that serum miRNA levels may be informative biomarkers for different pathological states or diseases (Dennis Lo *et al.,* 1997; Weber *et al.,* 2010). To date, several miRNAs have been identified as potential biomarkers for IBD. These miRNAs could provide diagnosticians with an effective and non-invasive tool for better understanding a patient's disease risk, their level or type of inflammation, and even give insight into a patient's response

to therapy (Casado-Bedmar & Viennois, 2022). Aside from IBD, miRNAs also play a role in various other human diseases, including other inflammatory diseases, autoimmune disorders (i.e. rheumatoid arthritis) and neurodevelopmental diseases (i.e. Alzheimer's disease) (Ardekani & Naeini, 2010; Soifer *et al.,* 2007). The identification for non-invasive biomarkers, such as miRNAs, for early tumor detection or disease diagnosis has been a central focus of modern cancer research, as early diagnosis would significantly improve patient quality of life and overall disease prognosis (X. Chen *et al.,* 2008).

2.0 Aims of Scientific Study

To this date, an association between host-secreted miRNAs and commensal gut microbiota has been reported (Liu, et al., 2016), but the dynamics behind these interactions are still not well understood. Previous studies have shown that bacterial cells in the gut are able to uptake miRNAs, as supported by a significant increase in concentration of luminal miRNAs in germ free mice and antibiotic-treated mice compared to their SPF-colonized counterparts (Liu, et al., 2016). A previous investigation using fluorescently labelled miRNAs visually demonstrated that bacterial cells co-localize with host miRNAs, and this study also identified a decrease in co-localization between bacterial cells and miRNA scramble controls, suggesting that these interactions might be sequence dependent. However, these interactions have not been effectively studied or visualized in a complex microbial community. In the present study, we aim to establish whether the association between miR-21 and human gut microbiota derived from fecal samples is specific or non-specific by comparing the differential association of miR-21 and a miR-21 scramble control mimic with the gut microbiota. Additionally, we are interested in investigating the dynamics of these interactions. We will identify changes in miRNA concentrations across both the pellet (bacterial cell-rich) and supernatant (bacterial cell-free) fractions to better establish if the miRNAs are taken up and degraded by the gut microbiota or if diffusion of miRNAs occurs between cell fractions.

Aside from better understanding the dynamics of these miRNA-microbiota interactions, we also aim to gain more detailed insights into the composition of the bacterial communities associating with miRNAs and if and how miRNAs impact the growth and gene expression of members of these microbial communities. Using fluorescence-labelled miRNA mimics, fluorescence-activated cell sorting and downstream 16S rRNA gene amplicon sequencing, we aim to identify which bacterial taxa within fecal samples are associating with miR-21 and if this microbial community differs significantly from that which is associating with miR-21 Scramble. To better understand the potential impacts miRNAs have on bacterial growth and gene expression, we will study the growth of the commensal gut bacteria, *Bacteroides thetaiotaomicron* (*Bt*), in the presence of different miRNAs or small RNA molecules. These *in vitro* growth studies will elucidate if miRNAs boost or impair the growth of *Bt* and if these observed effects are unique to miRNAs specifically or are observed with the amendment of any small RNA molecule. Once this is understood, we will supplement these results with a transcriptomic study that will show how these miRNAs impact *Bt* gene expression. A better understanding of which genes and operons are up- or down-regulated by these miRNAs will give important insight into how these regulatory molecules are ultimately able to impact bacterial growth and physiology.

In summary, this study will combine different techniques to better understand the dynamics of the associations between miR-21 and the human intestinal microbial communities, and the potential effects that miR-21 has on bacterial growth and gene expression. The extensive influence that host-secreted miRNAs may exert on the intestinal community remains significantly underexplored, and this study aims to produce a comprehensive report of the complex miRNA-microbiome interactome.

3.0 Methods and Materials

3.1 Media Preparation

3.1.1 Phosphate Buffered Saline (1 x PBS)

1.0 Liter of 1 x PBS medium was prepared by adding the required reagents (Table 1) to 800 mL of distilled water and adjusting the final pH to 7.4 using 1M hydrochloric acid. Milli-Q water was then added for a final volume of 1.0 Liter, and the medium was autoclaved for 15 minutes at 121 °C. An aliquot was then transferred over a flame into an autoclaved 100 mL Schott flask to be stored for use in the anaerobic tent.

3.1.2 M9 Minimal Medium

The 10 x M9 salt solution was prepared by dissolving the required reagents (Table 1) in 800 mL water and adjusting the solution to a final pH of 7.2 using 10M sodium hydroxide. Milli-Q water was then added for a final volume of 1.0 Liter, and the solution was autoclaved for 15 minutes at 121 °C. The YCFA Vitamin Mix was prepared according to the protocol for medium 1611 (YCFA Medium (Modified)) in DMSZ, and the reagents are summarized in Table 1. The 100 x Trace Elements Solution was prepared by dissolving 5g of EDTA in 800 mL distilled water and adjusting the pH to 7.5 using 1.0 M NaOH. The remaining reagents listed in Table 1 were then added, water was added to a final volume of 1.0 Liter, and the final solution was vacuum sterilized using a 0.22-μm filter. The 10 x M9 salt solution, Vitamin Mix and 100 x Trace Elements Solution were added with additional reagents (Table 1) to prepare the M9 incubation medium, and the final medium was filter sterilized using a 0.22-μm filter unit under vacuum into an autoclaved 100 mL Schott flask to be stored in the anaerobic tent for incubation set-up.

3.1.3 Bacteroides Minimal Media (BMM)

500 mL of the Mineral 3B solution was prepared by dissolving the reagents outlined in Table 1 in 500 mL Milli-Q water. The solution was then autoclaved for 15 minutes at 121 °C. 100 mL of Bacteroides Minimal Media (BMM) was made by dissolving 0.1 g glucose and 0.1 g L-cysteine in 91.75 mL nuclease free water. Then the remaining reagents outlined in Table 1 were added for a final volume of 100 mL. The medium was then filter sterilized using a 0.22-μm filter unit under vacuum into an autoclaved 100 mL Schott flask and moved into the anaerobic chamber. The same procedure was repeated for the BMM without glucose, with the only amendment being that glucose was not added.

Table 1: Preparation of the various solutions and media used throughout the various experiments.

10x M9 Salt Solution (per 1 L)		**100 x Trace Elements (TE) Solution (per 1 L)**		**YCFA Vitamin Mix (per 1 L)**	
Reagent	**Quantity**	**Reagent**	**Quantity**	**Reagent**	**Quantity**
$Na_2HPO_4•2H_2O$	75.2 g	EDTA	5.0 g	Biotin	2.0 mg
KH_2PO4	30.0 g	$FeCl_3•6H_2O$	498 mg	Folic Acid	2.0 mg
NaCl	5.0 g	$ZnCl_2$	84 mg	Pyridoxine-HCl	10.0 mg
NH_4Cl	5.0 g	$CuCl_2•2H_2O$	765 µL	Thiamine-$HCl•2H_2O$	5.0 mg
1 x PBS (per 1 L)		$CoCl_2•2H_2O$	210 µL	Riboflavin	5.0 mg
Reagent	**Quantity**	H_3BO_3	1.6 mL	Nicotinic acid	5.0 mg
NaCl	8.0 g	$MnCl_2•4H_2O$	8.1 µL	D-Ca-pantothenate	5.0 mg
KCl	0.2 g			Vitamin B_{12}	0.1 mg
$Na_2HPO_4•2H_2O$	1.81 g			p-Aminobenzoic acid	5.0 mg
KH_2PO4	0.24 g			Lipoic acid	5.0 mg
M9 Medium (per 1 L)		**Mineral 3B Solution (per 1 L)**		**Bacteroides Minimal Media (per 1 L)**	
Reagent	**Quantity**	**Reagent**	**Quantity**	**Reagent**	**Quantity**
Glucose (water-free)	0.05 g	KH_2PO_4	9.0 g	Mineral 3B Solution	5.0 mL
L-Cysteine	0.1 g	NaCl	9.0 g	Glucose	0.1 g
10 x M9 salt solution	10 mL	$MgCl_2•6H_2O$	0.2 g	L-Cysteine	0.1 g
Vitamin Mix (YCFA)	1 mL	$CaCl_2•2H_2O$	0.26 g	Hemin Solution	1.0 mL
100 x TE solution	1 mL	$CoCl_2•6H_2O$	0.01 g	Vitamin B_{12} (0.01%)	0.1 mL
1M $MgSO_4$	0.1 mL	$MnCl_2•4H_2O$	0.1 g	$FeSO_4$	0.15 mL
1M $CaCl_2$	0.03 mL	NH_4Cl	5.0 g	10% (w/v) $NaHCO_3$ solution	2.0 mL
		Na_2SO_4	2.5 g		

3.2 Fecal Slurry Incubations for miR-21 and miR-21 Scramble Association Experiment

Human fecal samples were collected from three healthy adult individuals who had not taken antibiotics in the previous 3 months. All participants submitted an informed consent form and self-sampled using a sterile polypropylene tube with the attached sampling spoon (Sarstedt, Product Number: 80.622, Nümbrecht, DE). The study protocol was approved by the University of Vienna Ethics Committee (reference #00161). All data is completely anonymized and adheres to University regulations (Ge *et al.*, 2022). All reagents and laboratory equipment were introduced into the anaerobic chamber minimally one day prior to experimentation via an Airlock (Coy Lab Products) to reduce oxygen levels. Additionally, all Eppendorf tubes and pipette tips used to set up incubations were nuclease free, to prevent miRNA degradation, and nuclease-free water was always used to prepare custom buffers and solutions that came in contact

with miRNAs. Samples were freshly collected and introduced into the anaerobic tent via the Airlock upon immediate arrival at the laboratory. All fecal slurries and incubations were prepared, stored, and incubated in a vinyl Anaerobic chamber (Coy Lab Products) with an atmospheric composition of 5% H_2, 10% CO_2 and 85% N_2. This experiment was repeated with two additional donors, following the same protocol (2.21-2.6).

3.2.1 Preparation of Fecal Slurry

One spoonful of fecal sample was collected (approximately 1 gram). 1 gram of fecal sample was resuspended in 10mL of 1 x PBS and vortexed thoroughly for 2-4 minutes, to generate a 10% (w/v) fecal slurry. The sample was then left for 10 minutes, so that larger particles could settle to the bottom (Fig. 4A). 1 mL of the pre-settled mixture was transferred to a new 50 mL falcon tube and diluted ten times with 9 mL sterile M9 medium. The mixture was thoroughly vortexed and left to the side again to allow larger particles to settle. An aliquot of the diluted, pre-settled fecal slurry was then transferred to a new 15 mL falcon tube and will be referred to from here on out as the working fecal slurry. One working fecal slurry (4.5 mL) was used for live cell incubations, and the other (3.5 mL) was used for control incubations with ethanol- fixed cells (Fig. 4B).

3.2.2 Cell Fixation

As a control, cells were fixed using 96% ethanol to determine whether microRNAs bind to or enter dead/inactive cells (Fig. 4B). Following preparation of the working fecal slurry, 3.5 mL of the diluted, pre-settled fecal slurry was aliquoted for cell fixation. The sample was centrifuged for 5 minutes (4°C at 14000 rpm) and resuspended in the same volume ice-cold 1 x PBS. Next, one volume ice-cold 96% (v/v) ethanol was added and mixed into the resuspended sample via inversion. The mixture was then stored at -20°C for 1 hour, then spun down again for 5 minutes (4°C at 14000 rpm). All liquid was removed and discarded, and the recovered pellet was resuspended in the same initial volume of sterile M9 medium in the anerobic tent.

3.2.3 Live and Fixed Cell Incubations and Sampling

Incubations were set up in duplicates and labeled according to the scheme summarized in Figure 4. Prior to incubation set-up, time points were chosen (T0, T1, T2, T4, T6, and T24) to ensure a sufficient volume of working fecal slurry was aliquoted to each incubation. Because 6 time points were selected and 100 μL was sampled per time point, 750 μL live and fixed working fecal slurry were aliquoted to the respective, pre-labelled 1.5 mL Eppendorf tubes for incubation. Human miR21 (Sequence: 5’ – UAGCUUAUCAGACUGAUGUUGA - 3’; MISSION® microRNA Mimic, Sigma-Aldrich), or 250 nM miR21 scramble (Sequence: 5’ - GCAUAUUCGGUCGUUAUAAGAU - 3’; MISSION® microRNA Mimic, Sigma-Aldrich) diluted in water were added for a final concentration of 250 nM. A water control where the same volume of water only (3.75 μL) was added was also included. The T0 timepoint was sampled immediately after the addition of nuclease free water, miR21 or miR21 scramble (Fig. 4C). The remaining samples were then collected 1 hour, 2 hours, 4 hours, 6 hours and 24 hours after the addition of DEPC water, miR21 or miR21 Scramble. Immediately after sampling, the samples

were spun down for 5 minutes (4°C at 14000 rpm), and the supernatant was extracted and stored at -80°C (Fig. 4D). The cell fraction (pellet) was then washed with one volume ice-cold 1 x PBS and spun down again for 5 minutes (4°C at 14000 rpm). The supernatant was then extracted and discarded, and the recovered pellet was stored at -80°C.

3.2.4 Fecal RNA Isolation

The Norgen Biotek Total RNA Purification Kit (Catalog number: 17200) was used to isolate and purify total RNA from the supernatant and pellet cell fractions. Norgen's kit can be used to purify all sizes of RNA, including miRNAs, which was of particular interest in this study. The total RNA was extracted from the various incubation cell fractions following the manufacturer's guidelines for total RNA isolation. For the initial cell lysis step, Tris-EDTA (TE) lysis buffer was prepared by adding Tris-HCl buffer (20 mM, pH = 8.0), EDTA (2 mM) and Triton-X (1.2%) to DEPC-water for a final volume of 50 mL. The pellet fractions of each sample were homogenized in 100 μL TE buffer, with 10 mg/mL freshly added lysozyme (SKU: 62970-5G-F, Sigma-Aldrich), and incubated at 37°C for 30 minutes. Following this, pellet and supernatant fractions were treated the same for all downstream steps. The provided lysis buffer, which contains guanidinium salts, was added to all samples to lyse the cells. After thoroughly vortexing the lysate, ethanol was added, and the entire lysate was loaded onto the spin column. Norgen Biotek's resin preferentially binds RNA based on ionic concentration, so only RNA will bind to the column, while all remaining proteins will be removed with the flowthrough. After RNA has successfully bound to the column, the column was washed three times using the provided washing buffer. Lastly, the purified RNA product was eluted in 25 μL RNase-free water. The final RNA product was stored at -80°C for subsequent downstream analysis.

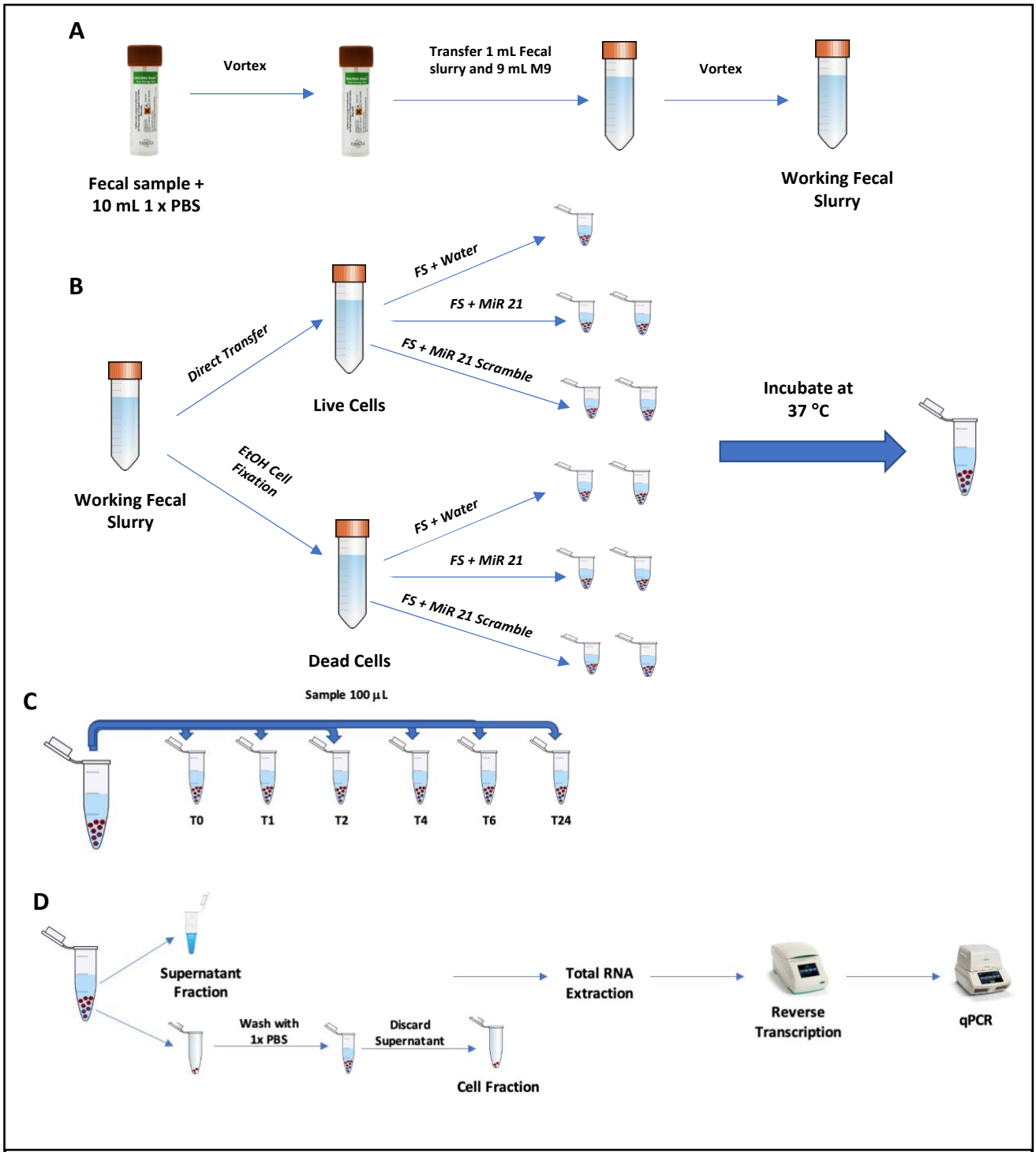

Figure 4: Procedural schematic for fecal slurry preparation for live and fixed cell incubations and sampling. (A) Preparation of the fecal slurry. (B) Incubation set-ups for both live and dead bacterial cell incubation, including the different amendments and controls added to each incubation. (C) Summary of the different sampling time points. (D) Separation of samples into supernatant and pellet fractions and subsequent downstream analysis.

3.2.5 Complementary DNA (cDNA) Synthesis

After extraction of the total RNA from the cell and supernatant fractions, reverse transcription was performed to synthesize cDNA for downstream analysis with qPCR. All reverse transcription and qPCR reactions were set up in a UVP PCR² Workstation (Analytik Jena) to ensure a clean working environment. 1:10 dilutions of all total RNA samples were created using 2 μL RNA product and 18μL RNase free water. 5 μL of the diluted RNA product was mixed thoroughly with 3 μL of the 5 X RT primers and incubated at 85°C for 5 minutes, followed by 60°C for 5 minutes. Different 5 x RT primers were used for analysis with miR21 (Catalog number: 4427975, Thermo Fisher Scientific) versus miR21 scramble (Catalog number: 4398987, Thermo Fisher Scientific) (Table 8). During the incubation, the master mix was prepared according to the manufacturer's instructions using a miRNA reverse transcription kit (Catalog number: 4366596, Thermo Fisher Scientific) and kept on ice. Following incubation, 7 μL of master mix was added to each reaction tube for a total volume of 15 μL, and the reverse transcription reaction was performed in the thermal cycler (T100™ Thermal Cycler, Bio-Rad Laboratories), following the thermal program outlined in Table 2. As a control, a mock cDNA synthesis reaction was also performed, in which no reverse transcriptase was added to the samples of interest. Following completion of the reactions, the cDNA products were stored at -20°C.

Table 2: Thermal protocol for the reverse transcription reaction. RT reaction was performed using standard cycling with a reaction volume of 15 μL.

Step	Temperature	Time
Reverse Transcription	16° C	30 minutes
	42° C	30 minutes
Stop Reaction	85° C	5 minutes
Hold	4° C	Hold

3.2.6 MiRNA Quantification with qPCR

To quantitatively measure the concentration of miRNAs in the various cDNA products, qPCR was performed using the TaqMan™ Fast Advanced Master Mix (catalog number: 4444556, Thermo Fisher Scientific). 18.67 μL of the Master Mix, which consisted of the 20 X small RNA assay, the TaqMan™ Fast Advanced Master Mix, and nuclease-free water, was added to each well, followed by 1.33 μL of cDNA of the samples of interest for a total volume of 20 μL. Different TaqMan™ MicroRNA Assays were used for analysis with miR21 (Catalog number: 4427975, Thermo Fisher Scientific) vs miR21 scramble (Catalog number: 4398987, Thermo Fisher Scientific). In addition to standards, nuclease free water was added to the Master Mix on its own as a control to ensure no contamination of the master mix. All samples and controls were plated in triplicate on a 96-well standard (0.2 mL) reaction plate (catalog number: HSP9601, Bio-Rad Laboratories), which was sealed and ran in the thermal cycler (CFX96™ real-time PCR system, Bio-Rad Laboratories) using the appropriate fast cycling mode and

thermal protocol, as specified by the manufacturer and outlined in Table 3. The results of the qPCR reaction were then analyzed using the CFX Maestro software program.

Table 3: Thermal protocol for the real-time PCR reaction performed to calculate miRNA concentration in fecal slurry incubation samples. PCR reaction was performed in a 96-well standard (0.2 mL) plate

Step	Temperature	Time	Cycles
UNG Activation	50° C	2 minutes	1
Enzyme Activation	95° C	20 seconds	1
Denature	95° C	3 seconds	40
Anneal/Extend	60° C	30 Seconds	

The standards were produced by generating a serial dilution of the miRNA of interest. In the case of miR21, the first dilution was made so that the concentration was equivalent to that which was initially added to all the incubations (250 nM). This was done my adding 1 μL of the 50 μM miR21 stock solution to 200 μL nuclease free water. The second dilution was then made by adding 2 μL of the 250 nM dilution to 18 μL nuclease free water. The third solution was then made from this second dilution and so on until there were a total of 7 dilutions ranging in miR21 concentration from 250 nM to 0.00025 nM. The standards for the miR21 scramble were produced in the same manner. Following the preparation of these serial dilutions, the reverse transcription reaction was performed, this time without further diluting the samples. Following cDNA synthesis, qPCR was performed to measure the Cq values of the various standards. The same procedures, including Master Mix preparation, incubation and run procedures were used on the standards as with all other samples. Standard curves were then generated using the results from the qPCR and mapping miRNA concentration of the standards against Cq value. The acquired regression line equation was then used to calculate miRNA concentration in all the samples based on their respective Cq values. The final calculated miRNA concentrations were then corrected to account for the 1:10 dilution prior to cDNA synthesis and the four-fold increase in concentration following total RNA extraction.

3.3 Gel Electrophoresis

To verify the integrity of the isolated RNA product, agarose gel electrophoresis was performed on a subset of samples from different time points. A 1.2% agarose gel with Gel Red nucleic acid gel stain (Biotium) was made and loaded with the chosen samples and ran at 90 volts. 1 μL of 6x loading dye was added to 3 μL of the RNA product of the chosen samples and ran alongside 2 μL of GeneRuler 1 kb (Catalog number: SM0311, Thermo Fisher Scientific) for comparison. The negatively charged RNA molecules will migrate towards the anode in the presence of the electrical current according to the size of the molecular components, with larger components travelling through the gel slower than smaller components. After completion of the run, the gel was imaged using an ultraviolet transilluminator (Gel Doc™ XR+ Molecular Imager, Bio-Rad Laboratories).

3.4 Fecal Slurry Incubations with miR21 in the presence of an RNAse inhibitor

Live and dead fecal slurry incubations were prepared using the same aforementioned procedure (3.3), with either the addition of miR21 or miR21 with an RNase inhibitor (catalog number: 4469082, Thermo Fisher Scientific). The incubations were set up in duplicate and labeled according to the scheme summarized in Supplemental Figure 1. The same concentration of miR21 (250 nM) was added to all the incubations containing either the live or dead fecal slurry and incubated at 37°C for 10 minutes. After this initial incubation period to allow sufficient time for microbiota-miRNA associations, all the samples were spun down, and the supernatant was removed and discarded. The pellets were then washed with and re-suspended in M9 medium. The samples were spun down again, and the pellets were washed and re-suspended once more in M9 medium. These additional washing steps were included to sufficiently deplete any extracellular miRNAs adhering to the surface of cells, so as to only quantify miRNAs in association with the cells. Following the second pellet resuspension, RNase inhibitor was re-added to the amendments previously inoculated with RNase inhibitor, and the first sample was taken from all incubations (T0) after vortexing. Sampling continued at the defined time points (Sup. Fig. 1). Because the pellets were already thoroughly washed in the anaerobic tent prior to the initial sampling, additional washing outside of the tent was not necessary. Instead, all the samples were spun down, and the supernatant and pellet were stored separately at -80°C. Only the pellets were used in downstream analysis, which included RNA extraction and miRNA quantification using qPCR. Additionally, the ethanol fixed (“dead”) samples were omitted from downstream analysis. Supplemental Figure 1 summarizes the procedure followed for fecal slurry preparation for cell incubation and the subsequent sampling for the amended miR21 incubation experiment.

3.5 MiR21 Stability Incubation

An additional incubation was set up, in which 250 nM of miR21 was added to 600 μL M9 medium. 100 μL was sampled every hour for 6 hours (T0, T1, T2, T4, T6). Because no bacterial cells are present in this control incubation, the sample is immediately stored as the supernatant fraction at -80°C. These fractions were then subjected to downstream analysis, which included RNA extraction, cDNA synthesis and miRNA quantification using qPCR.

3.6 Ethanol Fixation Growth Analysis

The live and dead fecal slurries were prepared according to previous procedures (see 3.3). Following the preparation of the live fecal slurry, two serial dilutions were created by transferring 100 μL of the live slurry to an autoclaved Eppendorf tube with 900 μL 1 x PBS and vortexed well. The same was done for the ethanol-fixed fecal slurry following a wash and resuspension in M9 medium. 100 μL of the undiluted fecal slurries and serial dilutions were added and spread onto BHI agar plates and incubated at 37°C for 72 hours under anaerobic conditions.

3.7 Fecal Sample Incubations with Fluorescently Labelled microRNAs

3.7.1 Fecal Sample Incubations and Sampling

Three different fecal samples were collected from the same three donors used in the previous miRNA incubation experiments (see 3.2) and introduced into the anaerobic tent. Working fecal slurries were prepared for each fecal sample according to the protocol previously summarized in section 3.3.1. Prior to the addition of amendments, 500 μL of each slurry was removed and added to a clean, nuclease-free Eppendorf tube and centrifuged (10,000 rpm, 5 mins). The supernatant was removed and discarded, and the fecal pellets were stored at -80 °C for downstream DNA extraction to profile the microbiome of each donor. Following this step, the fecal slurries from all 3 donors were combined into a clean 50 mL falcon tube, so as to create a single working fecal slurry representative of all 3 donors for the experiment.

For the miRNA samples, each sample replicate was set up and processed one at a time to prevent miRNA degradation by the bacterial cells and minimize fluorescent dye bleaching. During all steps of the workflow, all samples were carefully protected from light to preserve the fluorescence signals.

All samples (water control, miR21, miR21 scramble) were set up in duplicate, and 1000 μL of the working fecal slurry was aliquotted into 6 separate 2 mL Eppendorf tubes. To set up the negative control incubations, 5 μL nuclease free water was added to 2 Eppendorf tubes containing 1 mL fecal slurry. The samples were vortexed and washed with 1 x PBS and following centrifugation the supernatant was discarded, and the pellet was re-suspended in 1000 μL 1 x PBS. To set up the fluorescent miRNA incubations, 250 nM of fluorescently tagged miR21 (Sequence: 5'- [6FAM]UCAACAUCAGUCUGAUAAGUCUA [dT][dT]- 3' ; Merck Millipore) and miR21 scramble (Sequence: 5'-[6FAM]AUCUUAUAACGACCGAAUAUUGC[dT][dT]- 3'; Merck Millipore) was added to an Eppendorf tube containing 1000 μL fecal slurry. The approximate fluorescence excitation and emission maxima for the 6-FAM tag (ATTO 488) labelling the miRNAs are 490 nm and 525 nm, respectively. The samples were gently vortexed and incubated at 37 °C for 30 minutes. After the incubation, the samples were vortexed, washed with 1 x PBS and the sample pellet was re-suspended in 1000 μL 1 x PBS. Following the washing step with 1 x PBS, the samples were put on ice and removed from the tent for ethanol fixation and nucleic acid staining. The same process was repeated for the duplicate of each sample following FACS analysis with the first duplicate.

3.7.2 Ethanol Fixation

In order to preserve their current state for nucleic acid staining and cell sorting, ethanol fixation was performed on all samples. 100% ethanol (v:v) was added to each sample, and the tubes were inverted to mix. The samples were fixed at -20 °C for 30 minutes, centrifuged (16,000 rpm, 4 °C, 5 min.), the supernatant was discarded, and the pellet was re-suspended in 2000 μL 1 x PBS.

3.7.3 SYTO62 Staining

All samples (except for one of the water control sample duplicates) were stained with 2 uM STYO62 red fluorescent cell-permeable, nucleic acid stain (Catalog number: S11344, Thermo Fisher Scientific) in the dark for 30 minutes. The approximate fluorescence excitation and emission maxima for SYTO62 are 649 nm and 680 nm, respectively. This staining was important during fluorescence-activated cell sorting to assist with gating by helping to distinguish real cell events from debris.

3.7.4 Fluorescence-activated Cell Sorting (FACS)

The incubation experiment with fluorescently labelled miRNAs and subsequent cell sorting were repeated with samples from the same 3 donors mentioned in previous experiments (Section 3.2). During sample preparation, the FACS Melody™ System was set-up, cleaned and calibrated using BD™ CS&T (Catalog number: 656504) and BDFACS Accudrop (Catalog number: 345249) bead solutions in filter-sterilized 1 x PBS (all solutions passing through the FACS are filter sterilized). Following system calibration, all samples were transferred into 5 mL FALCON® tubes and passed through a 35 μM pore cell strainer cap (Catalog number: 352235, Corning) and analyzed and sorted on purity mode using the BD FACS Melody™ Cell Sorter. The gating for the SYTO62 counterstain was adjusted based on the stained and unstained water control samples and the 1 x PBS control. The gates for the ATTO 488+ and ATTO 488- populations was adjusted based on the SYTO62-stained water control sample and the ATTO488-tagged miRNA samples (Sup. Fig. 5). Fluorescent events were monitored using a 561 nm laser and 697/58 nm filter (SYTO62 detection) and a 488 nm laser and a 527/32 nm filter (ATTO 488 detection). At times when the concentration of cells was too high, the samples were diluted with an additional ½ volume 1 x PBS. All fluorescent miRNA incubation samples were sorted, so that each sorted fraction contained approximately 25,000 ATTO 488+ and 25,000 ATTO 488- events. All sorts, as well as two 10 μL aliquots of the 1 x PBS used to dilute the samples were subsequently stored at -80 °C for downstream processing.

3.7.5 DNA Extraction from FACS Sorted Cells

The innuPREP DNA Mini Kit (Catalog number: 845-KS-1041250, Analytik Jena) was used to extract DNA from all cell sorts- this includes sorts from both the original and amended experiments, as well as the 1 x PBS aliquots used during both experiments. Additionally, 50 μL of fixed sample (pre-sorting) was included as another control. Prior to extraction, all kit buffers and TE lysis buffer (before lysozyme addition) were UV-radiated for 30 minutes in a UVP PCR² Workstation (Analytik Jena). Following UV radiation, 20 mg/mL of fresh lysozyme was added to the TE lysis buffer (previously prepared in 3.3.4). Cells were harvested from the sorts via centrifugation (7500 rpm, 5 min), but the supernatant was not removed to prevent any loss of cells. The cells were then re-suspended in 180 μL of the enzymatic lysis buffer, vortexed (1 min.), spun-down, and incubated (37 °C, 45 min, 400 rpm). 25 μL of the provided Proteinase K was added to each sample, followed by a quick vortex (5 sec), spin down and incubation (50 °C, 15 min, 400 rpm). Following lysis, 400 μL Binding Solution TBS was added to each sample and

mixed by vortexing. The lysate and binding solution mixture was then applied to a spin filter and centrifuged (2 min, 10,000 rpm). The collection tube with the filtrate was discarded and the spin filter was placed in a new collection tube. The spin filter was then washed with 500 μL Washing Solution HS, centrifuged (1 min, 10,000 rpm) and placed into a new collection tube. This washing step was repeated with 750 μL Washing Solution MS. The tubes were centrifuged (2 min., 10,000 rpm) again to remove all traces of ethanol, and the spin filter was placed into a clean 1.5 mL elution tube. 20 μL of nuclease-free water was added to each tube, and the samples were all incubated for 5 minutes at room temperature. The final DNA product was eluted via centrifugation (1 min, 10,000 rpm), and all samples were stored at -20 °C.

3.7.6 Polymerase Chain Reaction and Gel Electrophoresis for DNA Extracts

The concentrations of DNA extracted from the cell sorts were too low to quantify with Qubit, so 16S rRNA PCR amplification and gel electrophoresis were carried out to confirm that the DNA extraction was clean and successful. The PCR reaction was performed with all DNA extracts and the PCR water to control for any contamination in the PCR reaction mix. In this experiment, the V4 region of the 16S rRNA gene was targeted using the 515F-mod and 806R-mod primers (Apprill *et al*., 2015; Parada *et al*., 2016) (Table 8). The PCR reaction was prepared by adding 1 μL DNA template to 19 μL of the PCR master mix, prepared according to Table 4, and the PCR reaction was run in a thermocycler (T100™ Thermal Cycler, Bio-Rad Laboratories) using the protocol outlined in Table 5.

Table 4: Summary of reagents used in the 16S rRNA PCR reaction.

Reagent	Volume per 20 μL Reaction
10 x Dream Taq Buffer	2.0 μL
2 mM dNTP-Mix	2.0 μL
MgCl2	1.6 μL
10 μM 515F Primer	0.4 μL
10 μM 806 R Primer	0.4 μL
BSA	0.125 μL
Dream Taq DNA Polymerase	0.125 μL
Nuclease-free Water	12.35 μL
DNA Template	1.0 μL
Total	20.0 μL

After the PCR reaction, all samples were run on a 1.2% Agarose gel (45 min, 90 V) in order to ensure that the samples were amplified successfully. Only the DNA samples that presented with a successful amplification were submitted for 16S rRNA amplicon sequencing.

Table 5: Thermal protocol for the 16S rRNA PCR reaction. The reaction was performed using standard cycling with a reaction volume of 20 μL.

Step	Temperature	Time	Cycles
Initial Denaturing	95° C	3 minutes	1
Denaturing	95° C	30 seconds	30
Annealing	52° C	45 seconds	
Elongation	72° C	1 minute	
Final Elongation	72° C	10 minutes	1

3.7.7 16S rRNA Amplicon Sequencing

For high throughput sequencing of 16S rRNA gene amplicons, amplicon pools were extracted from the raw sequencing data, according to the two-step PCR amplicon sequencing workflow and downstream sequencing pipeline of the Joint Microbiome Facility (JMF) (Herbold *et al*., 2015; Pjevac e*t al.,* 2021). In the first PCR reaction, the V4 region of the 16S gene was targeted and amplified with specific primers, H-515F-mod and H-806R-mod that added a universal head sequence to each amplicon (Table 8). In the second PCR reaction, this amplicon was subsequently tagged with a primer that targeted the head sequence and affixed a barcode to each end of the amplicons. These barcoded PCR amplicons were then purified, normalized and subjected to downstream analysis according to the JMF amplicon sequencing pipeline (Herbold *et al*., 2015; Pjevac *et al*., 2021). The DADA2 R package (Callahan *et* al., 2016a; Rangel *et al.,* 2022) was employed for demultiplexing amplicon sequencing variants (ASVs) using a pre-defined protocol (Callahan *et al,* 2016b; Rangel *et al.,* 2022). Taxonomy was assigned to 16S rRNA gene sequences based on SILVA taxonomy using the DADA2 classifier (Callahan *et al,* 2016b; Rangel *et al.,* 2022). Amplicon sequence libraries were analyzed using the vegan (v 2.6.4) and phyloseq (v 1.42.0) packages of the software R (v 4.2.2) and DESeq2 (v 1.38.3; Love *et al.,* 2014) implemented in phyloseq was used to identify any significant differences in ASV, genera and family abundance across the different FACS sorted fractions. Microbiome Analyst was employed for additional analysis of the relative abundance of different taxa in the samples, as well as in the creation of the dendrogram displaying clustering of the different samples[1].

3.8 In vitro Experiments using Pure Cultures of Bacteroides thetaiotaomicron

3.8.1 Bacteroides thetaiotaomicron Growth Curves

Bacteroides thetaiotaomicron (*Bt*) strain VPI-5482 (DSM2079) was pre-grown on a Brain Heart Infusion (BHI) Agar plate from a pre-existing glycerol stock. After 72 hours of growth, a large, singular colony was picked to inoculate 5 mL liquid *Bacteroides* Minimal Media (BMM) and grown overnight. After the first 16 hours of growth, the culture transitioned to exponential phase. 50 μL of the pre-grown culture was then taken at exponential phase to inoculate 5 mL BMM in a fresh hungate tube. The optical density (OD600) was then measured every 30 minutes to analyze the rate of growth and create a growth curve for *Bt*.

[1] https://microbiomeanalyst.ca/

3.8.2 Growth of Bacteroides thetaiotaomicron in the Presence of Small RNA Molecules

After analyzing the growth pattern of *Bt* in liquid culture in hungate tubes, the same procedure (3.9.1) was repeated using a 96 well plate. A colony was picked from the pre-grown *Bt* on the BHI plate and used to inoculate 5 mL BMM, and the culture was incubated and allowed to grow overnight at 37°C. Fresh BMM was prepared both with and without the addition of glucose. BMM without glucose was prepared using the same procedure described (3.2.3), with the only amendment being the omission of glucose. 1100 μL of BMM with glucose and 1100 μL of BMM without glucose were aliquotted into 4 different 2.0 mL Eppendorf tubes each and 250 nM of each treatment was added (5.5 μL of 50 μM stock of hsa-miR-21-5p, 5.5 μL of 50 μM stock of hsa-miR-21 scramble, 3.25 μL of 100 μM stock of small RNA oligonucleotide control (sequence: 5'- GGAACGCCAACCGAAGUCUA - 3')). In the fourth Eppendorf tube, 5.5 μL of nuclease free water was added as a negative control. Prior to the addition of the pre-grown *Bt* culture (at exponential phase), 200 μL of each aliquotted media with the various treatments were transferred in duplicate into the 96 well plate as a negative control to ensure no contamination of the prepared BMM. 7 μL of the *Bt* culture was then added to the remaining 700 μL in the various Eppendorf tubes, and then 200 μL of each sample was transferred in triplicate to the 96-well plate. The plate was loaded into the anaerobic tent reader, and the appropriate protocol was run for 48 hours. This experiment was repeated with the use of BMM without glucose and 200 μL of BMM media alone was added to all remaining empty wells. Additionally, all samples and controls were plated in the middle wells of the plate to avoid excess sample evaporation during growth.

3.8.3 Cell Quantification

After 18 hours of growth in the anaerobic plate reader, 2 μL of each sample and replicate was collected and stored on ice for bacterial cell quantification using the QUANTUM ™ Total Cell Staining Kit (logos biosystems). A 10:1 dilution of each sample was made with 1 x PBS by adding 9 μL of 1 x PBS to 1 μL of sample. 1 μL of QUANTUM™ Total Cell Staining Dye and 1 μL of QUANTUM™ Total Cell Staining Enhancer was added to the sample dilution, and the mixture was vortexed, spun down and incubated in the dark at room temperature for 5 minutes. 8 μL of QUANTUM™ Cell Loading Buffer was added, and the mixture was mixed gently via pipetting up and down so as to not create bubbles. 6 μL of the sample mixture was loaded into a QUANTUM™ M50 Cell Counting Slide. The sample slide was then centrifuged at 300 RCF for 15minutes and subsequently inserted into the QUANTUM Tx™ Microbial Cell Counter. The cells were counted at a light intensity of 5.

3.9 Transcriptomics Experiment

3.9.1 Sample Preparation

Prior to the day of the experiment, a culture of *Bt* was prepared according to the previous pure culture studies described in 3.9.1. In this experiment, the same 4 conditions described in procedure 3.9.2 were used again- water control (nuclease free), small RNA control, miR21, and miR21 scramble. 80 mL of BMM was inoculated with 800 μL of a pure culture of *Bt* in a small 100 mL Schott flask. 6.5 mL of the inoculation was then aliquoted into 12 different hungate tubes (3 tubes per condition) and incubated at 37 °C until mid-exponential phase (OD600 = ~0.5). Once the cultures reached mid-exponential phase, 250 nM (16.25 μL of 100 μM stock solutions, 16.25 μL water control) of each treatment was added to the respective tubes in triplicate, and the cultures were then incubated with these small RNA molecules for an additional hour at 37 °C, after which all tubes were removed from the tent for subsequent fixation with phenol.

3.9.2 Cell Fixation using Phenol

Prior to experimentation, a mixture of acidic-phenol (water equilibrated) and molecular grade ethanol was prepared in a 50 mL falcon tube by adding 2.5 mL phenol to 47.5 ethanol. The mixture was inverted to mix and stored on ice in the fume hood. Following removal from the tent, the samples were swiftly moved into a fume hood, where a 1:10 volume of the phenol/ethanol mixture was added to each sample (650 μL mixture into 6.5 mL sample). The samples were vortexed gently to mix, followed by a 5-minute incubation on ice. All samples were then transferred into clean 15 mL falcon tubes and centrifuged (5000 rpm, 4 °C) for 10 minutes. Following centrifugation, the supernatant was carefully removed and discarded, and the pellets were stored at -80 °C for subsequent downstream RNA purification.

3.9.3 Total RNA Extraction from Bacteroides thetaiotaomicron Pellets

Prior to extraction, 50 mL fresh TE buffer (20 mM Tris-HCl buffer [pH = 8.0], 2 mM EDTA, 1.2% Triton-X, and nuclease free water) was prepared and UV-irradiated for 30 minutes before use. The Norgen Biotek Total RNA Purification Kit (Catalog number: 17200) was used to isolate and purify total RNA from the sample pellets. The pellets were homogenized in 100 μL nuclease free TE buffer, with 1 mg/mL freshly added lysozyme (SKU: 62970-5G-F, Sigma-Aldrich), and incubated at 37°C for 15 minutes. Following this, the extraction protocol previously described in section 3.3.4 was followed, and the final RNA product was eluted in 41 μL nuclease free water.

3.9.4 DNase Treatment

In order to remove any trace amounts of contaminating DNA present in the RNA extracts, a DNase treatment was performed on each sample. The reagents summarized in Table 6 were added to each sample tube with the crude RNA extract. The samples were then incubated in a

thermoshaker at 37°C with gentle shaking (250 rpm) for 30 minutes, after which an additional 1 μL of Turbo DNase (Catalog number: AM2238, Thermo Fischer Scientific) was added to each tube and the incubation step was repeated (30 min, 37°C, 250 rpm).

Table 6: Summary of reagents added to each DNAse reaction tube

Reagent	**Per 50 μL reaction**
Nucleic acid crude extract (sample)	41 μL
10 x Turbo DNase buffer	5 μL
RNase Inhibitor (40U/μL)	1 μL
0.1M DTT	1 μL
Turbo DNase	1 μL
Add Additional 1μL DNase (after 30 min. incubation)	1 μL
Final Volume	50 μL

3.9.5 RNA Purification

Following DNase treatment, the Zymo RNA Clean & Concentrator Kit (Catalog number: R1015, Zymo Research) was used to clean and purify the final RNA product. Prior to clean-up, an adjusted RNA binding buffer was prepared by mixing equal volumes of the supplied Zymo RNA Binding Buffer and 100% ethanol. 2 volumes of the adjusted RNA binding buffer were then added to each sample (100 μL buffer added to 50 μL sample) and gently mixed. The sample/buffer mixture was then transferred to a Zymo-Spin™ Column and centrifuged (13,000 rpm, 30 sec). For this experiment, the procedure for the extraction of large RNAs (> 200 nt) was followed, and these are retained in the column. The flow through from the previous centrifugation step was discarded, and 400 μL RNA Prep Buffer was added to each column and centrifuged (13,000 rpm, 30 sec). The flow through was discarded, and the column was washed with 700 μL RNA Wash Buffer ad centrifuged (13,000 rpm, 30 sec). This wash step was then repeated with 400 μL RNA Wash Buffer and centrifuged (13,000 rpm) for 1 minute to dry the column. The column was then transferred to a clean, RNase-free tube, and the RNA product was eluted in 41 μL in preparation for a second DNase treatment. The DNase treatment and RNA clean-up steps (3.10.4- 3.10.5) were repeated twice more for a total of 3 rounds, and the final RNA product was eluted in 24 μL nuclease free water. 2 μL of each elute were removed and stored in a separate RNase-free tube for RNA quantification, and all tubes were stored at -80 °C.

3.9.6 RNA Quantification

The purified RNA was quantified using the Qubit 4 Fluorometer (Catalog number: Q33238, Thermo Fisher Scientific) and Qubit RNA Broad Range (BR) Assay Kit (Catalog number: Q10210, Thermo Fisher Scientific). The Qubit working solution was prepared by diluting the Qubit RNA BR Reagent 1:200 in Qubit RNA BR Buffer. Qubit assay tubes (catalog number:

Q32856, Thermo Fisher Scientific) were set up for each sample and for the 2 standards included with the kit. Each sample and standard was added to the respective assay tube containing the appropriate volume of working solution (Table 7) and vortexed gently for 3 seconds, after which all samples were incubated in the dark at room temperature for 2 minutes. Following incubation, the standards were used to properly calibrate the fluorometer, after which the samples were analyzed and the concentration of the original sample was measured.

Table 7: Summary of Assay tube preparation for RNA Quantification by Qubit™

Solution	Standards	Samples
Working Solution	190 μL	199 μL
Standard (from kit)	10 μL	----------
Purified RNA	----------	1 μL
Total in each Assay Tube	200 μL	200 μL

3.9.7 TapeStation Automated Electrophoresis for RNA Sample Quality Control

For quality control of the RNA samples, automated electrophoresis was performed using the Agilent 4150 TapeStation system. Due to the high concentrations of RNA measured during the quantification step (3.10.6), the RNA ScreenTape kit (Catalog number: 5067-5576, Agilent) was used to assess sample integrity. The TapeStation system evaluates the degree of RNA degradation in each sample by calculating the ratio between the 23S and 16S ribosomal RNAs (Cholet *et al.,* 2019). This degree of degradation is then reported as an RNA Integrity Number equivalent (RIN^e) on a scale of 1-10, where a low RIN^e is indicative of a highly degraded RNA sample, while a high RIN^e is indicative of an intact RNA sample.

Prior to sample preparation, the RNA ScreenTape device (Catalog number: 5067-5576, Agilent) was flicked and loaded into the TapeStation instrument. All RNA samples and reagents were thawed on ice, vortexed, and spun down before use. 1 μL of each RNA sample and 5 μL of RNA Sample Buffer (Catalog number: 5067-5577, Agilent) were added into their respective positions in the tube strip, keeping the first position free. In the first position, 5 μL RNA Sample Buffer was added with 1 μL RNA Ladder (Catalog number: 5067-5578, Agilent). All samples were vortexed (1 min, 2000 rpm) and subsequently spun down (1 min). All samples were then incubated for 3 minutes at 72 °C, cooled on ice, spun down (1 min), and loaded into the TapeStation instrument, ensuring proper alignment so that the tube containing the ladder is in position A1 on the tube strip holder. The samples were then run, and the results summarizing RNA concentrations and RNA Integrity Numbers were displayed on the TapeStation Analysis software.

3.9.8 Transcriptomics Sequencing and Data Analysis

Following quality control, all purified RNA samples were submitted to the Joint Microbiome Facility (JMF) for transcriptomics sequencing. The absence of any residual DNA contamination was confirmed via qPCR using the 16S rRNA gene targeted primers (Pjevac *et al.,* 2021; Apprill *et al*., 2015; Parada *et al*., 2016) and all RNA extracts were additionally depleted of rRNA.

Sequencnig libraries were prepared, pooled and sequenced by the JMF. Following sequencing, reads were quality filtered and trimmed and mapped to the provided *Bt* reference genome (Xu *et al.*, 2003). Mapped read pairs were then counted using featureCounts (Liao *et al.*, 2014; Overbeeke *et al.,* 2022), and a subsequent differential expression analysis was performed using the DESeq2 package (v 1.38.3; Love *et al.,* 2014; Overbeeke *et al.,* 2022) in the software R (v 4.2.2) to define the differences between the controls and small RNA-treated conditions. Databases including NCBI[2], QuickGO[3], and InterPro[4] were used to manually annotate differentially expressed genes identified in the differential expression analysis. Additional packages in the software in R, including ComplexHeatmap (v 2.14.0) were used to visualize the results of the differential expression analysis.

3.10 Primers

Table 8: List of specific primers and their sequences used throughout the study.

Primer	Primer Sequence (5'-3')	Primer Use
hsa-miR-21-5p	UAGCUUAUCAGACUGAUGUUGA	Reverse transcription of miR-21to cDNA
hsa-miR-21-5p Scramble control	GCAUAUUCGGUCGUUAUAAGAU	Reverse transcription of miR-21scramble to cDNA
hsa-miR-21-5p	UAGCUUAUCAGACUGAUGUUGA	miRNA-21 quantification using qPCR
hsa-miR-21-5p Scramble control	GCAUAUUCGGUCGUUAUAAGAU	miRNA-21 scramble quantification using qPCR
515F-mod	GTGYCAGCMGCCGCGGTAA	Amplification of the V4 region of the 16S rRNA gene
806R-mod	GGACTACNVGGGTWTCTAAT	Amplification of the V4 region of the 16S rRNA gene
H-515F-mod	GCTATGCGCGAGCTGCGTGYCAGCMGCCGCGGTAA	16S rRNA Amplicon Sequencing- First Step PCR
H-806R-mod	TAGCGCACACCTGGTAGGACTACNVGGGTWTCTAAT	16S rRNA Amplicon Sequencing- 1st Step PCR

[2] https://www.ncbi.nlm.nih.gov/data-hub/genome/GCA_000011065.1/
[3] https://www.ebi.ac.uk/QuickGO

[4] https://www.ebi.ac.uk/interpro/

4.0 Results

4.1 Live Gut Microbiota Associates with miR21

To determine if miR21 was stable in the incubation medium, and whether microbiota cells actively contribute to miR21 depletion, live and dead fecal slurry incubations (preparation detailed in methods) were set up with the addition of miR21. Samples were taken at the specified time points, the cell-rich and cell-free fractions were separated via centrifugation, and RNA was extracted from these fractions and quantified with qPCR. MiR21 concentrations were calculated using the logarithmic equation produced from a standard curve calculated using miR21 standards of known concentrations and respective Cq values determined by qPCR (Sup. Fig. 2). The samples used for standard curve generation were subjected to the same downstream processing as all incubation samples, to account for any loss in miRNA concentration during RNA extraction and cDNA synthesis. The standard curve produced a high R^2 value, indicating that the serial dilutions and qPCR analysis worked well. Additional corrections to the final standard curve equation were subsequently added to account for the changes in concentrations during downstream analysis. During total RNA extraction, the purified RNA product from the 100 μL incubation sample was eluted in 25 μL of nuclease-free water, meaning the resulting concentration was 4-fold higher. Additionally, prior to cDNA synthesis, 2 μL of the extracted RNA was diluted in 18 μL of nuclease-free water, meaning the sample was diluted 10-fold.

The calculated concentrations for the various time points analyzed were then converted to graphically depict the concentration of miR21 in the incubation vial across the various time points. Figure 5 shows these changes across the cell-free fractions of the different populations (live cells, dead cells, incubation medium). Analysis of the change in miR21 concentrations across the various supernatant (cell-free) fractions assessed by qPCR (as detailed in the methods) elucidated a significant decrease in miR21 concentration over time in incubations with live cells as compared to populations with either dead cells (ethanol fixed samples) or populations with no cells (incubation medium only) (Fig. 5). This shows a significantly larger decrease in miR21 concentration over time in the live cell incubations, which indicates some form of association between the live gut microbial cells and miR21, confirming previous observations of an association between miRNAs and gut microbiota (Liu, *et al.,* 2016). The incubation with miR21 in the presence of incubation medium alone was added as an additional control to emphasize that miR21 concentrations remain stable in medium.

In contrast, the incubation with miR21 in the presence of dead cells shows a significantly slower rate of miR21 depletion or degradation. To confirm whether ethanol fixation is an effective negative control, both live and dead fecal slurries were prepared and plated on BHI agar. If ethanol fixation is effective in killing gut microbiota and inhibiting growth, then it can be used as a control to determine whether the associations between the microbiota and miRNAs are dependent upon live cells actively taking up the miRNAs, or if these miRNAs are also able to adhere to the surface of dead cells. Following the 72-hour incubation period, the plates on which the undiluted and diluted live fecal slurries were growing exhibited a high degree of growth, with

the undiluted live fecal slurry showing the most growth. In comparison, the plates on which the dead fecal slurry was growing showed a significantly impaired growth, with both serial dilutions of the dead fecal slurry exhibiting no growth. Supplemental Figure 4 shows the pictures taken of the plates. On the plate with the undiluted dead fecal slurry (plate 4), approximately 7 colonies (5 larger colonies and 2 smaller colonies) grew during incubation. On the plates with the serial dilutions of the dead fecal slurry (plates 5 and 6), no growth is observed, suggesting that the ethanol fixation was overall effective in killing the microbial cells. This indicates that the process of ethanol fixation successfully inhibits growth of the microbiota in the fecal samples, rendering it an effective negative control.

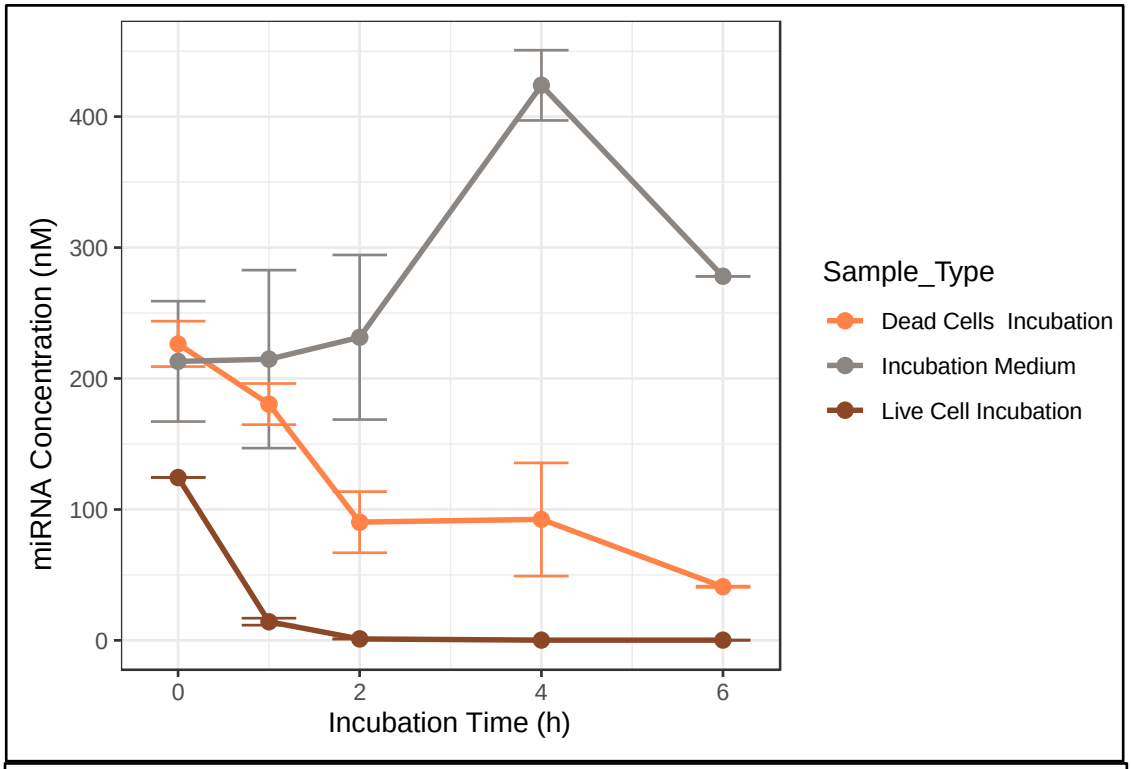

Figure 5: Change in miRNA concentration over time across the cell-free (supernatant) fractions of different incubations. Incubations with ethanol-fixed/dead cells are indicated in orange, incubations with live cells are indicated in brown, and incubations in incubation medium alone is indicated in grey. The change in miRNA concentration was calculated to reflect the percent of the starting concentration (measured at T0) remaining in the sample at the different time points.

4.2 Association of the Gut Microbiota with miRNAs is Non-specific

In order to investigate whether the dynamics of associations between miRNAs and gut microbiota are sequence-dependent, an additional incubation experiment was set up using miRNAs with different sequences. All incubations were prepared in duplicate using freshly collected fecal samples from 3 different donors. Similar to the previous experiment, incubations with live and dead bacterial cells (derived from the fecal samples) were set up with the addition of miR21. As an additional control, another set of incubations were amended with miR21 scramble, which contains the same nucleotides as miR21 but arranged in a different order.

MiR21 and miR21 Scramble concentrations were calculated using the logarithmic equations produced from the miR21 (Sup. Fig. 2) and miR21 scramble (Sup. Fig. 3) standard curve graphs. The same changes in concentration during RNA extraction and cDNA synthesis were accounted for in the calculation of the miR21 scramble concentrations. The standard curve produced a high R^2 value, indicating that the serial dilutions and qPCR quantification also worked well for the miR21 scramble control. Figure 6 summarizes the differential association between live and dead cells with either miR21 or the miR21 Scramble control.

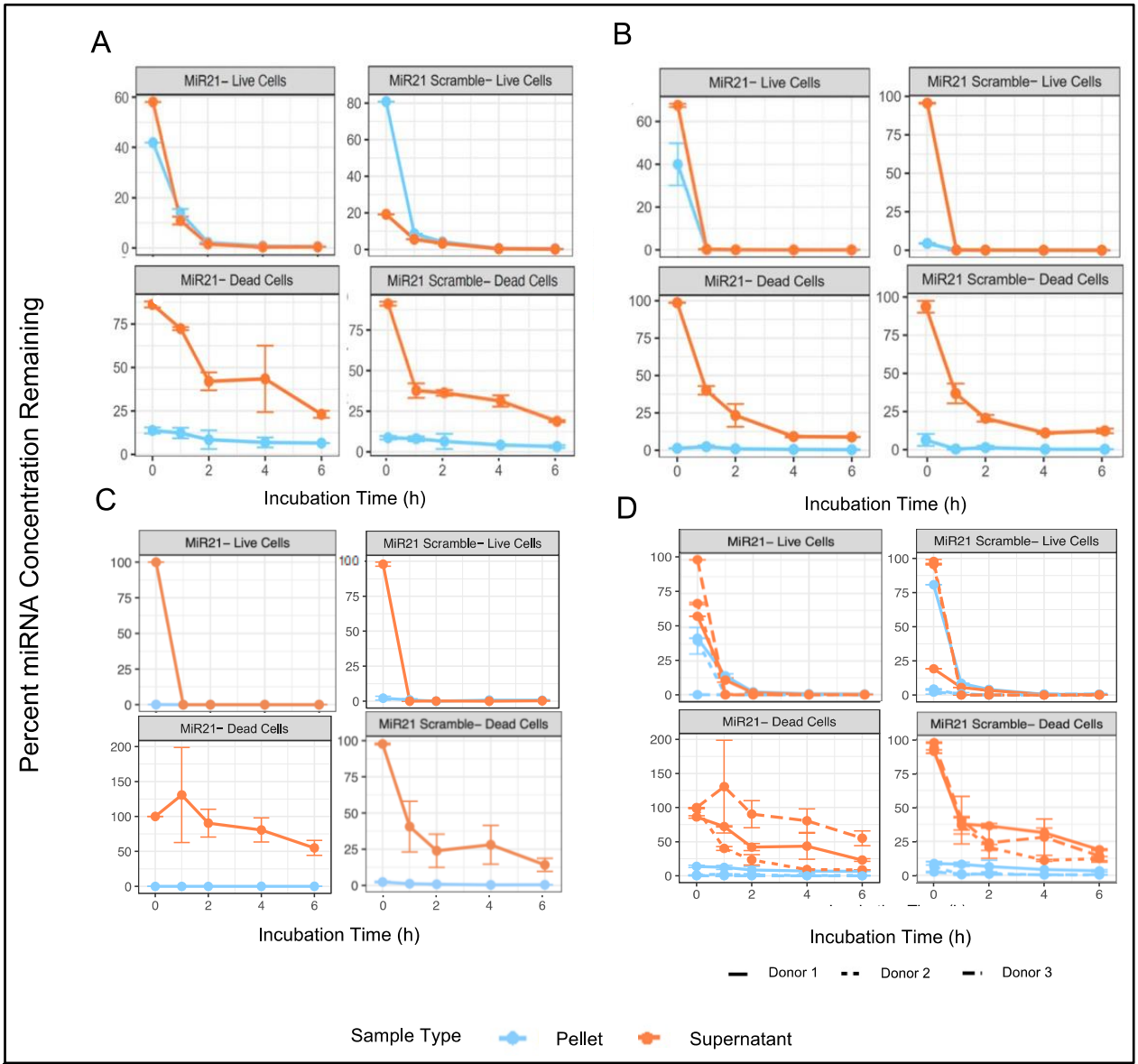

Figure 6: Percent of total miRNA concentration remaining over time in fecal slurry incubations from 3 different donors. Fecal slurry incubations were set up and amended with either 250 nM miR21 or 250 nM miR21 Scramble control and sampled at various time points. Figures 6A-6C summarize the percent of total miRNA concentration remaining in the cell-rich/pellet (blue) and cell-free/supernatant (orange) fractions of fecal slurries over time from Donor 1 (A), Donor 2 (B), and Donor 3 (C). Figure 6D shows the percent of total miRNA concentration remaining over time in all 3 different donors, with each donor represented by line style. The total miRNA concentration was defined as the sum of the miRNA concentrations in the pellet and supernatant fractions at time point T0.

Overall, there was no significant difference in the associations between microbiota cells and miR21 versus the miR21 scramble control, indicating that miR21 and miR21 scramble have similar dynamics. In most cases, most of the miRNA association occurred within the first 2 hours of incubation, as seen by the significant drop in percent of total miRNA concentration between time points T0-T2. Additionally, the percent of total miRNA concentration decreased more gradually in dead cells compared to live cells, suggesting that live cells associate more with the miRNAs. Lastly, changes in miRNA concentrations followed similar patterns in both the cell-free (supernatant) and cell-rich (pellet) fractions. Figure 6A-C summarize the change in miRNA concentration overtime in live and dead (ethanol-fixed) fecal slurry incubations from samples from 3 separate donors. Figure 6D summarizes the results of all 3 donor experiments to emphasize the overall similarity in miRNA dynamics across all 3 experiments. The standard curves used for calculating miR21 and miR21 scramble concentrations (equations previously defined) can be found in the supplemental material section of this study. In the case of donor 1, all samples fell within the points of the standard curve. However, in the case of donors 2 and 3, some samples fell outside of this standard curve. In these cases, the standard curve equation was extrapolated to calculate the miRNA concentration in those samples.

4.3 Association of the Gut Microbiota with miRNAs is Independent of RNase Activity

To determine if this disappearance of miRNA over time was simply due to RNase activity in the incubations, fecal slurry incubations with miR21 were set up again, this time with amendment of an RNase inhibitor. Based on the results from the first set of incubations, the sampling time points were adjusted so that they were shorter and more frequent. The time points chosen for these incubations were T0, T0.5, T1, T1.5, T2 and T4. In this set of incubations, the live and dead fecal slurries were prepared using the same procedure as the previous incubations (Methods 3.3.1) with a freshly collected fecal sample from a single donor. However, rather than including a water control in this set of incubations, an RNase inhibitor amendment was included (using the live fecal slurry), to investigate the potential affect that RNases have on the concentration of miRNAs in the incubations. The cell-rich and cell-free fractions were separated in the anaerobic chamber via centrifugation, and only the cell-rich (pellet) fractions (after washing) were used for downstream analysis.

The RNase inhibitor used in these experiments has been reported to effectively inhibit RNase A, B and C but not effectively inhibit other RNases (I, T1, T2, H, U1, U2 or CL3), including bacterial RNAses[5]. The RNase inhibitor amendment had no significant impact on the change in miR21 concentration over time in the cell-rich fractions. However, additional studies using other RNase inhibitors that inhibitor a wider range of bacterial or host-secreted RNases would need to be performed in order to definitively confirm whether these microbiota-miRNA associations occur in an RNase-independent manner. Figure 7 depicts the percent of total miRNA remaining in incubations with live cells and miR21 with and without the addition of an RNase inhibitor across the various time points. Another set of miR21 standard serial dilutions was produced for this

[5] https://www.thermofisher.com/at/en/home/life-science/dna-rna-purification-analysis/rna-extraction/rna-extraction-products/rnase-inhibitors.html

experiment, and since no significant deviation in average Cq value was observed, the same standard curve and logarithmic equation produced from the previous incubation experiment were used to calculate miR21 concentrations (see 4.2 and Sup. Fig. 2). The same changes in concentration during downstream analysis were accounted for in these calculations.

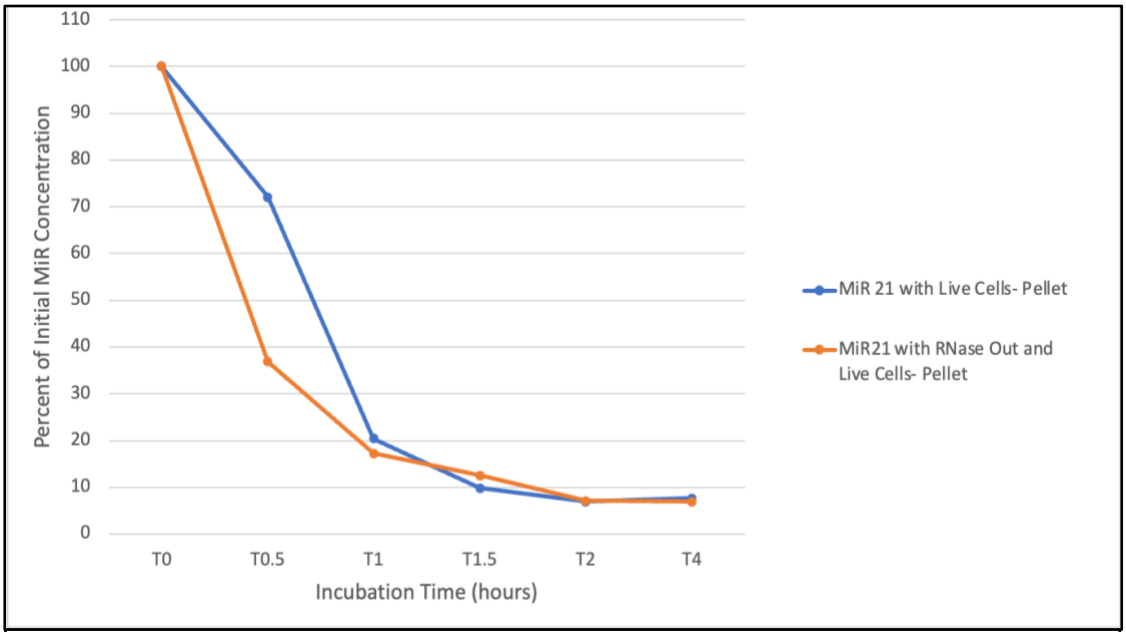

Figure 7: Percent of total miRNA concentration remaining over time in live cell incubations with miR21 versus miR21 in combination with an RNase Inhibitor. The total miRNA concentration was defined as miRNA concentration measured T0.

4.4 Bacterial Communities that Associate across the miRNA-positive gates compared to miRNA-negative gates, irrespective of miRNA sequence

In order to gain deeper insight into miRNA-microbiota associations, fluorescence activated cell sorting of fecal slurry incubations with different fluorescently labelled miRNAs was performed, in order to understand whether different miRNAs associate with distinct bacterial communities. Fluorescently labelled miRNAs were tagged with an Atto488 fluorophore so that miRNA-associated cells could be identified and sorted. Thus, Atto488-positive (Atto488+) fractions are the miRNA-associated fractions, whereas Atto488-negative (Atto488-) fractions are the miRNA-negative fractions. To visualize similarities or variations in the compositions of ASVs associating with the different FACS sorted fractions, β diversity analyses was performed. Figure 8A shows the principal coordinate analysis plot (PcoA) of all FACS sorted fractions in incubations with either miR21 or miR21 scramble created using Bray Curits distances, at the ASV composition level. The plot additionally includes the 3 different donors' samples to show how individual donor community compositions compare to the different sort populations. Figure 8B is a dendrogram representing the hierarchical clustering of the different populations.

Both the PcoA plot and the dendrogram highlight that the different FACS sorted fractions cluster together based on sort population, rather than what miRNA was supplemented in the

incubations. This is evident by all Atto488+ gates (shown in blue) clustering together, while all Atto488- gates (shown in purple) cluster together, regardless of miRNA added (represented by the marker shape). This supports the trends identified in the relative abundance plots (Fig. 9), which showed more inter-gate differences in relative abundance at the family level, as opposed to intra-gate variability. Additionally, these plots highlight that the supplementation with miRNAs has a greater impact on the composition of the bacterial community as opposed to the sequence of the miRNA itself. This is confirmed by the differential abundance analysis, which concluded that only a single ASV was significantly depleted in the presence of miR21, when compared to the incubations with miR21 scramble. Additionally, this is in line with results from the previous incubations experiments with different miRNAs (section 4.3), which showed that associations between bacteria and miRNAs in the gut are not sequence dependent.

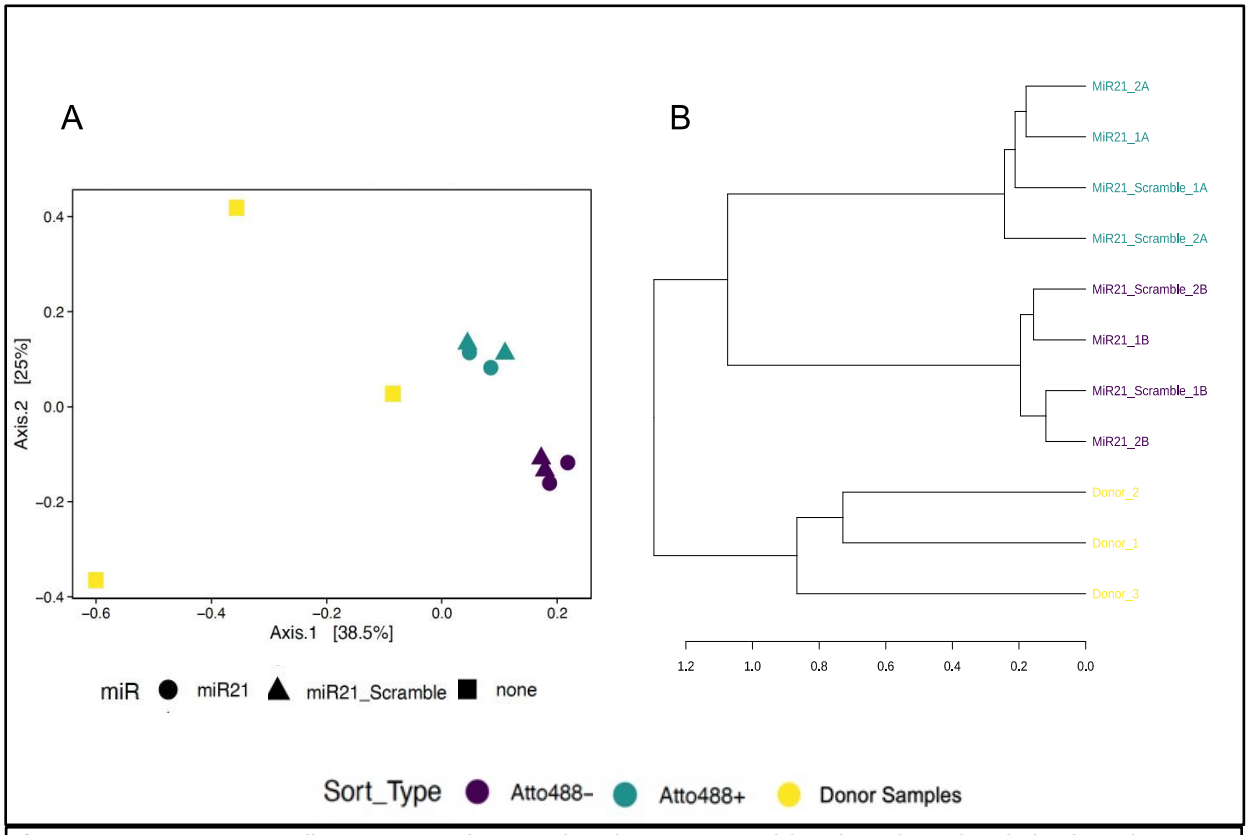

Figure 8: 16S rRNA amplicon sequencing results of FACS sorted fractions from fecal slurries of 3 donors combined. (A) Principal coordinate analysis (pCoA) based on Bray Curtis distances summarizing the β-diversity of the analyzed FACS sorted fractions associating with different miRNAs. The miRNA with which the samples were incubated is represented by shape, while the FACS sorted fraction is indicated by color. (B) Dendrogram summarizing the hierarchical clustering of the different FACS sorted fractions associating with different miRNAs. The different FACS sorted fractions are indicated by color. All fractions were sorted from the combined fecal samples of three different donors.

Figure 9 compares the relative abundance of FACS sorted fractions from incubations with miR21 versus miR21 scramble. The panel labelled “Donors” summarizes the relative abundance at the family level of the bacterial communities present in the 3 different donors, whose fecal samples were mixed and subsequently used for the fecal slurry incubations in all

FACS experiments. For the 3 donors' samples, an aliquot was collected from each donor fecal sample (prior to combining all samples), and DNA was extracted and subsequently submitted for sequencing along with all other extracts from the FACS sorted fractions, meaning the donors samples were not subjected to sorting. Fecal samples used for the previous miRNA incubation experiments (descried in section 4.3) were collected from these same 3 donors, to avoid variability in microbial communities across the different experiments throughout the study.

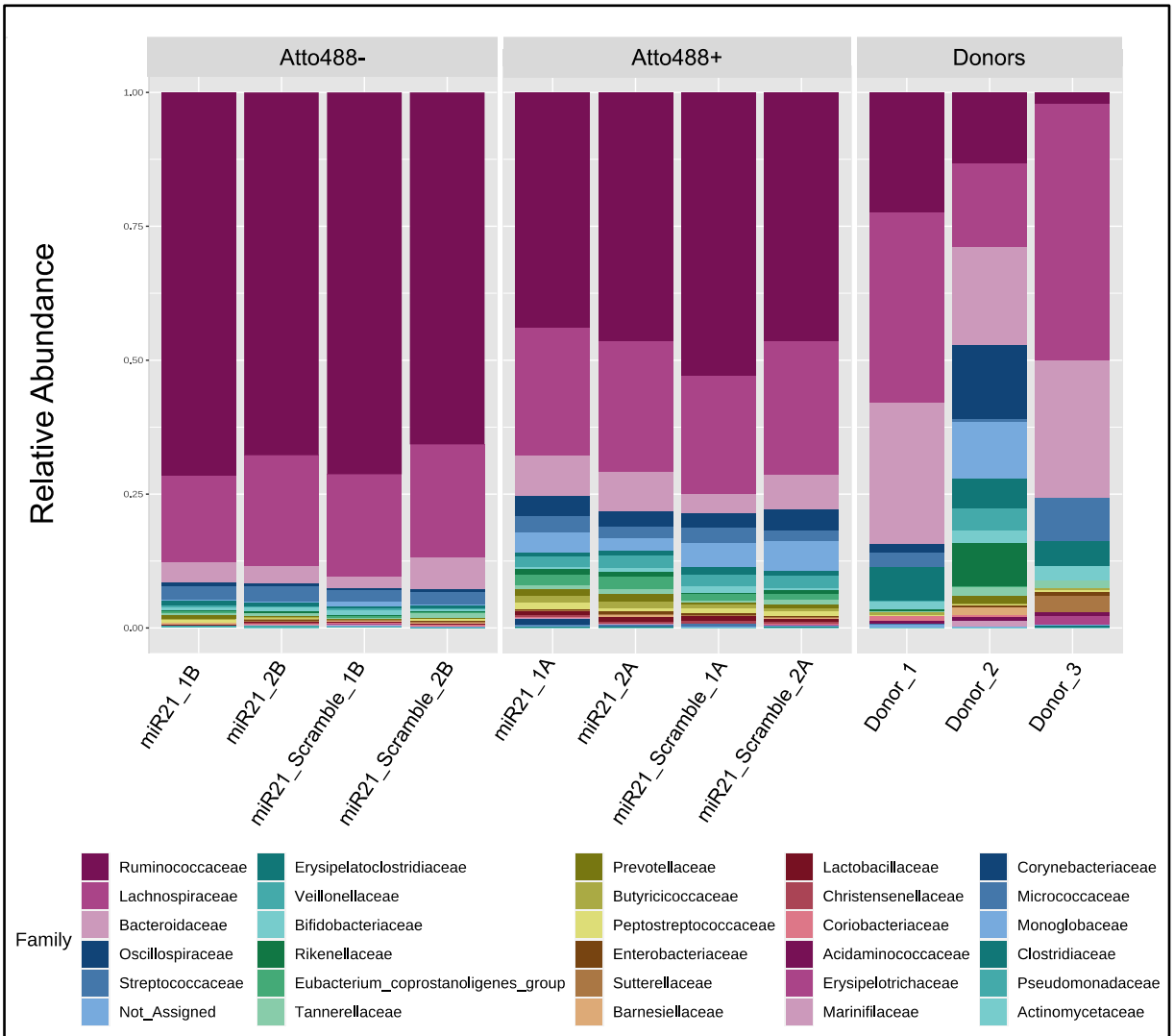

Figure 9: Relative abundance of bacteria populations interacting with either miR21 or miR21 scramble in FACS sorted fractions from the fecal samples of 3 different donors. The "Donors" panel shows the relative abundance of bacteria in each individual donor, but samples from all donors were combined for all FACS experimentation.

To assess whether a unique bacterial community associates with different miRNAs, the relative abundance of bacteria at the family level was analyzed across the different FACS sorted fractions and compared to the community of the 3 different donors. Figure 9 summarizes the relative abundance of bacterial communities at the family level in Atto488+ (meaning miRNA

Associated) FACS sorted fractions (Atto488+) versus Atto488- (meaning miRNA negative) FACS sorted fractions. The different FACS sorted populations and respective gating strategies are summarized in Supplemental Figure 5. In all FACS sorted fractions, the dominant bacterial family is *Ruminococcaceae*, followed by *Lachnospiraceae*. This differs slightly from the bacterial communities present in the 3 donors, where *Lachnospiraceae* is the dominant bacterial family, followed by *Bacteroidaceae* and *Ruminococcaceae*. All Atto488- FACS sorted fractions have a similar relative abundance at the family level, with no significant differences across incubation type. This same pattern is also noticed across all Atto488+ FACS sorted fractions. When comparing FACS sorted fractions at the family level, there is an increased abundance of *Ruminococcaceae* in Atto488- FACS sorted fractions. Conversely, there is a larger abundance of the family *Bacteroidaceae* in Atto488+ FACS sorted fractions. However, these observations must be confirmed through other forms of analysis, as relative abundance does not accurately reflect the absolute abundance of the different bacterial communities.

To confirm which bacteria are specifically enriched or depleted across different FACS sorted fractions from fecal slurry incubations with different miRNAs, differential abundance analysis was performed. Figure 10 summarizes which bacteria, at the genus level, are significantly ($p<0.05$) enriched or depleted across all miRNA-positive FACS sorted fractions (irrespective of miRNA sequence) versus all miRNA-negative FACS sorted fractions. Overall, there are a wide array of ASVs significantly enriched and depleted in the miRNA-associated fractions, indicating that several taxa are capable of associating with miRNAs. At the phylum level, predominantly *Firmicutes* and some *Bacteroidota* ASVs were enriched in the presence of miRNAs. In contrast, all ASVs belonging to either the *Actinobacteriota* or *Proteobatceria* phyla that were observed to be differentially abundant were significantly depleted in the miRNA-associated fractions. These observations indicate that *Firmicutes* and *Bacteroidota* may preferentially associate with miRNAs. Additionally, some *Firmicutes* ASVs and one *Bacteroidota* ASV were significantly depleted in miRNA-positive fractions. At the family level, one or more ASVs belonging to *Aeromondaceae*, *Coriobacteriacea*, *Pseudomonadaceae* and *Yersiniacea* families were depleted in miRNA-positive fractions, whereas *Butyricicoccacea*, *Christensenellaceae*, *Lactobacillaceae*, *Oscillospiraceae*, *Rikenellaceae* and *Veillonellaceae* were all enriched in miRNA-positive fractions. The family *Bacteroidaceae* was observed to be both significantly enriched and depleted in miRNA-positive fractions, indicating that miRNAs may be selectively interacting with specific *Bacteroides* species (Fig. 10). At the species level, *B. cellulosilyticus/intestinalis/timonensis* and *B. uniformis* were both significantly enriched in the miRNA-positive gates, whereas *B. finegoldii* was significantly depleted in the miRNA-positive gates. Other bacterial families including *Lachnospiraceae* and *Streptococcaceae* were also found to have varying abundances in miRNA-positive gates, with some ASVs being enriched while others were depleted.

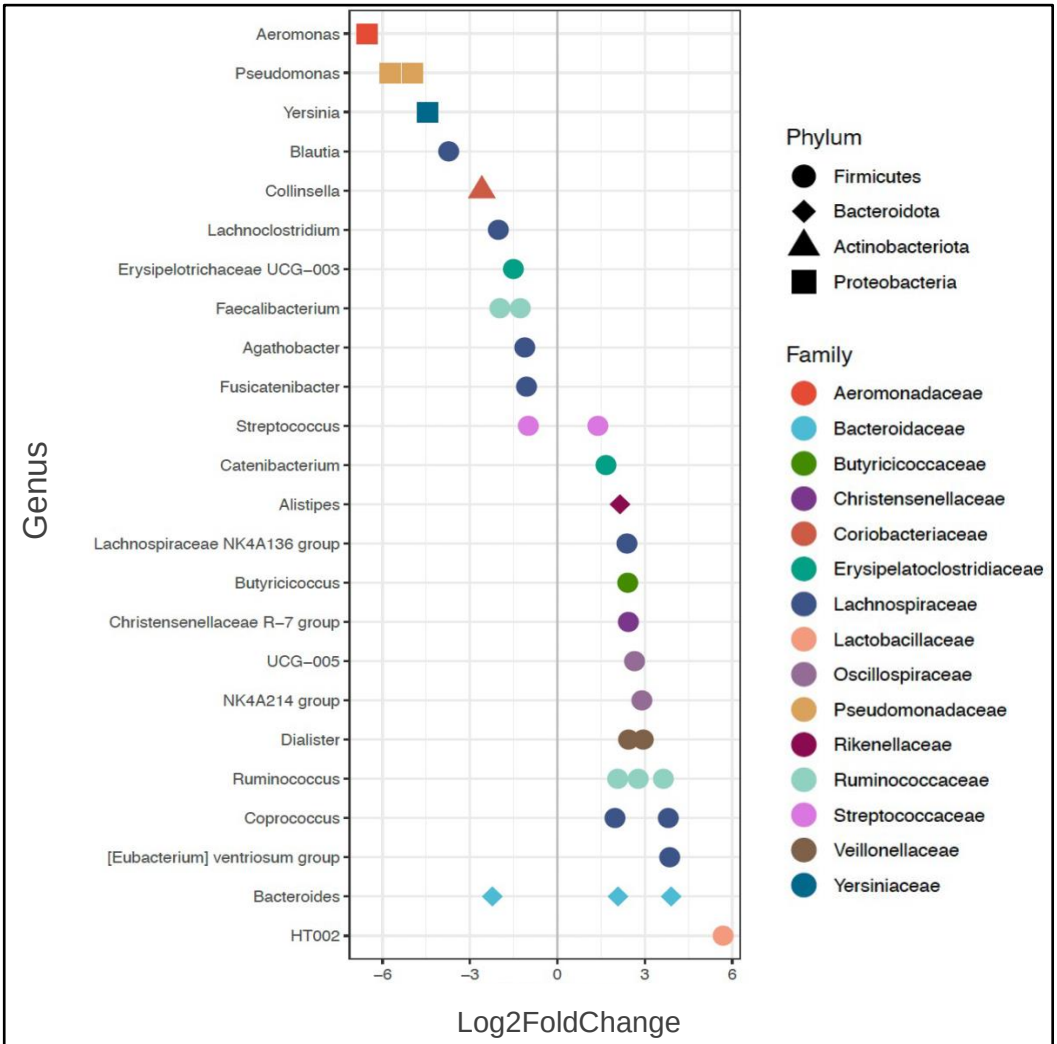

Figure 10: Differential abundance analysis of bacterial populations of FACS sorted fractions. The above figure summarizes all ASVs whose abundance significantly differs across miRNA-positive gates compared to miRNA-negative gates, regardless of sequence. Each dot represents a different ASV, grouped by genus (y-axis), family (color), and phylum (shape). The x-axis represents the log2 fold change in expression of the respective ASV across treatments. All differential abundance analysis was performed using the Phyloseq and DESeq2 packages in R, and all ASVs passed a threshold of significance with an adjusted p-value of .05 or less. All fractions were sorted from the combined fecal samples of three different donors.

To better understand any sequence-specific influences on bacterial abundances across the different incubations, differential abundance analysis was performed, this time focusing on the differences in the relative abundances of ASVs within communities identified in the miRNA-positive FACS sorted fractions versus miRNA-negative FACS sorted fractions from fecal slurry incubations supplemented with either miR21 or miR21 scramble separately. Figure 11 summarizes the sequence-specific changes in bacterial communities in the presence of either miR21 scramble (Fig. 11A) or miR21 (Fig. 11B), analyzed separately. Overall, supplementation

with miR21 resulted in more variations in the miRNA-associating bacterial community, as shown by a significantly larger number of differentially abundant ASVs in the fractions associating with miR21 compared to those associating miR21 scramble. At the phylum level, *Firmicutes* showed most significantly different associations, with several ASVs having varying abundances across the different incuations. In contrast *Bacteroidota* showed more variation across the different incubations, indicating that this phylum may be more sensitive to miRNA supplementation. In incubations supplemented with miR21 scramble, *B. finegoldii* was depleted, whereas *B. uniformis* was enriched in incubations supplemented with miR21.

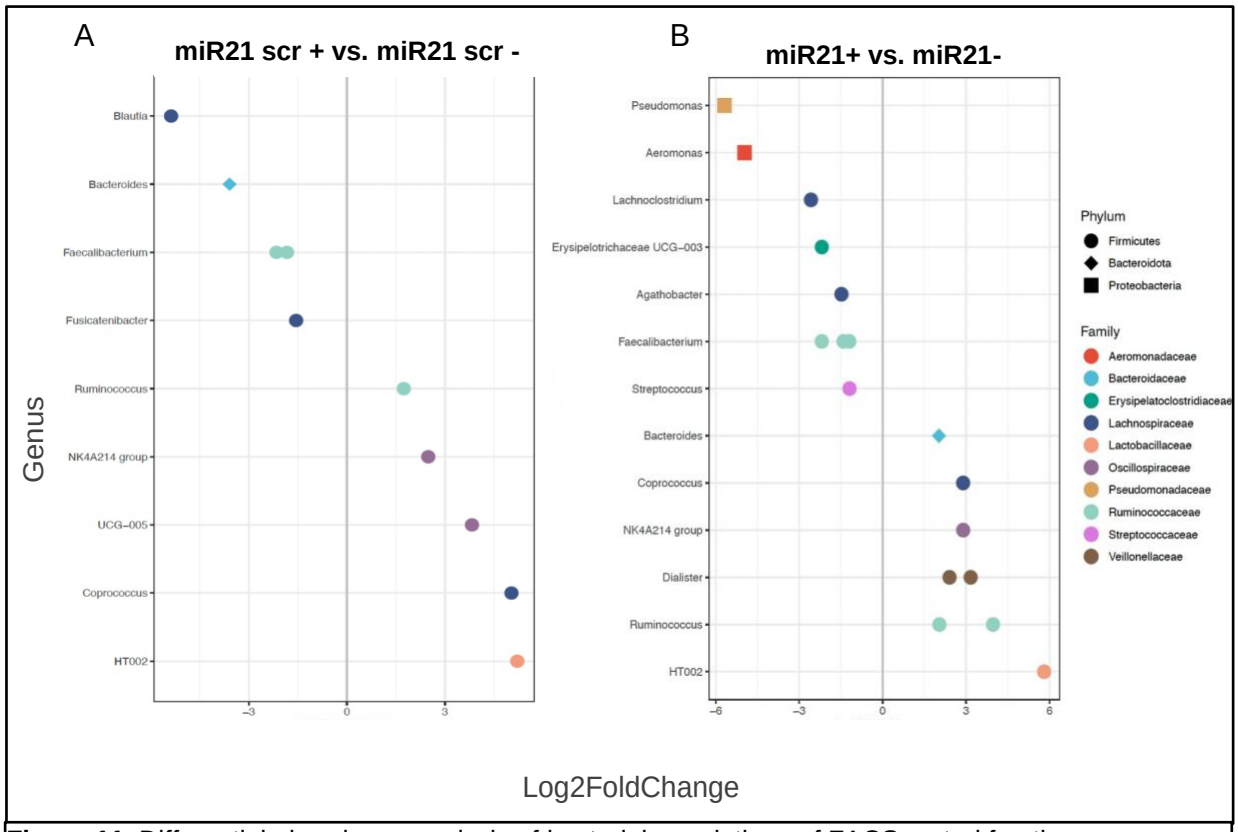

Figure 11: Differential abundance analysis of bacterial populations of FACS sorted fractions associating with different miRNAs. Panel A summarizes all ASVs whose abundance significantly differs in the presence of miR21 scramble, while panel B summarizes all ASVs whose abundance significantly differs in the presence of miR21. Each dot represents a different ASV, grouped by genus (y-axis), family (color), and phylum (shape). The x-axis represents the log2 fold change in expression of the respective ASV across treatments. All differential abundance analysis was performed using the Phyloseq and DESeq2 packages in R, and all ASVs passed a threshold of significance with an adjusted p-value of .05 or less. All fractions were sorted from the combined fecal samples of three different donors.

Differential abundance analysis was additionally performed to identify any ASVs specifically enriched or depleted in miRNA positive gates sorted from incubations with miR21, compared to miRNA positive gates sorted form incubations with miR21 scramble control. Only a single ASV, identical to *Ruminococcus bromii*, was identified to be depleted (log2FC= -1.75) in the presence of miR21, indicating that miRNA sequence has a minimal impact on the bacterial community. All

significant differentially abundant ASVs across all miRNA incubations mentioned in section 4.5 are summarized in Supplemental Tabl.

4.5 Supplementation of miRNAs Significantly Boosts Bacteroides thetaiotaomicron Growth in Pure Culture

After analyzing which bacteria are associating with miRNAs, *B. thetaiotaomicron* (*Bt*) was selected for additional experiments to understand the impacts of miRNA supplementation in pure culture. The 16S rRNA amplicon sequencing results elucidated that *Bacteroides* species were sensitive to miRNA supplementation, and *Bt* is a very well-studied commensal in the gut. Additionally, previous experimentation has demonstrated that *Bt* can associate with miRNAs, specifically with miR21. For these reasons, this specific strain of *Bacteroides* was selected for *in vitro* growth experimentation and subsequent transcriptomic sequencing analysis. For all pure culture growth experiments, an additional small noncoding RNA control was included to confer whether any observable effects on *Bt* growth are specific to miRNA supplementation, or if the same effect is observed when the culture medium is supplemented with any small RNAs. Overall, supplementation with miRNAs resulted in a significant boost in *Bt* growth compared to no amendment. The amendment of the miR21 scramble control caused the largest boost in *Bt* growth compared to all other conditions, including miR21.The amendment of the small RNA control additionally resulted in a significant increase in growth, albeit lesser than that resulting from supplementation with both miRNAs. Therefore, it cannot be determined if this boost in growth is a unique result of miRNA supplementation or if *Bt* is able to utilize any RNAs to boost growth. Figure 12 shows the different growth curves of the various pure culture incubations amended with the different small RNAs or water control (Fig. 12A), as well as the respective area under the curve (AUC) calculations used to assess overall differences in growth across the different incubations (Fig. 12B). Statistical significance was calculated using a t-test, comparing the different amendments to the incubation with no amendment (water control).

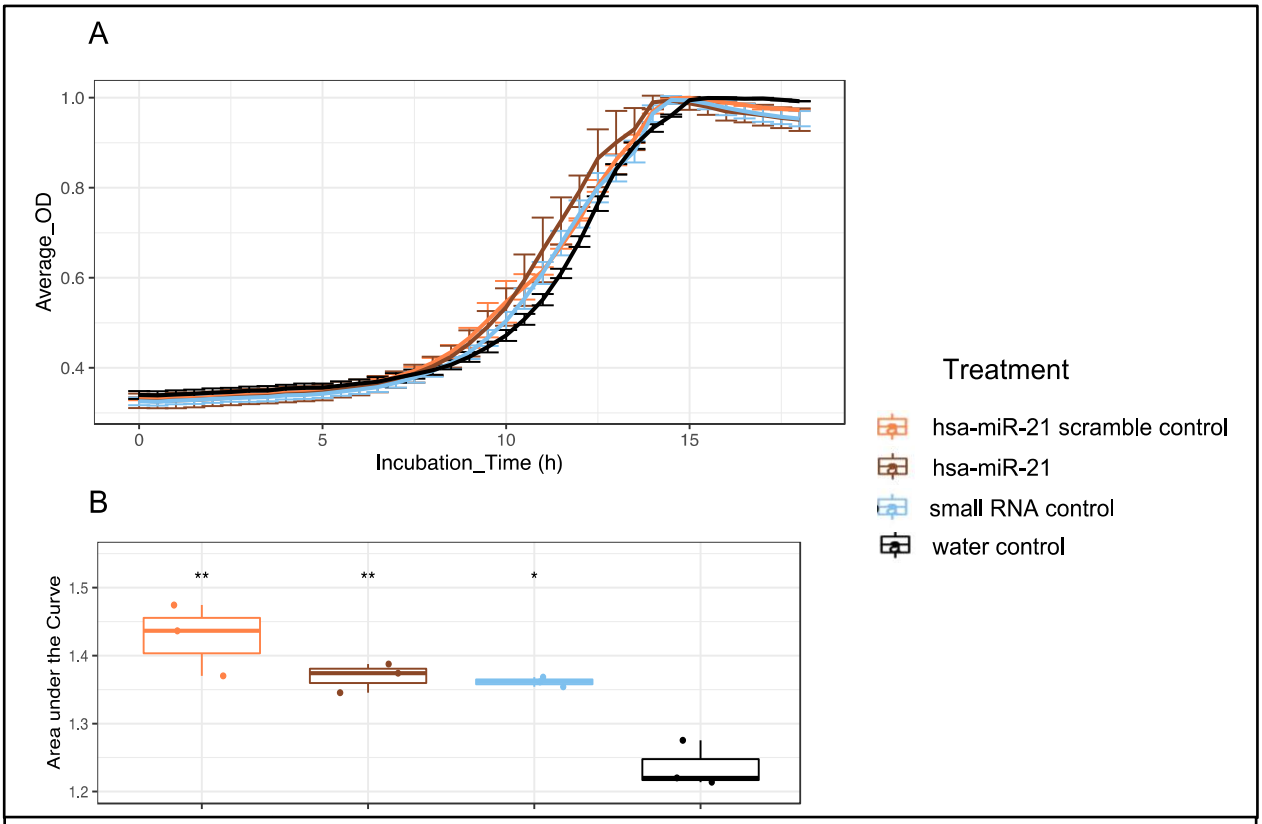

Figure 12: Impact of supplementation with small RNA molecules on *B. thetaiotaomicron* growth. (A) Growth of *B. thetaiotaomicron* in Bacteroides Minimal Media (BMM) in the presence of miR21 (brown), miR21 Scramble (orange), a small RNA control (blue) and no amendment (black). All incubations were set up and grown in triplicate, with the respectively colored line representing the average of all replicates. Growth patterns were observed for 18 hours, with optical density (600 nm) measurements recorded every 30 minutes. (B) Bacterial growth in the presence of the various small RNA molecules was quantified by calculating the area under the curve (AUC) under each respective growth curve. Statistical significance was calculated using a t-test comparing the means of the AUC of the water control versus the AUC with the different small RNA treatments.

4.6 MiR21 Significantly Downregulates Gene Expression in Bacteroides thetaiotaomicron

Following *in vitro* growth analysis, similar pure culture incubations with *Bt* were set up and transcriptomic sequencing was performed to elucidate any impacts that miRNAs have on bacterial gene expression. All incubations (in triplicates) were grown until exponential phase before supplementation with the various miRNA treatments and controls and collected for RNA extraction after 1 hour of incubation. The same small RNA control was included in this experiment as an additional control for any baseline impacts that small RNA molecules have on *Bt* gene expression. TapeStation analysis, which performs automated electrophoresis for sample quality control, was performed on all samples to measure the RNA Integrity Number (RIN). All samples successfully passed quality control, except for the third water triplicate which had the lowest RIN of all samples (6.5). Because of this, only 2 water replicates were included

in downstream analysis, while all three replicates were included for the remaining treatments. Transcriptomic sequencing was performed and differential expression analysis was performed using the DESeq2 package in R (v 1.38.3; Love *et al.,* 2014).

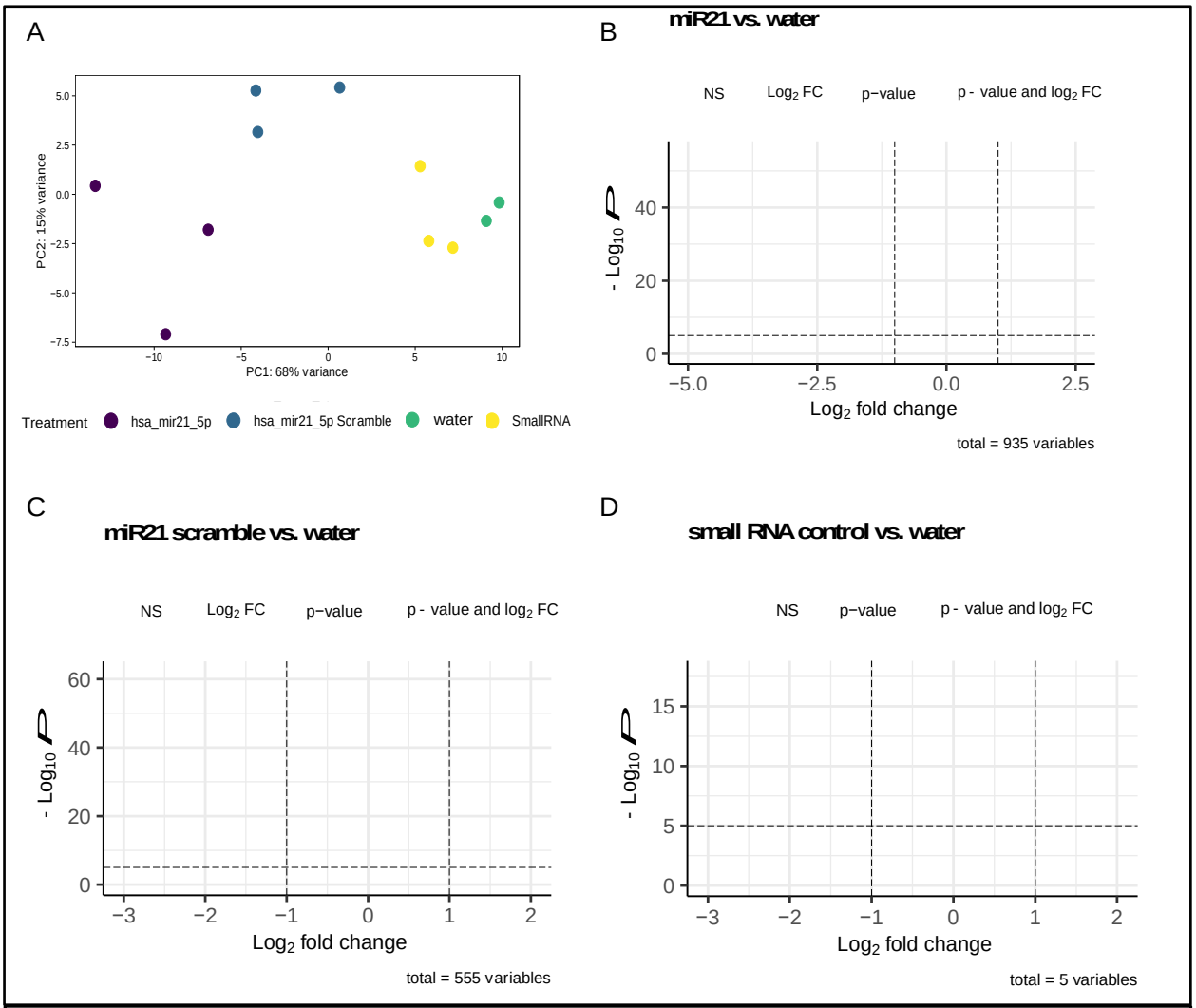

Figure 13: Transcriptomic sequencing results of *B. thetaiotaomicron* in pure culture supplemented with small RNA molecules. (A) Principal coordinate analysis (pCoA) based on Bray-Curtis distances summarizing the β-diversity of the analyzed samples incubated with different small RNA molecules. The different small RNA molecules (treatments) are represented by color. (B-D) Volcano plots representing the upregulated and downregulated differentially expressed genes (DEGs) in *B. thetaiotaomicron* incubated with miR21 and the water control (B), miR21 scramble and the water control (C), and the small RNA control and the water control (D). In all volcano plots, the x-axis represents the log2fold change and the y-axis represents -log10 (adjusted p values). All DEGs were identified and analyzed using the DESeq2 package in R. DEGs represented by a green dot have a log2 fold change with an absolute value greater than or equal to 1, all DEGs represented by a blue dot have an adjusted p-value of .05 or less and are differentially significant, and all DEGs represented by a red dot have both a log2 fold change with an absolute value greater than or equal to 1 and are differentially significant.

B-diversity analysis was performed to compare the transcriptomic profiles across all different treatments, and the PcoA plot (based on Bray Curtis distances) in Figure 13A visually

represents this. Both the water control and the small RNA control cluster together, away from both miRNA treatments, indicating that the transcriptomic profile induced by miRNA supplementation is unique from that induced by the small RNA control. Additionally, it highlights the similarity between gene expression profiles of the water control incubation and the small RNA control incubation, which supports the results of the differential expression analysis identifying only 3 DEGs in the small RNA control compared to the water control. All 3 replicates from each respective miRNA treatment cluster together, signifying an overall similarity across transcriptome profiles of the different replicates. This additionally highlights that miR21 and miR21 scramble have unique impacts on the *Bt* transcriptome, as both clusters of replicates from the different miRNA treatments cluster separately.

Differential expression analysis effectively identified all significantly differentially expressed genes across the different treatments (miR21, miR21 scramble and small RNA control) compared to the water control, and these results are summarized in the volcano plots in Figure 13B-D. Supplementation with miR21 had the greatest impact on the *Bt* transcriptome, as evident by 185 differentially expressed genes (DEGs) identified in the miR21 incubation compared to the incubation with water (Fig. 13B). Supplementation with miR21 scramble yielded 63 DEGs compared to the water control (Fig. 13C), whereas supplementation with the small RNA control only showed 3 observable DEGs compared to the water control (Fig. 13D).

In order to effectively analyze the myriad of DEGs induced by miRNAs compared to the water control, a threshold of a log2 fold change greater than or equal to the absolute value of 1 was applied as a filter to the DEGs visualized in Figures 13B-D. These results and the functional annotations of the identified DEGs can be found in Supplemental Tables 1-3. Figure 14A summarizes all these genes significantly upregulated or downregulated in the presence of a small RNA molecule (miR21, miR21 scramble, and small RNA control) compared to the water control. All genes depicted in Figure 14A have a log2 fold change greater than or equal to 1 or less than or equal to -1, with a p-value of 0.05 or less. Of the 185 genes differentially expressed in the presence of miR21, 49 are also differential expressed in the miR21 scramble incubation as well, and these 49 DEGs represent the overall impact that miRNA supplementation has on the gene expression profile of *Bt*. This finding that supplementation with either miR21 or miR21 scramble control downregulates several genes in *Bt* supports previous research that suggests miRNAs control gene expression through degradation of bacterial mRNA (O'Brien et al., 2018). While several of these down-regulated, miRNA-specific genes are uncharacterized, many of them encode for DNA binding proteins, ribosomal proteins, transcriptional regulators and transfer RNAs (tRNAs) (Sup. Tables 1-2).

4.7 MiR21 Significantly Induces Differential Expression of Several Gene Clusters

The heatmap of DEGs in Figure 14A also highlights a cluster of genes that are upregulated in the presence of miR21. Following gene annotation, this gene cluster was identified with high confidence as the gene operon encoding the various enzymes involved in the L-tryptophan and Indole biosynthesis pathway. These genes can be identified with the Gene IDs BT0527- BT0533 and are all significantly upregulated in the presence of miR21 compared to all other conditions

(Fig. 14B), highlighting the specific effect that supplementation with miR21 has on this pathway. Several other groups of sequential genes from the same strand, referred to as gene clusters, were identified to be differentially expressed in the presence of miR21 compared to all other treatment conditions (Fig. 14B), but this gene cluster controlling L-tryptophan and Indole synthesis is the only cluster in which all genes are consistently significantly upregulated by miR21. All other gene clusters are predominantly down-regulated by miR21. An additional gene cluster was found to be exclusively upregulated in the presence of miR21 compared to miR21 scramble but not identified as differentially expressed in any other conditions, including the small RNA control (Fig. 14C). This gene cluster (BT1883-BT1886) was identified to potentially have an RNA-related role. No significant difference in expression of this gene cluster is observed in the miR21 treatment compared to either the small RNA control or the water control.

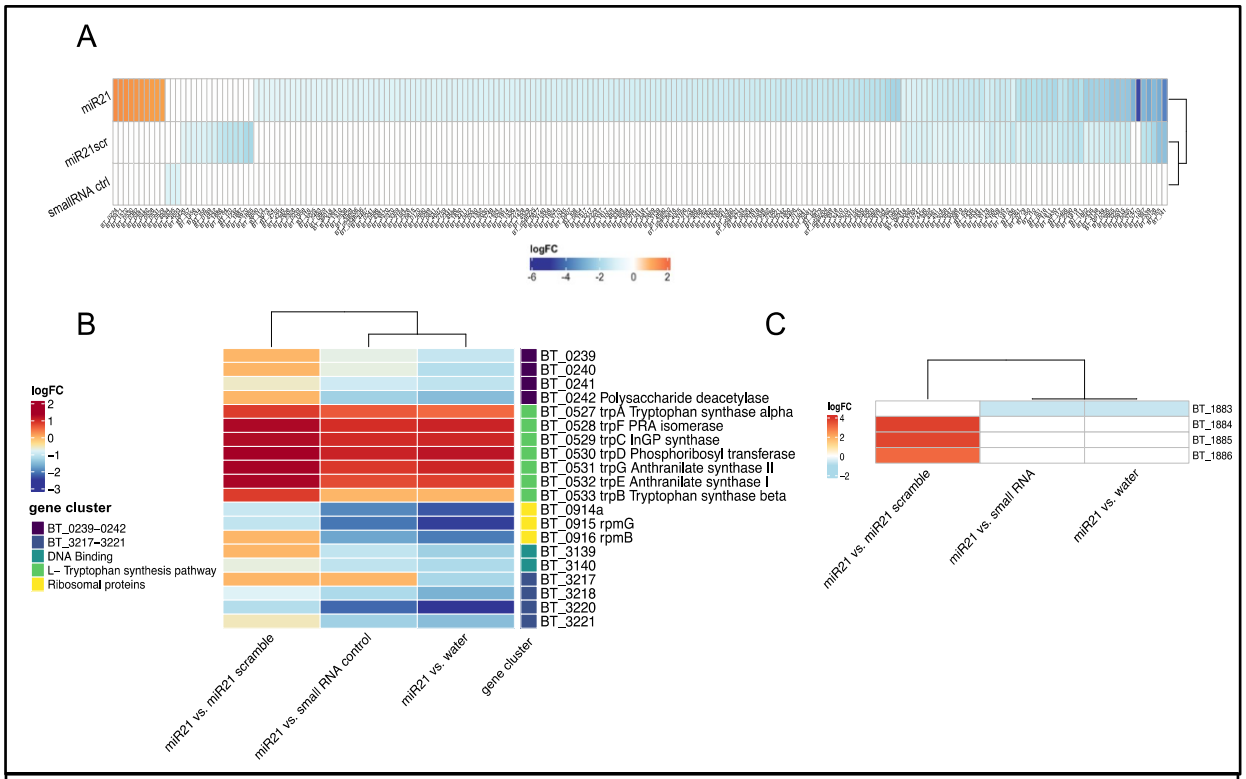

Figure 14: Summary of genes significantly differentially expressed in *B. thetaiotaomicron* when grown in pure culture with different small RNA molecules. (A) Heatmap showing all differentially expressed genes (DEGs) between all small RNA treatments and the water control with a log fold change absolute value greater than or equal to 1. (B) Heatmap summarizing entire gene clusters differentially expressed in the presence of miR21 compared to all other treatments. (C) Heatmap highlighting the fold change in expression of the BT_1883-BT_1886 gene cluster in the presence of miR21 compared to all other treatments. (A-C) All DEGs were identified and analyzed using the DESeq2 package in R, and all heatmaps contain DEGs that meet the significance with an adjusted p-value of 0.05 or less.

5.0 Discussion

5.1 MiRNA Association Experiments with miR21 and miR21 scramble mimics Reveals a Strong Association between Live Gut Microbiota and miRNAs that is Non-specific

Although studies have previously shown that miRNAs are present in the gut and play a role in the regulation of gut microbiota diversity and the development of pathogenic phenotypes in the host, there are still many outstanding questions regarding the specific intricacies of these microbiota-miRNA associations. In the first part of this study, we aimed to investigate distinctive dynamics behind host microbiome associations with miR21 and a miR21 scramble control. Both live and ethanol-fixed (dead) fecal slurries were prepared to understand if miRNAs are only taken up and/or degraded by live microbiota cells or if miRNAs can still associate or adhere to the surface of dead cells. MiR21 was incubated alone in incubation medium to measure its relative stability over time. Any variability in miR21 concentrations measured at the selected time points could be attributed to the presence of RNases in the incubation medium or to the fact that RNAs are relatively unstable molecules and degrade rapidly. MiR21 was found to be relatively stable in incubation medium alone, especially compared to when it is added to incubations with live cells. It was also confirmed that there is an association between live gut microbiota cells and miR21 that does not occur in the amendment with killed gut microbiota cells. To confirm whether this association between the host gut microbiota and miRNAs is sequence specific, either miR21 or a miR21 scramble control were added to incubations set up using both live and dead fecal slurries. No significant difference of change in concentration was observed between incubations with miR21 and those with miR21 scramble, suggesting that the dynamics of miR21 and miR21 scramble are very similar. These results contradict with those of a previous study in which *E. coli,* cultured in the presence of fluorescently labelled miRNAs and their scrambled controls, exhibited a significantly lower degree of co-localization with hsa-mir-1226-5p scramble compared to hsa-mir-1226-5p (Liu, *et al.*, 2016).

In order to confirm these observations and test for interindividual variability (as each individual has a distinct microbiome), this experiment was also performed with fecal samples from two additional donors (Fig. 6B-C). Overall, the same patterns were observed across all 3 donors with only minor variations. The most notable variation across the 3 donor experiments is that over time (from the first experiment with the sample from donor 1 to the third experiment with donor 3), the speed of miRNA depletion seems to increase. This is evident not only when comparing live versus dead cell incubations, but also when comparing the miRNA concentrations across pellet and supernatant fractions. As opposed to the incubations from donor 1 where a significant percentage of the starting miRNA concentration can be measured in the live incubations cell pellets at time point 0, the same incubations from donor 2 show a drastic decrease in this initial miRNA concentrations in the pellet. This decrease becomes even starker in the third donor experiment suggesting that the overall miRNA stability may have been compromised throughout the period of the study. Despite these differences, however, the same patterns are still conserved across all 3 donors, indicating that they are experimentally

significant. In the case of all 3 donors, there is no significant difference in miRNA association patterns in incubations supplemented with miR21 versus miR21 scramble, confirming that this association between gut bacteria and miRNAs is not sequence specific. Additionally, all 3 donor experiments demonstrated a significantly faster depletion of miRNA in live cell incubations compared to dead cell (ethanol-fixed) incubations. This further confirms that this depletion or association with miRNAs is microbiota-dependent.

An initial observation from the first set of incubations that was striking was that most of the miRNA degradation/ decrease in miRNA concentration occurred within the first 2 hours. This rapid degradation period was especially surprising, considering that the median half-life of some of the most abundant miRNAs is around 11 hours (Zlotorynski, 2019). If miR21 does in fact play a role in bacterial growth and gene regulation, we would expect it to persist for longer periods of time in the cells. For this amended experiment, we used shorter, more frequent sampling times to better investigate the dynamics that occur during the early hours of incubation. After the first hour of incubation, we quantified that only approximately 20% of the initial miRNA concentration was remaining (Fig. 7), again confirming the short half-life of miR21 in these incubations. In addition to this quick drop in concentrations, we also observed that the miRNA concentration followed similar patterns across both the pellet and supernatant fractions. To isolate most of the miRNAs in the pellet fraction and focus on the association between bacterial cells and miRNAs, additional washing steps were added prior to starting the incubations. Lastly, an additional incubation with RNase inhibitor was also included in the amended experiment to determine if bacterial RNases were responsible for the change in miRNA concentrations observed in the previous experiment. We found that the addition of RNase inhibitor had no significant effect on the changes in miRNA concentrations observed (Fig. 7). As previously mentioned, the RNase inhibitor used in these experiments has been reported to effectively inhibit RNase A, B and C but not effectively inhibit other RNases, including RNase I, T1, T2, H, U1, U2 or CL3[6]. RNase I and members of the RNase H family (HI and HII) are endoribonucleases present in bacteria and have been purified previously from *E. coli* (Bechhofer & Deutscher, 2019). RNase T2 represents a family of human secreted RNases that function as RNA scavengers (Lu *et al.,* 2018), emphasizing that there are still other bacterial and host RNases not inhibited by the selected RNase Inhibitor. Therefore, the observation that there was no significant effect of the addition of RNase inhibitor on miRNA concentrations does not rule out the possibility that there are other uninhibited bacterial RNases at work. To better measure the impact that bacterial RNases may have on miRNAs, an RNase activity assay could be performed to evaluate the RNase activity in these incubations in real time.

[6] https://www.thermofisher.com/at/en/home/life-science/dna-rna-purification-analysis/rna-extraction/rna-extraction-products/rnase-inhibitors.html

5.2 Fluorescence-Activated Cell Sorting of fecal samples supplemented with miR21 and miR21 scramble mimics Reveals Unique miRNA-Associating Bacterial Communities

Previous studies have shown that miRNAs are capable of modulating the gut microbiota (Johnston *et al.,* 2018; Liu *et al.,* 2016), so a better understanding of the differences in community composition across miRNA-associated and miRNA-negtative populations can elucidate potential mechanisms for how miRNAs influence human health. The most highly abundant bacterial families identified in the miRNA-associated fractions, irrespective of miRNA sequence, were *Lactobacilliaceae*, *Veillonellaceae*, and *Oscillospiraceae,* whereas the bacterial families with the lowest abundance in the miRNA-associated fractions *were Pseudomonadaceae, Aeromonadaceae, and Yersiniaceae*. These families all belong to the phylum *Firmicutes*, whereas the families with a significant lower abundance all belong to the phylum *Proteobacteria*. In contrast to *Firmicutes*, whose members are capable of producing the essential short chain fatty acid, butyrate, and play a key role in maintaining intestinal homeostasis (Venegas *et al.,* 2019), an increase in *Proteobacteria* has been shown to positively correlate with human disease and a dysbiotic gut (Méndez-Salazar et al., 2018). This initial observation that several *Firmicutes* species associate with miRNAs, while many *Proteobacteria* species associate less so with miRNAs suggests that predominantly beneficial bacteria preferentially associate with miRNAs.

In addition to those discussed above, several bacterial families were observed to have more varying abundances in the miRNA- positive fractions, with some genera being enriched while others being depleted. These include the families *Lachnospiraceae*, *Ruminococcaceae* and *Bacteroidaceae*. For example, within the family *Ruminococcaceae*, the genus *Ruminococcus* was found to associate with the miRNAs, whereas the genus *Faecalibacterium* was not. Both these genera play key roles in immune homeostasis and previous studies have shown that significant decreases in these populations are observed in patients suffering from IBD. In the case of *Lachnospiraceae*, genera *Blautia*, *Lachnoclostridium*, *Agathobacter* and *Fusicatenibacter* were all depleted in the miRNA-associated fractions, whereas genera *Coprococcus* and *NK4A136* and *Eubacterium ventriosum* groups were enriched in them. In previous studies, IBD patients have presented with varying abundances of *Lachnospiraceae* based on condition. A decreased abundance of *Blautia* species was observed in patients suffering from UC, whereas a decreased abundance in *Coprococcus* was observed in patients suffering from CD. However, many studies have provided inconsistent results regarding *Lachnospiraceae* abundances and disease pathologies, indicating that the variations observed in this study (Fig. 10) may be due to natural fluctuations across this bacterial family in different individuals.

Additionally, many ASVs from *Bacteroidaceae* proved to have varying abundances across the miRNA-associated fractions. *B. cellulosilyticus/intestinalis/ timonensis* and *B. uniformis* were found to both associate miRNAs, whereas *B. finegoldii* was in much lower abundance in the miRNA-associated fractions. When comparing the incubations with different miRNAs, those with miR21 scramble only showed a depletion in *B. finegoldii*, whereas incubations with miR21 only

showed an enrichment of *B. uniformis*. This shows that the observed differences in *Bacteroides* abundance may be sequence-specific. Although the previous incubation experiments showed no major differences in dynamics of miR21 versus miR21 scramble, these results show that some *Bacteroides* species may preferentially associate with miR21 over miR21 scramble. However, differential abundance analysis comparing miR21 and miR21 scramble positive gates, did not identify any *Bacteroides* species as being significantly differentially abundant. The only ASV significantly differentially abundant in miR21 positive gates compared to miR21 scramble positive gates was that of *Ruminococcus bromii*, a keystone commensal capable of producing essential SCFAs like butyrate and whose byproducts are often used as fuel for other gut commensals including *B. thetaiotaomicron* (X. Chen *et al.,* 2008; Qiu *et al.,* 2022). However, the differential expression analysis from the separate incubations (miR21 and miR21 scramble) indicates that this ASV associates with both miRNAs, compared to the miRNA-negative FACS sorted gates, indicating that *R. bromii* significantly associates with both miR21 and miR21 scramble, but that it may preferentially associate with miR21 scramble. The observation that only a single ASV was differentially abundant across miR21 positive and miR21 scramble positive gates demonstrates that sequence specificity plays a minimal role in bacterial associations with miRNAs.

The variable abundances across *Firmicutes* and *Bacteroidota* highlight that some species from these phyla associate preferentially with miRNAs compared to others. Additionally, a lower abundance of some mutualistic bacteria including *Faecalibacterium* and *Bacteroides* ASVs suggests that miRNAs may not have an exclusively beneficial impact on the host gut microbial community. For example, when comparing miRNA positive gates versus negative gates in FACS-sorted fractions from incubations with miR21, *Faecalibacterium prausnitzii* was found to be significantly depleted (log2 FC = -1.41). *F. prausnitzii* is a key commensal, and patients with IBD have been reported to have a significantly lower abundance of it, as well as a lower abundance of other *Firmicutes*. This is concordant with previous experiments that have suggested that miR21 plays a role in IBD pathogenesis, as shown by an overall protective phenotype against colitis in miR21 knockout mice. One key mechanism through which miR21 has been shown to promote colitis is through increased permeability of the gut epithelium (Zhang *et al.,* 2015), which is a key part of the intestinal mucosa and plays a significant role in intestinal immunity (X. Chen *et al.,* 2008). Decreased abundance of *F. prausnitzii* has also been repeatedly associated with inflammation and compromised gut mucosa integrity (Qiu *et al.,* 2022), suggesting a potential mechanism through which miR21 induces a compromised gut epithelium and contributes to IBD development.

5.3 Transcriptome Analysis Reveals Significant Differences in Gene Expression between Control Groups and miRNA Treatment Groups

In vitro growth studies, in which pure cultures of *Bacteroides thetaiotaomicron* (*Bt*) were supplemented with either miR21, miR21 scramble, a small RNA control or water, showed that miRNA supplementation significantly boosted growth compared to both controls (Fig. 12A). However, it cannot be definitively concluded that this boost is specific to miRNAs, as the small RNA control also significantly boosted *Bt* growth compared to the water control (Fig. 12B).

Because the addition of any small RNA significantly boosted growth, it is possible that the bacteria is utilizing the supplemented RNA as a food source. Previous studies have demonstrated that *Bt* and several other *Bacteroides* species can utilize ribose as a source of polysaccharides (Glowacki *et al.,* 2020). Additional experiments were performed using pure cultures of *Bt* grown in a minimal media without glucose to understand whether *Bt* growth could be stimulated by the supplementation of small RNAs alone (not shown), but no growth was observed under any of the conditions. In order to verify whether *Bt* is in fact utilizing the RNAs as a full source, additional experiments may need to be repeated with a higher concentration of supplemented RNAs.

Following these *in vitro* growth experiments, transcriptomic sequencing was performed on *Bt* in pure culture supplemented with different small RNA molecules (miR21, miR21 scramble, small RNA control) in order to understand how these supplemented miRNAs influence the *Bt* transcriptome. Analyzing significant changes in *Bt* gene expression can elucidate mechanistically how these molecules are able to significantly boost growth. Based on the outcome of the growth experiments, it was hypothesized that many of the upregulated genes would be related to glucose utilization, but this was not the case. In fact, almost all genes differentially expressed in the presence of miR21 and miR21 scramble (compared to the water control) were downregulated and very few of them were identified to be related to polysaccharide metabolism (Fig. 14A). Using the water control as a base for comparison, 185 genes are significantly differentially expressed in the presence of miR21 (Sup. Table 1), 63 in the presence of miR21 scramble (Sup. Table 2) and only 3 in the presence of the small RNA control. These results alone highlight the high degree of similarity between the transcriptomic profiles of *Bt* supplemented with water and *Bt* supplemented with the small RNA control. The three genes significantly downregulated in the presence of the small RNA control belong to a gene cluster encoding cation efflux system proteins in *Bt* (Sup. Table 3). This gene cluster specifically corresponds to the AcrAB-TolC system, and previous experiments have already demonstrated that small RNAs are capable of repressing proteins in this efflux system (Parker & Gottesman, 2016). Previous experiments have demonstrated that repression of this system is often linked to increased sensitivity to antibiotics and overall decreased fitness (Nishino *et al.,* 2021). Thus, repression of this gene cluster by the small RNA control is likely not related to the increased growth observed in the *in vitro* growth experiments.

Of the 185 genes differentially expressed in the presence of miR21, 49 are also differentially expressed in the miR21 scramble incubation (bolded in Sup. Table 1), and these 49 DEGs represent the overall impact that miRNA supplementation has on the gene expression profile of *Bt*. While almost a fourth of these DEGs are functionally uncharacterized, more than a third of them are characterized as DNA binding proteins, ribosomal proteins, transcriptional regulators and transfer RNAs (tRNAs). This demonstrates that these supplemented miRNAs play a much more complex role in *Bt* gene expression and that its impacts extend far beyond boosting growth. Additionally, all 49 of these miRNA-specific DEGs were significantly downregulated. Although this significantly repressed gene expression profile contradicts the growth experiments, it is congruent with previous research on miRNAs, which have shown that host mRNA degradation is the predominant mechanism of miRNA-mediated gene regulation (Bartel,

2018; O'Brien *et al.,* 2018). This is additionally supported by the significant down regulation of several tRNAs, which can be attributed to miRNA-mediated inhibition of host mRNA translation (Shukla et al., 2011). Similar to the small RNA control, very few of these DEGs were functionally identified to be proteins involved in carbohydrate metabolism. One DEG that may potentially contribute to the observed boost in growth in the presence of miRNAs is BT4356. This gene encodes for the anti-sigma FecR, a transcriptional regulator shown to regulate polysaccharide utilization loci (PULs) in *E. coli* (Cao *et al.,* 2016). While sigma factors are responsible for activating transcription, anti-sigma factors act in the contrary and inhibit their respective sigma factors to repress transcription (Treviño-Quintanilla *et al.,* 2013). In the presence of both miR21 and miR21 scramble, this DEG was significantly down regulated. Decreased expression of this anti-sigma factor could correlate to increased expression of PULs and subsequent activation of genes involved in the utilization of monosaccharides such as glucose, which could account for the significant boost in *Bt* growth in the presence of miRNAs.

Transcriptomic analysis additionally revealed that supplementation with miR21 significantly altered the expression of several gene clusters (Fig. 14B-C). In total, 5 gene clusters were identified to be significantly differentially expressed in the presence of miR21 compared to all other treatments (Fig. 14B). While one cluster (BT3217-BT3221) has an unidentified function, the remaining have somewhat defined functions and can give insights into some potential mechanisms underlying miR21-mediated regulation of host functionalities. One of these clusters (BT0914a-BT0916) has been identified with a high confidence to encode at least part of the ribosomal protein operon *rpmB-rpmG*, which controls early ribosomal assembly and function (Aseev *et al.,* 2016). BT0915 was identified as *rpmG* which encodes for the ribosomal protein L33, while BT0916 was identified as *rpmB*, which encodes for the ribosomal protein L28. Although the function of BT0914a is still unknown, previous research has demonstrated that it likely has a ribosomal protein-related function due to its proximity to other well-described ribosomal proteins (Sberro *et al.,* 2019). All of these ribosomal proteins were significantly repressed in the presence of miR21. While significant repression of L33 has a minimal impact on ribosome assembly, repression of L28 significantly stalls ribosomal assembly and induces downstream accumulation of smaller subunits, ultimately repressing translation (Aseev *et al.,* 2016). While this finding does not align with the observation that miR21 and miR21 scramble significantly boost grown of *Bt* (Fig. 12A-B), it does support previous studies that have found miR21 to be a repressor of translation (Janas *et al.,* 2012). Previous studies have additionally shown that miR21 plays a significant role in inflammation and disease development, specifically in the case of IBD (Johnston et al., 2018). These observations that important ribosomal proteins are significantly repressed by miR21 further elucidate potential mechanisms of miR21-mediated disease pathogenesis, as a defect in ribosome biogenesis could potentially develop into ribosomopathies that lead to inflammation or diseases in the host (Tahmasebi *et al.,* 2018).

Additional gene clusters highlighted in the heatmap in Figure 14B encode for genes involved in DNA binding, transcriptional regulation and virulence. BT3139 and BT3140 are both putative DNA binding proteins with a helix-turn-helix (HTH) motif. The HTH domain is one of the most common DNA-binding domains and is often associated with transcriptional regulation (Aravind *et al*., 2005). Although the specific function of these genes is unknown outside of their

sequential motifs, their repression because of miR21 supplementation is likely a downstream effect of miR21-mediated transcriptional control. Supplementation with miR21 also significantly decreased expression of another gene cluster (BT0239-BT0242). The majority of the genes encoded by this cluster exert an unknown function, but BT0242 was identified as a gene encoding a putative polysaccharide deacetlyase, an enzyme in the Carbohydrate Esterase Family 4 that plays a potential role in bacterial virulence (Balomenou *et al.,* 2013). This group of enzymes has already been well studied in gram-positive species (i.e. *Bacillus anthracis* and *Staphylococcus epidermidis*) and plays a key role in peptidoglycan modification and biofilm formation, but it has been less examined across gram-negative *Bacteroides* species (Balomenou *et al.,* 2013; Vuong *et al.,* 2004). Biofilm formation is not unique to pathogenic bacterial strains, and many symbiotic bacteria including *Bt* have been shown to have the capacity for biofilm formation (Béchon *et al.,* 2020). This biofilm formation may be an important factor that helps *Bt* colonize the gut and mediate intestinal homeostasis and stability, so repression of genes that control these virulence factors might be an additional mechanism behind miR21-mediated inflammation. However, biofilm formation of gut symbionts is neither well studied nor understood, so additional studies would need to follow to better investigate if and how miRNAs regulate virulence factors of commensals.

Although the majority of DEGs identified in the presence of miR21 were significantly down regulated, a single gene cluster was shown to be significantly over expressed in the presence of miR21 compared to all other conditions. This operon is made up of 7 genes (BT0527-BT0533) that encode for the different enzymes involved in the pathway for Indole and L-tryptophan synthesis. Supplementation with either miR21 scramble or the RNA control did not induce any significant differences in expression of these genes, highlighting that over expression of this gene cluster is a unique impact of miR21 supplementation. Until now, the transcriptomic analysis in this study supported several other studies that found that miRNAs significantly repressed mRNA translation in bacteria, so the finding that this entire gene cluster was consistently over-expressed in the presence of miR21 is noteworthy. Tryptophan is an essential amino acid and a vital component of the human diet, as it plays an important role in protein synthesis and is a precursor for several metabolites and vitamins including serotonin, melatonin and niacin (Sainio *et al.,* 1996). Dietary supplementation of tryptophan has been shown to ameliorate inflammation and improve overall host health (Nikolaus *et al.,* 2017). Aside from dietary interventions, tTyptophan is primarily produced by the gut microbiota and plays a well-established role in the gut-brain axis. Perturbations in tryptophan concentrations significantly influence the serotonin system and therefore the regulation of host mood and cognitive function (L. M. Chen *et al*., 2021; Jenkins *et al.,* 2016). However, serotonin synthesis only accounts for a very small portion of tryptophan metabolism; the majority of tryptophan metabolism occurs via the tryptophan-kynurenine metabolic pathway (L. M. Chen *et al.,* 2021). Increased tryptophan metabolism has been extensively tied to IBD pathogenesis, and many patients suffering from UC or CD have been shown to have increased concentrations of downstream tryptophan metabolites such as kynurenine (Nikolaus *et al.,* 2017; Sofia *et al.,* 2018). This suggests that the increased L-tryptophan biosynthesis in the presence of miR21 may potentiate inflammation or disease pathogenesis. As previously mentioned, earlier experiments have suggested that miR21 plays a significant role in IBD pathogenesis and that mice completely depleted of miR21

exhibited a protective state from colitis (Johnston *et al.,* 2018). These transcriptomic results suggest a potential underlying mechanism behind this miR21-mediated inflammation.

The final gene cluster highlighted in Figure 14 is one which is exclusively over expressed in the presence of miR21 compared only to miR21 scramble treatment (Fig. 14C). This gene cluster (BT1883-BT1886) is depicted separately, as it is not differentially expressed in the presence of miR21 compared to neither the water nor the small RNA control. Therefore, this suggests a potentially miRNA-specific impact on the *Bt* transcriptome. Analysis identified BT1884 as encoding a putative cold shock protein (CSP) with homology to a well-described protein (*CspC*/*CspE*) in *Escherichia coli* and *Salmonella enterica* (Michaux *et al.,* 2017). In *Proteobacteria*, these CSPs have been shown to play an important role in RNA-protein interactions and regulating virulence and stress responses during infection (Michaux *et al.,* 2017; Prezza *et al.,* 2022). However, their function on commensals such as *Bt* has been poorly characterized. Similar to experiments studying the effect of *CspC*/*CspE* deletions on the bacterial host, deletions of BT1884 conferred increased sensitivity to antibiotics and impaired motility and biofilm formation (Prezza *et al.,* 2022). In the present study, supplementation with miR21 significantly overexpressed BT1884 and neighboring genes (log 2 FC > 3) compared to incubations with miR21 scramble. One of these neighboring genes, BT1885, was identified to encode a homolog of *RhlE*, an RNA helicase previously shown to play a critical role in rRNA processing and ribosomal maturation in *E. coli* (Prezza *et al.,* 2022). Overexpression of this putative RNA-binding protein (RBP) may point to the mechanism behind boosted growth in the presence of miR21, but it does not explain the concomitant boost in growth in the presence of miR21 scramble. Previous experimentation with *cspC* and *cspE* additionally highlighted that their deletion does not significantly impact growth patterns of their hosts (Michaux *et al.,* 2017). Overall, this suggests that miR21 specifically has a significant RNA-related role in *Bt,* and further investigation into RNA biology of *Bt* and other commensals is warranted to better understand the importance of these potential RBPs and their consequences on bacterial growth and survival.

6.0 Conclusion and Outlook

In conclusion, this study provides valuable insights into the intricate associations between miRNAs and the human gut microbiota, shedding light on their dynamics and potential implications for human health. The findings highlight that miRNAs maintain a preferential association with certain live gut microbiota taxa, pointing to a microbiota-dependent mechanism. Importantly, incubations with both miR21 and miR21 scramble demonstrated that this association is not sequence specific, as no significant differences were observed between miR21 and a miR21 scramble dynamics. Community acquisition and analysis using fluorescence-activated cell sorting further elucidated which ASVs preferentially associate with miRNAs, with enriched *Firmicutes* and depleted *Proteobacteria* identified in the miRNA positive gates, implying a potential anti-inflammatory state. However, varying abundances were observed of ASVs belonging to families such as *Lachnospiraceae*, *Ruminococcaceae*, and *Bacteroidaceae*, suggesting that certain bacterial species may associate more efficiently with miRNAs compared to others. Furthermore, the observation of a decreased association of miR21 with key commensal bacteria, such as *F. prausnitzii*, in the presence of miR21 raises concerns about its potential impact on gut microbiota homeostasis.

While *in vitro* growth studies showed that miRNA supplementation significantly increased bacterial growth, transcriptomic analysis demonstrated that these miRNAs, especially miR21, play a far more complex role in bacterial gene expression. MiR21 significantly repressed transcription of several genes in *Bt* involved in a variety of functions, confirming previous investigations that have claimed miRNAs as negative regulators of bacterial gene expression. More surprising, however, is that supplementation with miR21 significantly increased the expression of gene clusters controlling tryptophan biosynthesis and RNA binding. While miRNAs have previously been reported to promote mRNA translation (Truesdell *et al.,* 2012), this phenomenon is less documented. Therefore, the ability for miR21 to significantly upregulate such an important biosynthesis pathway is noteworthy, especially when focusing on the context of miR21 and IBD pathogenesis. Previous research has shown that miR21 likely plays a role in promoting inflammation and disease development in patients with IBD (Johnston *et al.,* 2018), and these results suggest that increased tryptophan metabolism and downstream metabolites may play a role in this miR21-mediated inflammation.

Future experiments can further investigate these complex dynamics between miRNAs and the gut microbiota, ultimately advancing our understanding of the functional consequences and clinical relevance of these associations. Additionally, metabolomics could be employed to better elucidate the impact that miR21 has on host metabolism, specifically in the context of tryptophan. These experiments will confirm whether observed overexpression of the tryptophan biosynthesis pathway in the presence of miR21 is coupled to increased tryptophan metabolites that may be contributing to inflammation in the gut. Lastly, additional *in vivo* experiments could be done to elucidate how these specific miRNA-microbiota interactions play out in the host. *In vivo* mouse models could be employed to investigate whether supplementation with miR21 in germ-free mice colonized with *Bt* results in a similar transcriptomic profile and if a diseased phenotype is produced.

Altogether, these findings contribute to our understanding of the complex interplay between miRNAs and the gut microbiota in the specific context of miR21. The finding that miR21 can regulate host metabolism via the transcriptional control of L-tryptophan and indole synthesis is an important finding that may explain the role of miR21 in inflammation and IBD pathogenesis. Further experiments investigating the role that miR21 plays in tryptophan and Indole synthesis and subsequent tryptophan metabolism pathways will complement these results and elucidate whether miR21 may be a therapeutic target in IBD treatment. The study also provides hope that tryptophan and end-product metabolites of its metabolism may serve as promising biomarkers in IBD diagnosis. Overall, this research provides a foundation for further exploration and highlights the importance of considering miRNA-microbiota interactions in the context of human health and disease.

7.0 Supplemental Materials

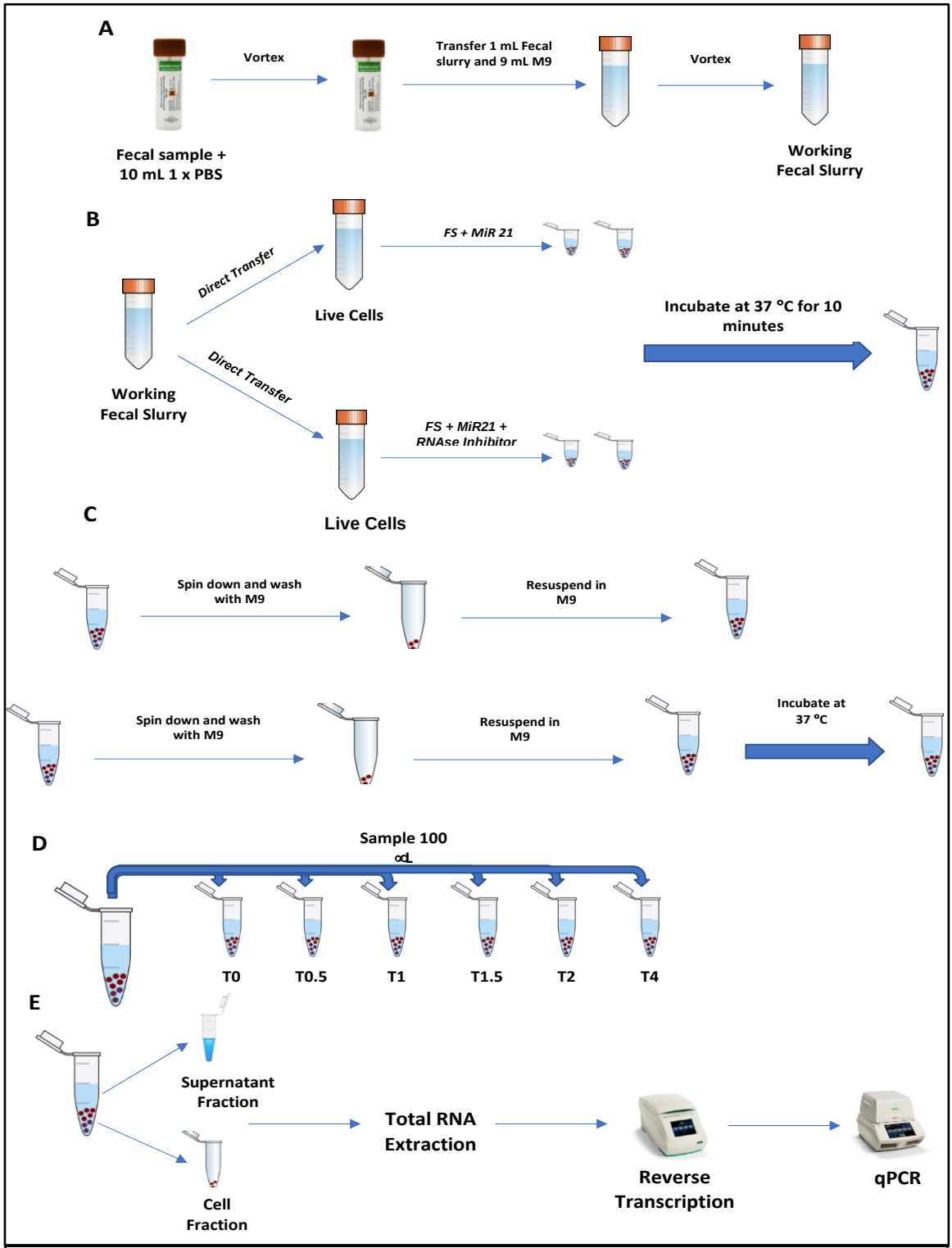

Sup. Figure 1: Procedural schematic for amended follow-up miR21 incubation experiment. (A) Preparation of the fecal slurry. (B) Incubation set-ups for live bacterial cell incubation, including the different amendments and controls added to each incubation. (C) Summary of the different sampling time points. (D) Separation of samples into supernatant and pellet fractions and subsequent downstream analysis.

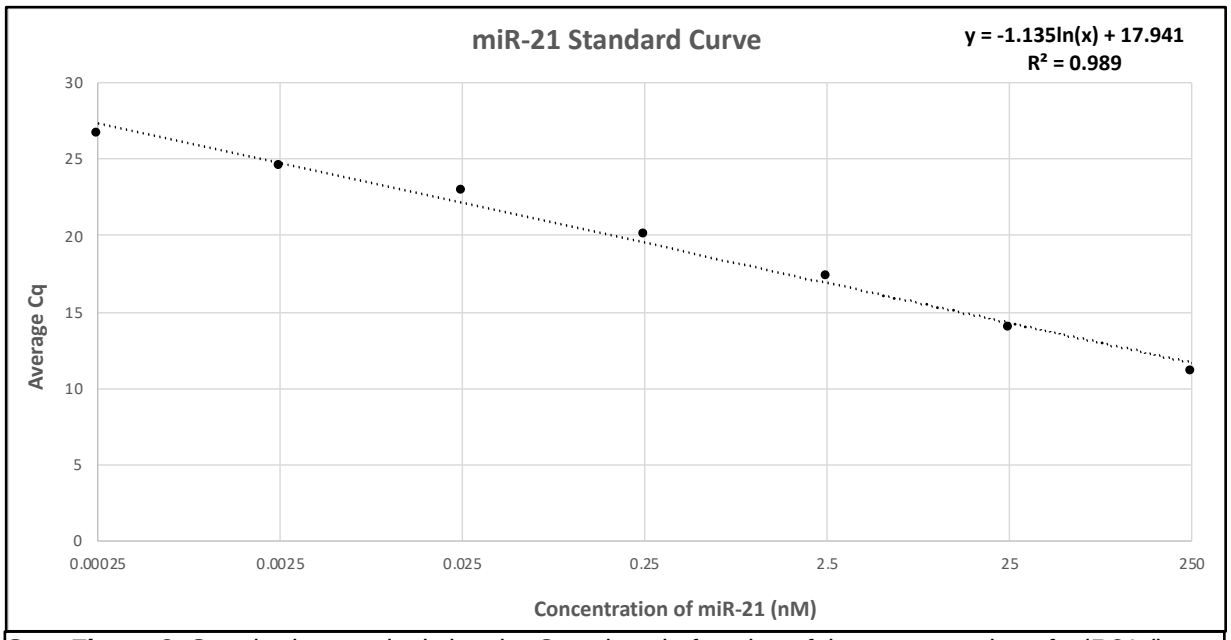

Sup. Figure 2: Standard curve depicting the Cq values in function of the concentration of miR21 (in nM), as determined using qPCR. Values for standards are shown in blue, and the above equation was used to calculate miRNA concentrations in all miR21 samples based on the acquired Cq value.

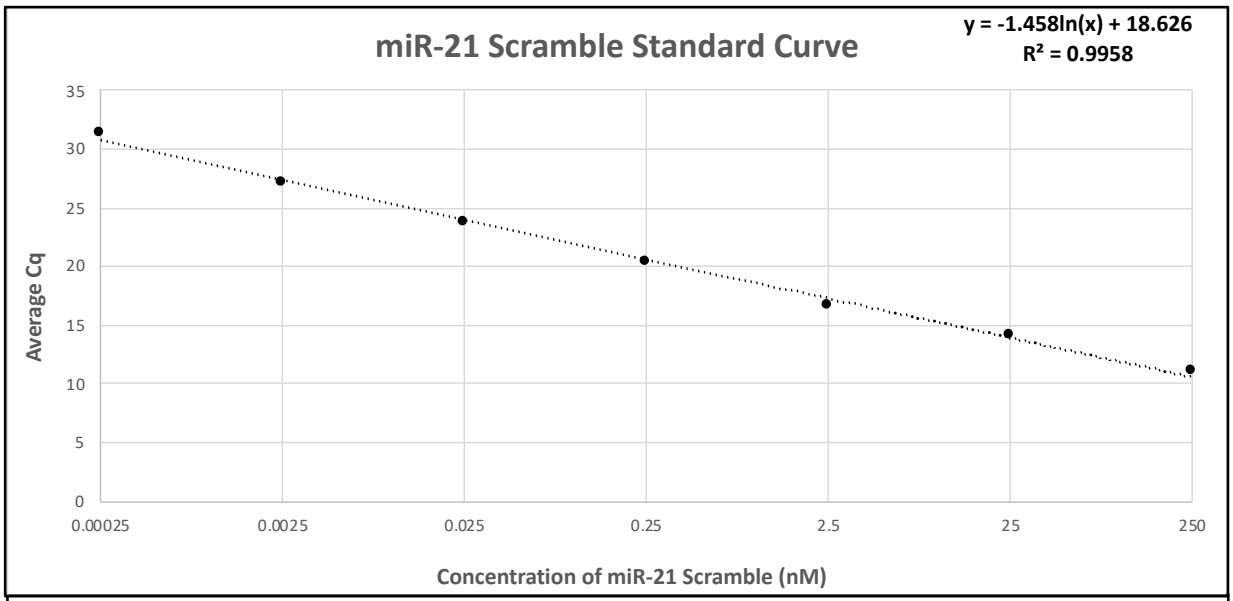

Sup. Figure 3: Standard curve depicting the Cq values in function of the concentration of miR21 scramble (in nM), as determined using qPCR. Values for standards are shown in blue, and the above equation was used to calculate miRNA concentrations in all miR21 scramble samples based on the acquired Cq value.

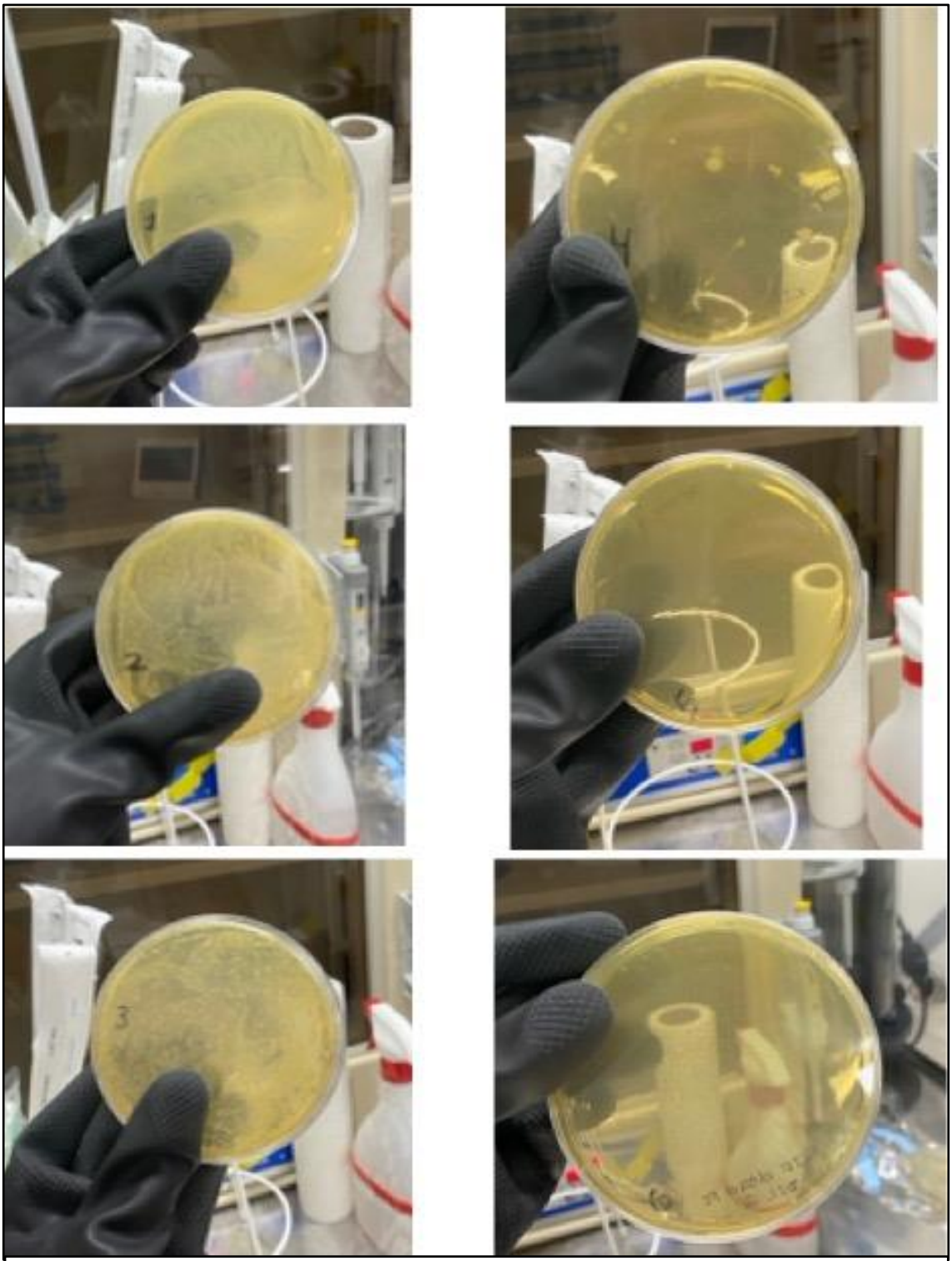

Sup. Figure 4: Pictures showing bacterial growth on BHI agar following 72-hour incubation period. The abbreviation TMC indicates there were too many colonies to count. (1) undiluted prepared fecal slurry with live cells; (2) 1:10 dilution of prepared fecal slurry with live cells; (3) 1:10 dilution of dilution on plate 2; (4) undiluted fecal slurry with dead cells; (5) 1:10 dilution of fecal slurry with dead cells; (6) 1:10 dilution of dilution on plate 5.

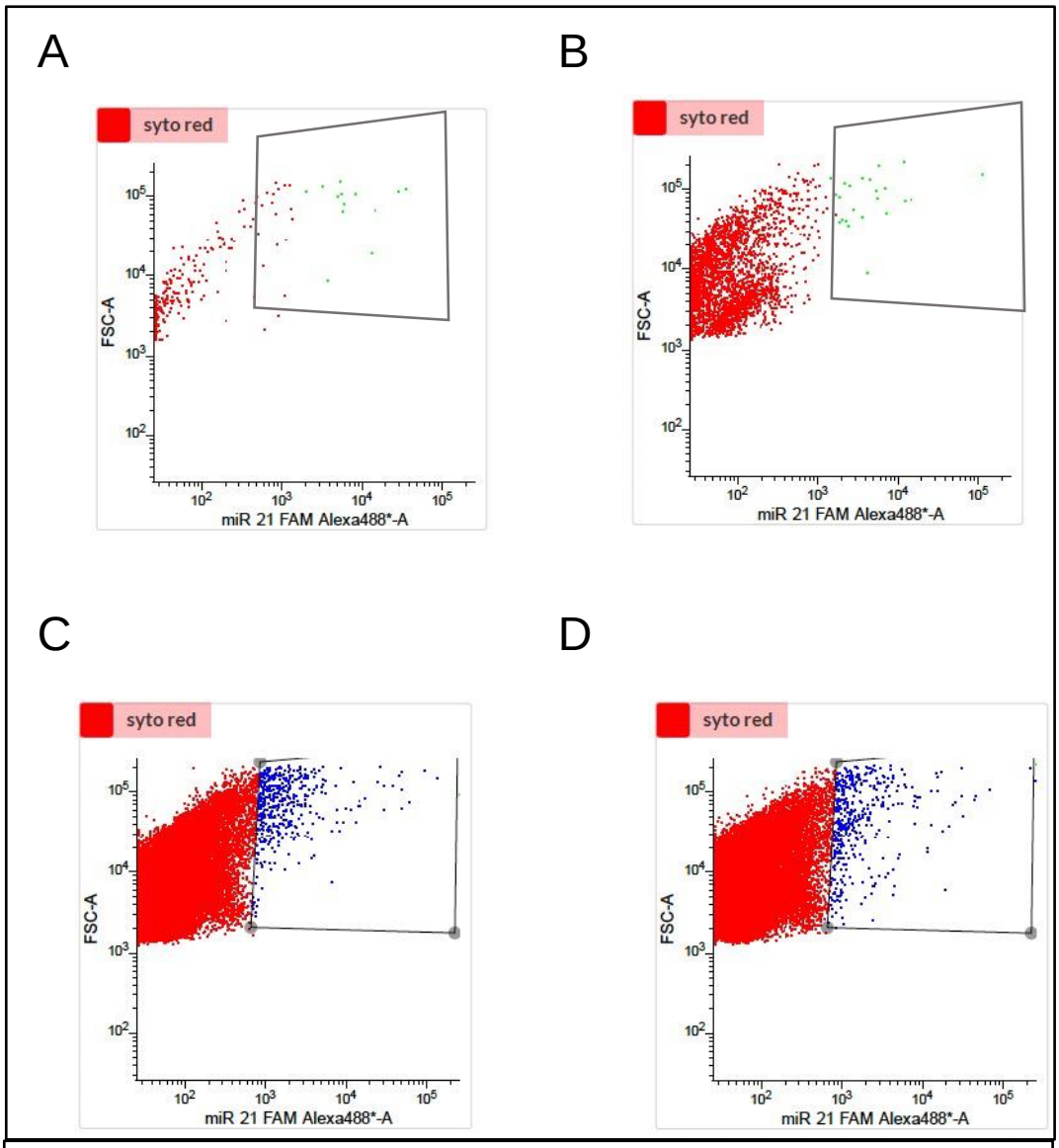

Sup. Figure 5: Representation of gating used for the FACS sorting of gut microbiota cells from fecal samples incubated with miRNAs. (A) Water control with no SYTO62 stain (SYTO 62 negative); (B) Water control with SYTO62 stain (SYTO62 positive); (C) miR21 Atto488; (D) miR21 Atto488 scramble. The gate outlined in C-D indicate the Atto488 positive cells, whereas the populations not included in the gate are considered Atto488 negative cells.

Sup. Table 1: Table summarizing the significantly differentially expressed genes with a log2 fold change absolute value greater than or equal to 1 in the miR21 treatment compared to the water control treatment. Bolded rows represent genes that are also significantly differentially expressed in the miR21 scramble control treatment compared to the water control treatment.

Gene_ID	baseMean	log2 Fold Change	pvalue	padj	padj. signif	Functional Category[7]
BT_0128	**174.3859**	**-2.7885**	**1.00E-27**	**4.20E-25**	********	**Lipoprotein**
BT_0170	83.1154	-1.1032	1.92E-05	2.62E-04	***	Putative conserved membrane protein
BT_0175	77.9489	-1.5463	2.83E-07	6.80E-06	****	Conserved hypothetical protein
BT_0224	30.8535	1.2915	0.0043	0.0218	*	Lipocalin-like protein
BT_0239	458.8802	-1.0172	3.30E-10	1.89E-08	****	Thiol: disulfide interchange protein
BT_0240	95.7042	-1.1471	3.38E-05	4.09E-04	***	TPR Repeat containing protein
BT_0241	2878.9931	-1.0603	2.38E-17	4.49E-15	****	Conserved hypothetical protein
BT_0242	4912.9419	-1.5129	5.16E-07	1.17E-05	****	Polysaccharide deacetylase
BT_0255	**80.9883**	**-2.5402**	**1.43E-16**	**2.45E-14**	********	**Conserved hypothetical protein**
BT_0256	**166.5383**	**-2.3376**	**2.03E-21**	**5.12E-19**	********	**Conserved hypothetical protein**
BT_0289	31.2343	-1.1088	0.0062	0.0287	*	Receptor domain protein
BT_0382	103.1617	1.1545	1.34E-05	1.89E-04	***	Polysaccharide biosynthesis
BT_0407	1696.3013	-1.2238	1.20E-04	0.0011	**	Conserved hypothetical protein
BT_0408	874.9234	-1.8336	6.32E-06	1.03E-04	***	Conserved hypothetical protein
BT_0471	27.1340	1.2482	0.0081	0.0360	*	Glycoside transferase family 4
BT_0481	34.2851	1.1244	0.0097	0.0413	*	Polysaccharide export protein
BT_0482	118.5197	1.0963	3.42E-05	4.13E-04	***	Tyrosine protein kinase
BT_0528	365.3414	1.0456	7.79E-08	2.36E-06	****	L-tryptophan synthesis pathway
BT_0529	487.5251	1.0158	2.48E-08	8.68E-07	****	L-tryptophan synthesis pathway
BT_0530	834.4414	1.1761	1.32E-12	1.43E-10	****	L-tryptophan synthesis pathway
BT_0531	692.6416	1.0260	4.51E-09	1.91E-07	****	L-tryptophan synthesis pathway
BT_0581	169.4600	-1.5595	8.93E-15	1.20E-12	****	Acetyltransferase
BT_0582	63.0264	-1.3006	1.81E-05	2.49E-04	***	Transcriptional regulator
BT_0586	230.7480	-1.0845	1.36E-08	5.24E-07	****	Conserved hypothetical protein

[7] https://www.ncbi.nlm.nih.gov/data-hub/genome/GCA_000011065.1/

BT_0616	55.1056	-1.3337	1.95E-05	2.64E-04	***	Transcriptional regulator
BT_0628	811.9341	-1.4434	1.39E-05	1.95E-04	***	Conserved hypothetical protein
BT_0631a	**1567.5328**	**-1.1211**	**1.67E-11**	**1.47E-09**	****	**Conserved hypothetical protein**
BT_0641	147.2988	-1.1089	2.60E-07	6.38E-06	****	Conserved hypothetical protein
BT_0646	1079.4332	-1.4463	1.14E-04	0.001093	**	Outer membrane protein
BT_t08	123.6353	-1.2243	4.56E-07	1.06E-05	****	tRNA-Gly
BT_0677	32.6344	-1.1883	0.0058	0.0272	*	Thioredoxin
BT_0747	**389.7053**	**-1.2168**	**3.01E-09**	**1.32E-07**	****	**phosphatidylinositol-4-phosphate 5-kinase**
BT_0779	**60.5722**	**-1.9271**	**1.52E-09**	**6.82E-08**	****	**Conserved hypothetical protein**
BT_0815	1067.7067	-1.1022	2.88E-14	3.62E-12	****	Conserved hypothetical protein
BT_0817	164.0469	-1.3151	1.17E-10	7.61E-09	****	Lipoprotein
BT_0819	**91.0514**	**-1.4928**	**1.50E-08**	**5.66E-07**	****	**Conserved hypothetical protein**
BT_0822	190.6412	-1.1449	8.87E-10	4.47E-08	****	Metallo-beta-lactamase hydrolase
BT_t10	**31.4814**	**-1.9239**	**4.03E-06**	**6.94E-05**	****	**tRNA- Lys**
BT_t11	**26.4107**	**-1.9360**	**7.32E-05**	**7.74E-04**	***	**tRNA- Lys**
BT_0841	60.9573	-1.5540	1.98E-07	5.27E-06	****	Conserved hypothetical protein
BT_t13	74.3840	-1.0015	3.26E-04	0.0026	**	tRNA- Pro
BT_0854	249.6739	-1.2329	8.15E-13	9.05E-11	****	Conserved hypothetical protein
BT_0868	49.8218	-1.8688	6.83E-08	2.10E-06	****	Hypothetical protein
BT_0869	266.6614	-1.0236	1.55E-09	6.89E-08	****	Conserved hypothetical protein
BT_t16	135.8279	-1.0189	8.89E-05	9.03E-04	***	tRNA- Arg
BT_0902	194.8759	-2.2513	2.87E-23	9.02E-21	****	Conserved hypothetical protein
BT_0914a	**1899.4449**	**-2.3056**	**2.69E-45**	**3.39E-42**	****	**Conserved hypothetical protein**
BT_0915	**2022.1876**	**-2.4685**	**1.27E-54**	**4.80E-51**	****	**50S ribosomal protein L33**
BT_0916	**2882.0012**	**-2.0442**	**1.21E-51**	**2.29E-48**	****	**50S ribosomal protein L28**
BT_t17	**45.0905**	**-1.6943**	**1.13E-06**	**2.35E-05**	****	**tRNA-OTHER**
BT_0938	235.0491	-1.4622	1.57E-16	2.57E-14	****	HNH_5 domain-containing protein
BT_1009	29.0956	-1.2654	0.0044	0.0220	*	Dihydroorotate dehydrogenase
BT_1262	17.4804	-1.3831	0.0082	0.0363	*	Transcriptional regulator
BT_1302	22.4664	-1.3867	0.0046	0.0226	*	Hypothetical protein
BT_t24	2743.0267	-1.0049	0.0023	0.0128	*	tRNA- Ile

BT_1309	240.1359	-1.4088	3.26E-11	2.62E-09	****	Conserved hypothetical protein
BT_1336	307.2167	-1.1633	1.43E-11	1.28E-09	****	Translation initiation inhibitor
BT_1345	92.0877	-1.2227	5.79E-06	9.60E-05	****	Glyosyltransferase
BT_1352	98.4976	-1.1481	5.15E-06	8.65E-05	****	Glycoside transferase family 4
BT_t25	237.8254	-1.5747	1.84E-04	0.0016	**	tRNA- Asp
BT_t26	**135.7012**	**-1.4855**	**9.76E-10**	**4.79E-08**	****	**tRNA- Asp**
BT_1428	326.0211	-1.1742	6.29E-10	3.26E-08	****	Conserved hypothetical protein
BT_1435	**1050.6427**	**-1.5330**	**1.18E-05**	**1.72E-04**	***	**Conserved hypothetical protein**
BT_1494	311.8481	-1.1554	6.04E-11	4.48E-09	****	Conserved hypothetical protein
BT_1510	121.9646	-1.0412	5.05E-06	8.51E-05	****	Conserved hypothetical protein
BT_1517	64.9218	-1.2432	3.20E-05	3.96E-04	***	Conserved hypothetical protein
BT_1572	73.1152	1.2257	1.12E-04	0.0011	**	RNA polymerase sigma factor
BT_1581	**69.5643**	**-1.6349**	**2.53E-08**	**8.77E-07**	****	**Hypothetical protein**
BT_1609	**65.7979**	**-1.5277**	**2.33E-07**	**5.94E-06**	****	**Conserved hypothetical protein**
BT_1612	**70.6638**	**-1.4915**	**2.94E-07**	**6.99E-06**	****	**Conserved hypothetical protein**
BT_1617	35.0217	-1.2596	8.68E-04	0.0058	**	RNA polymerase sigma factor
BT_1667	**252.9270**	**-2.8633**	**2.63E-08**	**8.93E-07**	****	**Antitoxin**
BT_1692	1169.4704	-1.4092	4.26E-16	6.43E-14	****	50S ribosomal protein L31 type B
BT_1755	**33.4298**	**-1.5207**	**1.16E-04**	**0.0011**	**	**24-amino acid repeat protein**
BT_1800	29.7918	-1.5266	2.26E-04	0.0019	**	2 component system sensor kinase
BT_1811	**197.7659**	**-2.0532**	**1.51E-21**	**4.07E-19**	****	**MerH regulator protein**
BT_1818	57.2129	-1.4546	1.16E-05	1.71E-04	***	Conserved hypothetical protein
BT_1819	**323.9933**	**-2.1413**	**2.21E-25**	**8.35E-23**	****	**Conserved hypothetical protein**
BT_1830	1187.9837	-1.1350	2.58E-12	2.63E-10	****	Chaperonin
BT_1862	**604.9875**	**-2.3362**	**6.82E-35**	**5.15E-32**	****	**Lipoprotein**
BT_1914	441.3977	-1.1610	3.10E-10	1.80E-08	****	thioredoxin
BT_1924	106.2213	-1.2111	2.88E-07	6.88E-06	****	Metal-dependent hydrolase
BT_1958	872.7168	-1.0188	6.94E-11	5.04E-09	****	Hypothetical protein
BT_2030	203.7364	-1.1514	2.16E-08	7.91E-07	****	Conserved hypothetical protein
BT_2031	50.8785	-1.6776	1.50E-06	2.93E-05	****	Hypothetical protein

BT_2037	141.7026	-1.2564	2.43E-08	8.59E-07	****	Conserved hypothetical protein
BT_2131	79.2529	-1.3007	5.57E-07	1.23E-05	****	Ubiquitin-like domain-containing protein
BT_2155	6116.6593	-1.7332	5.46E-29	2.58E-26	****	Hypothetical protein
BT_2164	69.5061	-1.0969	1.23E-04	0.0012	**	Transcriptional regulator
BT_2170	648.1768	-1.3406	1.07E-15	1.56E-13	****	Conserved hypothetical protein
BT_2229	945.5364	-1.2500	8.70E-24	2.99E-21	****	Thioredoxin
BT_2274	358.9925	-1.1637	5.45E-10	2.86E-08	****	Hypothetical protein
BT_t36	**40.9104**	**-1.1403**	**0.0065**	**0.0300**	*****	**tRNA- Lys**
BT_2280	**42.5459**	**-2.0551**	**6.59E-08**	**2.06E-06**	********	**Transposase**
BT_2328	40.4320	-1.0159	0.0047	0.0232	*	Conserved hypothetical protein
BT_2331	74.8057	-1.1226	4.34E-05	5.02E-04	***	Conserved hypothetical protein
BT_2361	**37.3965**	**-1.8062**	**1.22E-05**	**1.76E-04**	*******	**Conserved hypothetical protein, HTH Motif**
BT_2370	56.7752	-1.0940	5.01E-04	0.0036	**	Conserved hypothetical protein
BT_2388	236.7112	-1.3739	1.01E-09	4.89E-08	****	Conserved hypothetical protein
BT_2414	1759.2855	-1.4198	0.0015	0.0092	**	Ferredoxin
BT_2418	548.2887	-1.3142	5.26E-18	1.10E-15	****	Conserved hypothetical protein
BT_2435	**83.4921**	**-2.2814**	**2.65E-16**	**4.18E-14**	********	**MarR family transcriptional regulator**
BT_2462	18.2576	-1.4686	0.0045	0.0224	*	Anti-sigma factor (FecR protein)
BT_2466	**17.8313**	**-1.7675**	**0.0018**	**0.0104**	*****	**Conserved hypothetical protein**
BT_2483	62.3482	-1.0218	0.0012	0.0075	**	Hypothetical protein
BT_2526	518.5367	-1.1012	1.38E-11	1.27E-09	****	Hypothetical protein
BT_2538	65.0359	-1.0444	2.34E-04	0.0019	**	Conserved hypothetical protein
BT_2539	**1523.3006**	**-3.1232**	**2.34E-08**	**8.42E-07**	********	**Rubredoxin**
BT_2606	80.8506	-1.0148	8.65E-05	8.83E-04	***	Conserved hypothetical protein
BT_t41	**400.9208**	**-3.7060**	**1.39E-07**	**3.88E-06**	********	**tRNA- Pro**
BT_2669	250.8590	-1.3160	1.55E-10	9.59E-09	****	Conserved hypothetical protein
BT_2759	824.4607	-1.1191	0.0085	0.0373	*	Conserved hypothetical protein
BT_2786	1778.7497	-1.4734	1.60E-06	3.09E-05	****	30S ribosomal protein S15
BT_t50	**64.3441**	**-1.9123**	**1.29E-08**	**5.02E-07**	********	**tRNA- Asn**
BT_t51	**83.2873**	**-1.9497**	**5.24E-10**	**2.79E-08**	********	**tRNA- Asn**

BT_2830	2895.8406	-1.7489	8.40E-32	5.29E-29	****	DNA-binding protein
BT_2890	42.2248	-1.1039	0.0013	0.0080	**	Transposase
BT_2962	19.7732	-2.1199	8.38E-05	8.60E-04	***	Hypothetical protein
BT_3002	**117.2944**	**-1.1209**	**2.04E-06**	**3.83E-05**	****	**Transcriptional regulator**
BT_3010	47.8879	-1.6590	3.14E-06	5.54E-05	****	RNA polymerase anti-sigma factor (sigma-70 region)
BT_3058	**136.7261**	**-1.4199**	**8.57E-11**	**6.11E-09**	****	**Transcriptional regulator**
BT_3060	19.3280	-1.4200	0.0053	0.0253	*	Hypothetical protein
BT_3064	266.0206	-1.2969	2.07E-13	2.52E-11	****	Hypothetical protein
BT_3073	238.7517	-1.0020	3.99E-07	9.42E-06	****	TIM-barrel enzyme, putative dehydrogenase
BT_3098	**24.5727**	**-1.4480**	**0.0011**	**0.0070**	**	**Hypothetical protein**
BT_3138	**385.0040**	**-2.2741**	**1.92E-31**	**1.04E-28**	****	**Transmembrane protein**
BT_3139	74.2345	-1.3165	7.75E-05	8.13E-04	***	DNA binding protein
BT_3140	156.0088	-1.2034	1.43E-08	5.45E-07	****	DNA binding protein
BT_3154	19.1231	-1.9044	2.23E-04	0.0019	**	Two component system sensor kinase
BT_3166	58.8850	-1.3355	3.57E-05	4.26E-04	***	Conserved hypothetical protein
BT_3178	**62.9910**	**-1.2930**	**3.33E-05**	**4.05E-04**	***	**Beta-hexosaminidase precursor**
BT_3203	20.3862	-1.8406	0.0013	0.0081	**	Hypothetical protein
BT_3205	43.7318	-1.0207	0.0030	0.0159	*	Conserved hypothetical protein
BT_3217	56.7387	-1.2453	4.57E-05	5.26E-04	***	Conserved hypothetical protein
BT_3218	70.1253	-1.6118	1.12E-07	3.23E-06	****	Hypothetical protein
BT_3220	**528.3820**	**-2.5323**	**4.30E-38**	**4.06E-35**	****	**TPR-repeat containing protein**
BT_3221	287.9856	-1.4994	9.84E-18	1.96E-15	****	Hypothetical protein
BT_3262	38.4865	-1.1560	0.0018	0.0104	*	Conserved hypothetical protein
BT_3359	4743.5573	-1.0942	1.15E-20	2.56E-18	****	Acyl carrier protein
BT_3364	405.8464	-1.0347	4.79E-11	3.69E-09	****	Tyrosine protein kinase
BT_3402	**362.8163**	**-1.2457**	**3.25E-12**	**3.23E-10**	****	**Conserved hypothetical protein**
BT_3410	674.4084	-1.6441	8.66E-21	2.05E-18	****	Heavy metal-binding protein
BT_3430	**1235.9954**	**-2.1303**	**1.23E-07**	**3.49E-06**	****	**Ribosomal protein S20**
BT_t55	**97.5457**	**-3.0298**	**4.32E-23**	**1.26E-20**	****	**tRNA- Glu**
BT_3547	**25.6744**	**-1.4311**	**0.0017**	**0.0102**	*	**Hypothetical protein**
BT_3556	60.1874	-1.2063	6.99E-05	7.43E-04	***	Transcriptional regulator
BT_3570	55.5668	-1.0905	3.63E-04	0.0028	**	TPR-repeat containing protein

BT_3710	21.6362	-4.6167	5.58E-05	6.29E-04	***	50S ribosomal protein L34
BT_3747	35.9784	-2.9371	5.25E-10	2.79E-08	****	CoA-binding protein
BT_3748	30.5171	-1.1533	0.0063	0.0291	*	RNA polymerase sigma factor
BT_3769	**84.5712**	**-1.1696**	**1.85E-05**	**2.54E-04**	***	**Conserved hypothetical protein**
BT_3770	212.3284	-1.2142	1.05E-10	6.97E-09	****	Transcriptional regulator
BT_3865	**46.9726**	**-2.5138**	**2.51E-11**	**2.11E-09**	****	**Hypothetical protein**
BT_3879	48.1737	-1.5827	2.32E-06	4.26E-05	****	Translation initiation factor SUI1
BT_3901a	1793.8650	-1.0260	1.10E-09	5.12E-08	****	Conserved hypothetical membrane protein
BT_3989	65.2601	-1.6105	2.40E-07	6.01E-06	****	Hypothetical protein
BT_4005	182.9458	-1.3355	2.20E-10	1.32E-08	****	Conserved hypothetical protein
BT_4068	111.1964	-1.3772	6.52E-09	2.71E-07	****	Conserved hypothetical protein
BT_4235	220.6745	-1.0109	1.67E-07	4.57E-06	****	Hypothetical protein
BT_4314	**1830.1659**	**-1.4053**	**4.97E-17**	**8.93E-15**	****	**50S ribosomal protein L21**
BT_4356	**21.2597**	**-1.3799**	**0.0040**	**0.0205**	*	**Anti-sigma factor; FecR protein**
BT_4381	69.8517	-1.0845	1.56E-04	0.0014	**	Hypothetical protein
BT_4411	56.5357	-1.1372	1.86E-04	0.0016	**	Hypothetical protein
BT_4436	**95.2667**	**-1.2095**	**3.96E-06**	**6.87E-05**	****	**Bacterial Ig-like- group 2**
BT_4461	**36.9201**	**-1.3759**	**2.81E-04**	**0.0023**	**	**RNA polymerase sigma factor**
BT_4466	35.3356	-1.5353	6.14E-05	6.74E-04	***	HTH merR-type domain-containing protein
BT_4467	67.3487	-1.0575	4.84E-04	0.0036	**	Hypothetical protein
BT_4495	290.6160	-1.2969	7.97E-15	1.11E-12	****	Conserved hypothetical protein
BT_4528	31.1809	-1.0467	0.0096	0.0411	*	Metallophosphoesterase
BT_4529	45.7196	-1.1761	4.86E-04	0.0036	**	DNA-binding protein
BT_4534	**47.6943**	**-1.5363**	**2.03E-05**	**2.74E-04**	***	**Hypothetical protein**
BT_4590	275.8643	-1.3169	3.23E-13	3.81E-11	****	Conserved hypothetical protein
BT_4596	44.1340	-1.1238	0.0017	0.0100	**	Conserved hypothetical protein
BT_4646	103.9085	-1.2866	2.52E-07	6.27E-06	****	Conserved hypothetical protein
BT_4690	696.9397	-1.0009	4.99E-09	2.09E-07	****	Alpha-amylase precursor
BT_4697	201.9844	-1.1130	1.43E-07	3.96E-06	****	Transcriptional regulator
BT_4732	18.2497	-2.2052	1.04E-04	0.0010	**	Phage protein
BT_4733	38.5330	-1.4410	8.34E-05	8.60E-04	***	DNA-binding protein

BT_4755	557.4785	-1.0051	5.16E-10	2.79E-08	****	Two-component system sensor kinase
BT_p548204	114.0027	-1.5865	7.68E-09	3.12E-07	****	Zinc metalloprotease
BT_p548206	47.0202	-1.0486	0.0015	0.0093	**	Mobilization protein
BT_p548221	357.5256	-1.4207	9.31E-12	8.79E-10	****	Hypothetical protein
BT_p548225	31.5217	-1.1831	0.0033	0.0176	*	Hypothetical protein
BT_p548232	61.7491	-1.3259	4.80E-06	8.16E-05	****	Hypothetical protein
BT_p548236	96.4095	-1.0500	1.31E-05	1.85E-04	***	Hypothetical protein

Sup. Table 2: Table summarizing the significantly differentially expressed genes with a log2 fold change absolute value greater than or equal to 1 in the miR21 scramble treatment compared to the water control treatment.

Gene_ID	baseMean	log2 Fold Change	pvalue	padj	Padj. signif	Functional Category[8]
BT_0128	204.6404	-2.1714	7.36E-23	5.71E-20	****	Lipoprotein
BT_0189	39.4576	-1.2547	5.12E-04	0.0069	**	Anti-sigma factor
BT_0255	102.3007	-1.6459	2.12E-10	2.42E-08	****	Conserved hypothetical protein
BT_0256	213.3764	-1.4692	0.0023	0.0220	*	Conserved hypothetical protein
BT_0426	185.2470	-1.0181	1.22E-08	9.31E-07	****	Ferredoxin; iron-sulfur binding protein
BT_0631a	1721.0232	-1.0565	1.22E-16	4.30E-14	****	Conserved hypothetical protein
BT_0747	427.3499	-1.1504	1.36E-04	0.0023	**	phosphatidylinositol-4-phosphate 5-kinase
BT_0779	76.5593	-1.2190	1.85E-04	0.0029	**	Conserved hypothetical protein
BT_0784	1015.2597	-1.7177	5.65E-07	2.31E-05	****	RNA-binding protein
BT_0819	110.0082	-1.0500	1.61E-05	3.91E-04	***	Conserved hypothetical protein
BT_t10	37.5109	-1.4654	9.46E-05	0.0017	**	tRNA- Lys
BT_t11	29.0493	-1.8293	1.43E-04	0.0023	**	tRNA- Lys
BT_0914a	2516.2386	-1.3218	8.56E-04	0.0100	*	Conserved hypothetical protein
BT_0915	2670.3865	-1.4336	4.49E-04	0.0060	**	50S ribosomal protein L33
BT_0916	3653.7998	-1.3157	1.27E-04	0.0021	**	50S ribosomal protein L28
BT_t17	50.5673	-1.5072	5.00E-06	1.44E-04	***	tRNA-OTHER
BT_1232	16.9986	-1.8072	0.0025	0.0234	*	Hypothetical protein
BT_t26	161.6417	-1.0858	3.49E-07	1.54E-05	****	tRNA- Asp
BT_1435	1292.6420	-1.0335	2.90E-16	8.04E-14	****	Conserved hypothetical protein
BT_1456	36.5042	-1.1084	0.0033	0.0291	*	Thioredoxin
BT_1581	87.3340	-1.0531	2.73E-05	6.05E-04	***	Hypothetical protein
BT_1609	76.8266	-1.2084	5.83E-06	1.64E-04	***	Conserved hypothetical protein
BT_1612	79.5099	-1.2971	3.60E-06	1.08E-04	***	Conserved hypothetical protein
BT_1667	325.8446	-1.7668	0.0030	0.0268	*	Antitoxin
BT_1755	38.4929	-1.2455	0.0010	0.0117	*	24-amino acid repeat protein
BT_1811	245.8035	-1.3920	7.54E-04	0.0092	**	MerH regulator protein

[8] https://www.ncbi.nlm.nih.gov/data-hub/genome/GCA_000011065.1/

BT_1819	384.2671	-1.6678	4.77E-05	9.65E-04	***	Conserved hypothetical protein
BT_1862	855.0466	-1.0953	2.86E-04	0.0041	**	Lipoprotein
BT_1885	28.5905	-2.1502	2.92E-05	6.36E-04	***	ATP-dependent RNA helicase
BT_1886	105.1446	-1.5976	0.0052	0.0400	*	Oxidoreductase
BT_1887	326.8718	-1.8110	2.24E-04	0.0033	**	RNA-binding protein (rbpA)
BT_t34	125.6195	-1.1222	6.65E-07	2.63E-05	****	tRNA- Ser
BT_t36	38.7853	-1.6054	4.68E-05	9.51E-04	***	tRNA- Lys
BT_2280	50.2840	-1.5656	7.02E-06	1.91E-04	***	Transposase
BT_2361	47.9469	-1.0926	0.0018	0.0178	*	Conserved hypothetical protein, HTH Motif
BT_2435	111.9687	-1.2337	8.56E-06	2.23E-04	***	MarR family transcriptional regulator
BT_2466	20.2189	-1.5329	0.0042	0.0347	*	Conserved hypothetical protein
BT_2539	1979.3899	-1.8671	2.94E-04	0.0042	**	Rubredoxin
BT_t41	479.7940	-2.6518	2.19E-61	8.49E-58	****	tRNA- Pro
BT_t50	76.7915	-1.4603	8.44E-07	3.21E-05	****	tRNA- Asn
BT_t51	100.6242	-1.4423	9.03E-08	5.56E-06	****	tRNA- Asn
BT_3002	127.5196	-1.0859	5.89E-07	2.38E-05	****	Transcriptional regulator
BT_3058	162.6987	-1.0477	1.65E-08	1.23E-06	****	Transcriptional regulator
BT_3098	28.5398	-1.1495	0.0071	0.0498	*	Hypothetical protein
BT_3138	512.0319	-1.2719	2.30E-16	6.87E-14	****	Transmembrane protein
BT_3178	68.8535	-1.2138	8.67E-05	0.0016	**	Beta-hexosaminidase precursor
BT_3220	712.7767	-1.3776	3.26E-04	0.0046	**	TPR-repeat containing protein
BT_3402	402.2016	-1.1295	2.24E-14	4.58E-12	****	Conserved hypothetical protein
BT_3430	1572.6185	-1.3594	1.65E-29	3.21E-26	****	Ribosomal protein S20
BT_t55	109.7472	-2.6015	1.11E-21	7.17E-19	****	tRNA- Glu
BT_3547	29.6407	-1.1394	0.0057	0.0432	*	Hypothetical protein
BT_t57	119.2513	-1.0583	7.57E-07	2.94E-05	****	tRNA- Gly
BT_t58	48.3422	-1.1427	4.70E-04	0.0062	**	tRNA- Leu
BT_3769	91.5915	-1.1372	1.30E-05	3.20E-04	***	Conserved hypothetical protein
BT_3865	62.8696	-1.3669	8.07E-06	2.12E-04	***	Hypothetical protein
BT_3970	18.6581	-2.0942	6.97E-04	0.0087	**	Hypothetical protein
BT_4314	2194.9097	-1.0151	2.70E-26	3.49E-23	****	50S ribosomal protein L21

BT_4356	22.7234	-1.4057	0.0029	0.0265	*	Anti-sigma factor; FecR protein
BT_4436	103.3142	-1.1692	3.18E-07	1.45E-05	****	Bacterial Ig-like- group 2
BT_4461	43.0823	-1.0477	0.0031	0.0279	*	RNA polymerase sigma factor
BT_4534	57.2433	-1.0754	0.0015	0.0156	*	Hypothetical protein
BT_4542	29.0447	-1.2849	0.0022	0.0210	*	Type I Restriction enzyme
BT_t70	16.1463	-1.7678	0.0027	0.0250	*	tRNA- Ser

Sup. Table 3: Table summarizing the significantly differentially expressed genes with a log2 fold change absolute value greater than or equal to 1 in the small RNA control treatment compared to the water control treatment.

Gene_ID	baseMean	log2 Fold Change	pvalue	padj	Padj. signif	Functional Category[9]
BT_4693	330.9426	-1.1619	1.01E-15	2.44E-12	****	Cation efflux system protein
BT_4694	1051.6810	-1.1426	2.54E-17	1.22E-13	****	Cation efflux system protein
BT_4695	240.9785	-1.1529	1.62E-12	1.95E-09	****	Outer membrane efflux protien

[9] https://www.ncbi.nlm.nih.gov/data-hub/genome/GCA_000011065.1/

Sup. Table 4: Table summarizing the significantly differentially abundant ASVs in the different incubations with fluorescently labelled miRNAs.

Incubation with miR21: Atto488+ vs Atto488-					
	log2 Fold Change	**P val**	**Family**	**Genus**	**Species**
ASV_inb_ek4	-2.1879	7.2888E-11	Ruminococcaceae	Faecalibacterium	
ASV_i0z_5sv	4.3799	1.7696E-05	NA	NA	
ASV_jhl_q2w	2.0424	1.1345E-04	Ruminococcaceae	Ruminococcus	*bromii*
ASV_mbt_8vr	-1.4799	6.3829E-04	Lachnospiraceae	Agathobacter	
ASV_rpj_tca	2.8971	1.7107E-03	Oscillospiraceae	NK4A214 group	
ASV_k9o_dhg	3.9691	1.7620E-03	Ruminococcaceae	Ruminococcus	*bicirculans*
ASV_lfk_egf	-5.6767	3.6462E-03	Pseudomonadaceae	Pseudomonas	*veronii*
ASV_qvd_ehk	-2.1866	3.6462E-03	Erysipelatoclostridiaceae	Erysipelotrichaceae UCG-003	*bacterium*
ASV_t0z_6xv	2.0263	3.6462E-03	Bacteroidaceae	Bacteroides	*uniformis*
ASV_l2c_318	5.8082	4.3898E-03	Lactobacillaceae	HT002	
ASV_ai2_vbg	-1.2000	6.6726E-03	Ruminococcaceae	Faecalibacterium	
ASV_des_z79	3.1665	7.0852E-03	Veillonellaceae	Dialister	*invisus*
ASV_oha_idz	-2.5759	7.0852E-03	Lachnospiraceae	Lachnoclostridium	
ASV_qwa_h7y	-1.1897	7.4205E-03	Streptococcaceae	Streptococcus	
ASV_5am_qao	-1.4053	1.1917E-02	Ruminococcaceae	Faecalibacterium	*prausnitzii*
ASV_6f6_qy5	2.4072	1.1917E-02	Veillonellaceae	Dialister	
ASV_crs_b8j	2.7779	2.1678E-02	[Eubacterium] coprostanoligenes group	NA	
ASV_o8p_kmj	2.8953	2.1678E-02	Lachnospiraceae	Coprococcus	
ASV_tqb_amk	4.4042	2.1678E-02	[Eubacterium] coprostanoligenes group	NA	
ASV_4qc_wxb	-4.9744	2.3220E-02	Aeromonadaceae	Aeromonas	*veronii*
Incubation with miR21 scramble: Atto488+ vs Atto488-					
	log2 Fold Change	**P val**	**Family**	**Genus**	**Speies**
ASV_dhe_3st	-5.3715	2.1803E-04	Lachnospiraceae	Blautia	*stercoris*
ASV_mih_bqq	-1.5502	2.8055E-03	Lachnospiraceae	Fusicatenibacter	*saccharivorans*
ASV_inb_ek4	-2.1517	6.0716E-03	Ruminococcaceae	Faecalibacterium	

ASV_i0z_5sv	2.2016	6.2088E-03	NA	NA	
ASV_ai2_vbg	-1.8288	9.2122E-03	Ruminococcaceae	Faecalibacterium	
ASV_jhl_q2w	1.7397	9.2122E-03	Ruminococcaceae	Ruminococcus	*bromii*
ASV_o8p_kmj	5.0312	9.2122E-03	Lachnospiraceae	Coprococcus	
ASV_kvw_phv	-3.5862	3.0834E-02	Bacteroidaceae	Bacteroides	*finegoldii*
ASV_bon_cub	3.8240	3.2750E-02	Oscillospiraceae	UCG-005	
ASV_rpj_tca	2.4878	3.2750E-02	Oscillospiraceae	NK4A214 group	
ASV_l2c_318	5.2083	3.6483E-02	Lactobacillaceae	HT002	
Incubation with miRNAs: Atto488+ vs Atto488-					
	log2 Fold Change	**P val**	**Family**	**Genus**	**Species**
ASV_inb_ek4	-1.9736	1.2705E-12	Ruminococcaceae	Faecalibacterium	
ASV_rpj_tca	2.8983	3.7268E-07	Oscillospiraceae	NK4A214 group	
ASV_des_z79	2.9464	5.5872E-06	Veillonellaceae	Dialister	*invisus*
ASV_dhe_3st	-3.7305	5.5872E-06	Lachnospiraceae	Blautia	*stercoris*
ASV_o8p_kmj	3.8059	6.5952E-06	Lachnospiraceae	Coprococcus	
ASV_6f6_qy5	2.4428	1.0635E-05	Veillonellaceae	Dialister	
ASV_4qc_wxb	-6.5399	1.1295E-05	Aeromonadaceae	Aeromonas	*antarctica/ …/veronii*
ASV_l2c_318	5.6868	1.1308E-05	Lactobacillaceae	HT002	
ASV_i0z_5sv	3.0109	1.5839E-05	NA	NA	
ASV_k9o_dhg	2.7736	2.8649E-05	Ruminococcaceae	Ruminococcus	*bicirculans*
ASV_lfk_egf	-5.7304	3.1333E-05	Pseudomonadaceae	Pseudomonas	*antarctica/ …/veronii*
ASV_ai2_vbg	-1.2746	8.5224E-04	Ruminococcaceae	Faecalibacterium	
ASV_t0z_6xv	2.0788	8.5554E-04	Bacteroidaceae	Bacteroides	*uniformis*
ASV_tqb_amk	2.8641	1.4218E-03	[Eubacterium] coprostanoligenes group	NA	
ASV_jhl_q2w	2.0678	1.9670E-03	Ruminococcaceae	Ruminococcus	*bromii*
ASV_crs_b8j	2.1139	2.4905E-03	[Eubacterium] coprostanoligenes group	NA	
ASV_dk6_hg6	3.6368	2.4905E-03	Ruminococcaceae	Ruminococcus	
ASV_p2f_btm	-2.5927	2.4905E-03	Coriobacteriaceae	Collinsella	aerofaciens
ASV_bon_cub	2.6477	2.5874E-03	Oscillospiraceae	UCG-005	

ASV_cme_yc0	-4.9830	2.5874E-03	Pseudomonadaceae	Pseudomonas	*amygdali/…/tremae*
ASV_kvw_phv	-2.2305	2.8009E-03	Bacteroidaceae	Bacteroides	*finegoldii*
ASV_g7t_4vv	2.4363	3.5915E-03	Christensenellaceae	Christensenellaceae R-7 group	
ASV_qvd_ehk	-1.5097	3.5915E-03	Erysipelatoclostridiaceae	Erysipelotrichaceae UCG-003	*bacterium*
ASV_mbt_8vr	-1.1197	4.3481E-03	Lachnospiraceae	Agathobacter	
ASV_e9e_cr1	1.6679	4.5856E-03	Erysipelatoclostridiaceae	Catenibacterium	*mitsuokai*
ASV_mih_bqq	-1.0597	4.5856E-03	Lachnospiraceae	Fusicatenibacter	*saccharivorans*
ASV_qwa_h7y	-0.9968	4.7261E-03	Streptococcaceae	Streptococcus	
ASV_oha_idz	-2.0268	6.1683E-03	Lachnospiraceae	Lachnoclostridium	
ASV_1li_4fx	3.9060	7.0028E-03	Bacteroidaceae	Bacteroides	*cellulosilyticus/intestinalis/timonensis*
ASV_jxs_w1n	2.4136	7.1086E-03	Butyricicoccaceae	Butyricicoccus	
ASV_60x_hhi	-4.4464	9.5729E-03	Yersiniaceae	Yersinia	
ASV_ao4_xcw	3.7741	1.6209E-02	NA	NA	
ASV_lmo_pcd	3.6722	2.2390E-02	Oscillospiraceae	NA	
ASV_ekf_88p	2.1488	2.7691E-02	Rikenellaceae	Alistipes	*putredinis*
ASV_26g_hup	3.8537	3.0098E-02	Lachnospiraceae	[Eubacterium] ventriosum group	
ASV_kre_aut	2.3867	3.0098E-02	Lachnospiraceae	Lachnospiraceae NK4A136 group	
ASV_lvi_a0p	1.9760	3.0098E-02	Lachnospiraceae	Coprococcus	*eutactus*
ASV_7w6_t4q	1.3890	3.1070E-02	Streptococcaceae	Streptococcus	*australis/…/sanguinis*
Incubation with miRNAs: miR21 Atto488+ vs miR21 scramble Atto488+					
	log2 Fold Change	**P val**	**Family**	**Genus**	**Species**
ASV_jhl_q2w	-1.7514	2.7601E-03	Ruminococcaceae	Ruminococcus	*bromii*

8.0 References

Ahmed, F. E., Jeffries, C. D., Vos, P. W., Flake, G., Nuovo, G. J., Sinar, D. R., Naziri, W., & Marcuard, S. P. (2009). Diagnostic microRNA markers for screening sporadic human colon cancer and active ulcerative colitis in stool and tissue. *Cancer Genomics and Proteomics*, *6*(5).

Apprill, A., Mcnally, S., Parsons, R., & Weber, L. (2015). Minor revision to V4 region SSU rRNA 806R gene primer greatly increases detection of SAR11 bacterioplankton. *Aquatic Microbial Ecology*, *75*(2).

Aravind, L., Anantharaman, V., Balaji, S., Babu, M. M., & Iyer, L. M. (2005). The many faces of the helix-turn-helix domain: Transcription regulation and beyond. In *FEMS Microbiology Reviews,* 29(2).

Ardekani, A. M., & Naeini, M. M. (2010). The role of microRNAs in human diseases. In *Avicenna Journal of Medical Biotechnology,* 2(4).

Arijs, I., De Hertogh, G., Lemaire, K., Quintens, R., Van Lommel, L., Van Steen, K., Leemans, P., Cleynen, I., Van Assche, G., Vermeire, S., Geboes, K., Schuit, F., & Rutgeerts, P. (2009). Mucosal gene expression of antimicrobial peptides in inflammatory bowel disease before and after first infliximab treatment. *PLoS ONE*, *4*(11).

Arumugam M., Raes J., Pelletier E., Le Paslier D., Yamada T., Mende D.R., Fernandes G.R., Tap J., Bruls T., Batto J.M., *et al.* (2011). Enterotypes of the human gut microbiome. *Nature,* 473.

Aseev, L. V., Koledinskaya, L. S., & Boni, I. V. (2016). Regulation of ribosomal protein operons rplM-rpsI, rpmB-rpmG, and rplU-rpmA at the transcriptional and translational levels. *Journal of Bacteriology*, *198*(18).

Bäckhed, F., Ding, H., Wang, T., Hooper, L. V., Gou, Y. K., Nagy, A., Semenkovich, C. F., & Gordon, J. I. (2004). The gut microbiota as an environmental factor that regulates fat storage. *Proceedings of the National Academy of Sciences of the United States of America*, *101*(44).

Balomenou, S., Fouet, A., Tzanodaskalaki, M., Couture-Tosi, E., Bouriotis, V., & Boneca, I. G. (2013). Distinct functions of polysaccharide deacetylases in cell shape, neutral polysaccharide synthesis and virulence of Bacillus anthracis. *Molecular Microbiology*, *87*(4).

Balthazar, C. F., Guimarães, J. F., Coutinho, N. M., Pimentel, T. C., Ranadheera, C. S., Santillo, A., Albenzio, M., Cruz, A. G., & Sant'Ana, A. S. (2022). The future of functional food: Emerging technologies application on prebiotics, probiotics and postbiotics. *Comprehensive Reviews in Food Science and Food Safety*, *21*(3).

Bartel, D. P. (2018). Metazoan MicroRNAs. In *Cell*, 173(1).

Bechhofer, D. H., & Deutscher, M. P. (2019). Bacterial ribonucleases and their roles in RNA metabolism. *Critical Reviews in Biochemistry and Molecular Biology*, *54*(3).

Béchon, N., Mihajlovic, J., Vendrell-Fernández, S., Chain, F., Langella, P., Beloin, C., & Ghigo, J. M. (2020). Capsular polysaccharide cross-regulation modulates bacteroides thetaiotaomicron biofilm formation. *MBio*, *11*(3).

Bengmark, S. (2001). Pre-, pro- and synbiotics. In *Current Opinion in Clinical Nutrition and Metabolic Care,* 4(6).

Bi, K., Zhang, X., Chen, W., & Diao, H. (2020). Micrornas regulate intestinal immunity and gut microbiota for gastrointestinal health: A comprehensive review. In *Genes*, 11(9).

Callahan, B. J., McMurdie, P. J., Rosen, M. J., Han, A. W., Johnson, A. J. A., and Holmes, S. P. (2016a). DADA2: high-resolution sample inference from Illumina amplicon data. *Nat. Methods* 13.

Callahan, B. J., Sankaran, K., Fukuyama, J. A., McMurdie, P. J., and Holmes, S. P. (2016b). Bioconductor workflow for microbiome data analysis: from raw reads to community analyses. *F1000Res.* 5.

Cao, B., Zhou, X., Ma, J. *et al.* (2017). Role of MiRNAs in Inflammatory Bowel Disease. *Dig Dis Sci,* 62.

Cao, Y., Förstner, K. U., Vogel, J., & Jeffrey Smith, C. (2016). cis-encoded small RNAs, a conserved mechanism for repression of polysaccharide utilization in Bacteroides. *Journal of Bacteriology*, *198*(18).

Casado-Bedmar, M., & Viennois, E. (2022). MicroRNA and Gut Microbiota: Tiny but Mighty-Novel Insights into Their Cross-talk in Inflammatory Bowel Disease Pathogenesis and Therapeutics. *Journal of Crohn's and Colitis*, *16*(6).

Cerutti, H., & Casas-Mollano, J. A. (2006). On the origin and functions of RNA-mediated silencing: From protists to man. In *Current Genetics* (Vol. 50, Issue 2).

Cheng, A. M., Byrom, M. W., Shelton, J., & Ford, L. P. (2005). Antisense inhibition of human miRNAs and indications for an involvement of miRNA in cell growth and apoptosis. *Nucleic Acids Research*, *33*(4).

Chen, L. M., Bao, C. H., Wu, Y., Liang, S. H., Wang, D., Wu, L. Y., Huang, Y., Liu, H. R., & Wu, H. G. (2021). Tryptophan-kynurenine metabolism: a link between the gut and brain for depression in inflammatory bowel disease. In *Journal of Neuroinflammation*, 18(1).

Chen, X., Ba, Y., Ma, L., Cai, X., Yin, Y., Wang, K., Guo, J., Zhang, Y., Chen, J., Guo, X., Li, Q., Li, X., Wang, W., Zhang, Y., Wang, J., Jiang, X., Xiang, Y., Xu, C., Zheng, P., … Zhang, C. Y. (2008). Characterization of microRNAs in serum: A novel class of biomarkers for diagnosis of cancer and other diseases. *Cell Research*, *18*(10).

Cholet, F., Ijaz, U. Z., & Smith, C. J. (2019). Differential ratio amplicons (R amp) for the evaluation of RNA integrity extracted from complex environmental samples. *Environmental Microbiology*, *21*(2).

Cresci, G. A., & Bawden, E. (2015). Gut microbiome: What we do and don't know. In *Nutrition in Clinical Practice*, 30(6).

Dahlhamer, J. M., Zammitti, E. P., Ward, B. W., Wheaton, A. G., & Croft, J. B. (2015). *Morbidity and Mortality Weekly Report Prevalence of Inflammatory Bowel Disease Among Adults Aged ≥18 Years-United States, 2015*.

Dennis Lo, Y. M., Corbetta, N., Chamberlain, P. F., Rai, V., Sargent, I. L., Redman, C. W. G., & Wainscoat, J. S. (1997). Presence of fetal DNA in maternal plasma and serum. *Lancet*, *350*(9076).

Ding, T., & Schloss, P. D. (2014). Dynamics and associations of microbial community types across the human body. *Nature*, *509*(7500).

Feuerstadt, P., Louie, T. J., Lashner, B., Wang, E. E. L., Diao, L., Bryant, J. A., Sims, M., Kraft, C. S., Cohen, S. H., Berenson, C. S., Korman, L. Y., Ford, C. B., Litcofsky, K. D., Lombardo, M.-J., Wortman, J. R., Wu, H., Auniņš, J. G., McChalicher, C. W. J., Winkler, J. A., … von Moltke, L. (2022). SER-109, an Oral Microbiome Therapy for Recurrent Clostridioides difficile Infection . *New England Journal of Medicine*, *386*(3).

Flanagan, K., Vesley, C., Gawish R., Berry D., Pereira, F. C. (2022). "Dynamics of Associations between Host-Derived MicroRNAs with Human Gut Microbiota." *37. Jahrestagung der Österreichischen Gesellschaft für Hygiene, Mikrobiologie und Präventivmedizin (ÖGHMP),* Abstract.

Ge, Xiaowei *et al.* (2022). “SRS-FISH: A high-throughput platform linking microbiome metabolism to identity at the single-cell level.” *Proceedings of the National Academy of Sciences of the United States of America*, 119(26).

Gevers, D., Knight, R., Petrosino, J. F., Huang, K., McGuire, A. L., Birren, B. W., Nelson, K. E., White, O., Methé, B. A., & Huttenhower, C. (2012). The Human Microbiome Project: A Community Resource for the Healthy Human Microbiome. *PLoS Biology*, *10*(8).

Glowacki, R. W. P., Pudlo, N. A., Tuncil, Y., Luis, A. S., Sajjakulnukit, P., Terekhov, A. I., Lyssiotis, C. A., Hamaker, B. R., & Martens, E. C. (2020). A Ribose-Scavenging System Confers Colonization Fitness on the Human Gut Symbiont Bacteroides thetaiotaomicron in a Diet-Specific Manner. *Cell Host and Microbe*, *27*(1).

Guh, A. Y., & Kutty, P. K. (2018). Clostridioides difficile infection. In *Annals of Internal Medicine*, 169(7).

Harfe, B. D., McManus, M. T., Mansfield, J. H., Hornstein, E., & Tabin, C. J. (2005). The RNaseIII enzyme Dicer is required for morphogenesis but not patterning of the vertebrate limb. *Proceedings of the National Academy of Sciences of the United States of America*, *102*(31).

Heintz-Buschart, A., & Wilmes, P. (2018). Human Gut Microbiome: Function Matters. In *Trends in Microbiology*, 26(7).

Herbold, C. W., Pelikan, C., Kuzyk, O., Hausmann, B., Angel, R., Berry, D., & Loy, A. (2015). A flexible and economical barcoding approach for highly multiplexed amplicon sequencing of diverse target genes. *Frontiers in Microbiology*, *6(*JUL*)*.

Hill, C., Guarner, F., Reid, G., Gibson, G. R., Merenstein, D. J., Pot, B., Morelli, L., Canani, R. B., Flint, H. J., Salminen, S., Calder, P. C., & Sanders, M. E. (2014). The International Scientific Association for Probiotics and Prebiotics consensus statement on the scope and appropriate use of the term probiotic. *Nature Reviews Gastroenterology & Hepatology*, *11*(8).

Hooper, L. V., Midwedt, T., & Gordon, J. I. (2002). How host-microbial interactions shape the nutrient environment of the mammalian intestine. In *Annual Review of Nutrition*, 22.

Huntzinger, E., & Izaurralde, E. (2011). Gene silencing by microRNAs: Contributions of translational repression and mRNA decay. In *Nature Reviews Genetics*, 12(2).

Huttenhower, C., Gevers, D., Knight, R., Abubucker, S., Badger, J. H., Chinwalla, A. T., Creasy, H. H., Earl, A. M., Fitzgerald, M. G., Fulton, R. S., Giglio, M. G., Hallsworth-Pepin, K., Lobos, E. A., Madupu, R., Magrini, V., Martin, J. C., Mitreva, M., Muzny, D. M., Sodergren, E. J., … White, O. (2012). Structure, function and diversity of the healthy human microbiome. *Nature*, *486*(7402).

Iborra, M., Bernuzzi, F., Correale, C., Vetrano, S., Fiorino, G., Beltrán, B., Marabita, F., Locati, M., Spinelli, A., Nos, P., Invernizzi, P., & Danese, S. (2013). Identification of serum and tissue micro-RNA expression profiles in different stages of inflammatory bowel disease. *Clinical and Experimental Immunology*, *173*(2).

James, J. P., Riis, L. B., Malham, M., Høgdall, E., Langholz, E., & Nielsen, B. S. (2020). MicroRNA biomarkers in IBD-differential diagnosis and prediction of colitis-associated cancer. In *International Journal of Molecular Sciences*, 21(21).

Janas, M. M., Wang, E., Love, T., Harris, A. S., Stevenson, K., Semmelmann, K., Shaffer, J. M., Chen, P. H., Doench, J. G., Yerramilli, S. V. B. K., Neuberg, D. S., Iliopoulos, D., Housman, D. E., Burge, C. B., & Novina, C. D. (2012). Reduced Expression of Ribosomal Proteins Relieves MicroRNA-Mediated Repression. *Molecular Cell*, *46*(2).

Jenkins, T. A., Nguyen, J. C. D., Polglaze, K. E., & Bertrand, P. P. (2016). Influence of tryptophan and serotonin on mood and cognition with a possible role of the gut-brain axis. In *Nutrients*, 8(1).

Johnston, D. G. W., Williams, M. A., Thaiss, C. A., Cabrera-Rubio, R., Raverdeau, M., McEntee, C., Cotter, P. D., Elinav, E., O'Neill, L. A. J., & Corr, S. C. (2018). Loss of microRNA-21 influences the gut microbiota, causing reduced susceptibility in a murine model of colitis. *Journal of Crohn's and Colitis*, *12*(7).

Jo, M. H., Shin, S., Jung, S. R., Kim, E., Song, J. J., & Hohng, S. (2015). Human Argonaute 2 Has Diverse Reaction Pathways on Target RNAs. *Molecular Cell*, *59*(1).

Kamada, N., Seo, S. U., Chen, G. Y., & Núñez, G. (2013). Role of the gut microbiota in immunity and inflammatory disease. In *Nature Reviews Immunology*, 13(5).

Khan, I., Ullah, N., Zha, L., Bai, Y., Khan, A., Zhao, T., Che, T., & Zhang, C. (2019). Alteration of gut microbiota in inflammatory bowel disease (IBD): Cause or consequence? IBD treatment targeting the gut microbiome. In *Pathogens*, 8(3).

Kreuzer-Redmer S, Bekurtz JC, Arends D, Bortfeldt R, Kutz-Lohroff B, Sharbati S, Einspanier R, Brockmann GA. Feeding of Enterococcus faecium NCIMB 10415 Leads to Intestinal miRNA-423-5p-Induced Regulation of Immune-Relevant Genes. Appl Environ Microbiol. 2016.

Kriss, M., Hazleton, K. Z., Nusbacher, N. M., Martin, C. G., & Lozupone, C. A. (2018). Low diversity gut microbiota dysbiosis: drivers, functional implications and recovery. In *Current Opinion in Microbiology*, 44.

Kuzmenko, Anton et al. “DNA targeting and interference by a bacterial Argonaute nuclease.” *Nature* vol. 587(7835). 2020.

Lawrie, C. H., Gal, S., Dunlop, H. M., Pushkaran, B., Liggins, A. P., Pulford, K., Banham, A. H., Pezzella, F., Boultwood, J., Wainscoat, J. S., Hatton, C. S. R., & Harris, A. L. (2008). Detection of elevated levels of tumour-associated microRNAs in serum of patients with diffuse large B-cell lymphoma. *British Journal of Haematology*, *141*(5).

LeBlanc, J. G., Milani, C., de Giori, G. S., Sesma, F., van Sinderen, D., & Ventura, M. (2013). Bacteria as vitamin suppliers to their host: A gut microbiota perspective. In *Current Opinion in Biotechnology*, 24(2).

Lee, Y., Kim, M., Han, J., Yeom, K. H., Lee, S., Baek, S. H., & Kim, V. N. (2004). MicroRNA genes are transcribed by RNA polymerase II. *EMBO Journal*, *23*(20).

Li, K., Bihan, M., & Methé, B. A. (2013). Analyses of the Stability and Core Taxonomic Memberships of the Human Microbiome. *PLoS ONE*, *8*(5).

Liao Y., Smyth G. K., Shi W. (2014). Feature counts: an efficient general purpose program for assigning sequence reads to genomic features. *Bioinformatics* 30

Lisitskaya, L., Shin, Y., Agapov, A. *et al.* Programmable RNA targeting by bacterial Argonaute nucleases with unconventional guide binding and cleavage specificity. *Nat Commun* 13(4624). 2022.

Liu, S., Da Cunha, A. P., Rezende, R. M., Cialic, R., Wei, Z., Bry, L., Comstock, L. E., Gandhi, R., & Weiner, H. L. (2016). The Host Shapes the Gut Microbiota via Fecal MicroRNA. *Cell Host and Microbe*, *19*(1).

Liu, S., Rezende, R. M., Moreira, T. G., Tankou, S. K., Cox, L. M., Wu, M., Song, A., Dhang, F. H., Wei, Z., Costamagna, G., & Weiner, H. L. (2019). Oral Administration of miR-30d from Feces of MS Patients Suppresses MS-like Symptoms in Mice by Expanding Akkermansia muciniphila. *Cell Host and Microbe*, *26*(6).

Love, M. I., Huber, W., and Anders, S. (2014). Moderated estimation of fold change and dispersion for RNA-seq data with DESeq2. Genome Biol. 15(550).

Lu, L., Li, J., Moussaoui, M., & Boix, E. (2018). Immune modulation by human secreted RNases at the extracellular space. In *Frontiers in Immunology*, 9(MAY).

Méndez-Salazar, E. O., Ortiz-López, M. G., Granados-Silvestre, M. D. L. Á., Palacios-González, B., & Menjivar, M. (2018). Altered gut microbiota and compositional changes in firmicutes

and proteobacteria in mexican undernourished and obese children. *Frontiers in Microbiology*, *9*(OCT).

Michaux, C., Holmqvist, E., Vasicek, E., Sharan, M., Barquist, L., Westermann, A. J., Gunn, J. S., & Vogel, J. (2017). RNA target profiles direct the discovery of virulence functions for the cold-shock proteins CspC and CspE. *Proceedings of the National Academy of Sciences of the United States of America*, *114*(26).

Michielan, A., & D'Incà, R. (2015). Intestinal Permeability in Inflammatory Bowel Disease: Pathogenesis, Clinical Evaluation, and Therapy of Leaky Gut. In *Mediators of Inflammation*, 2015.

Mori, M. A., Ludwig, R. G., Garcia-Martin, R., Brandão, B. B., & Kahn, C. R. (2019). Extracellular miRNAs: From Biomarkers to Mediators of Physiology and Disease. In *Cell Metabolism*, 30(4).

Myhrstad, M. C. W., Tunsjø, H., Charnock, C., & Telle-Hansen, V. H. (2020). Dietary fiber, gut microbiota, and metabolic regulation—current status in human randomized trials. In *Nutrients*, 12(3).

Neumeier, J. and Meister, G. (2021). siRNA Specificity: RNAi Mechanisms and Strategies to Reduce Off-Target Effects. *Front. Plant Sci.*

Nguyen, T. A., Jo, M. H., Choi, Y. G., Park, J., Kwon, S. C., Hohng, S., Kim, V. N., & Woo, J. S. (2015). Functional anatomy of the human microprocessor. *Cell*, *161*(6).

Nikolaus, S., Schulte, B., Al-Massad, N., Thieme, F., Schulte, D. M., Bethge, J., Rehman, A., Tran, F., Aden, K., Häsler, R., Moll, N., Schütze, G., Schwarz, M. J., Waetzig, G. H., Rosenstiel, P., Krawczak, M., Szymczak, S., & Schreiber, S. (2017). Increased Tryptophan Metabolism Is Associated With Activity of Inflammatory Bowel Diseases. *Gastroenterology*, *153*(6).

Nishino, K., Yamasaki, S., Nakashima, R., Zwama, M., & Hayashi-Nishino, M. (2021). Function and Inhibitory Mechanisms of Multidrug Efflux Pumps. In *Frontiers in Microbiology* (Vol. 12). Frontiers Media S.A.

O'Brien, J., Hayder, H., Zayed, Y., & Peng, C. (2018). Overview of microRNA biogenesis, mechanisms of actions, and circulation. In *Frontiers in Endocrinology*, 9(AUG).

Okumura, R., & Takeda, K. (2017). Roles of intestinal epithelial cells in the maintenance of gut homeostasis. In *Experimental and Molecular Medicine*, 49(5).

Overbeeke A, Hausmann B, Nikolov G, Pereira FC, Herbold CW and Berry D (2022). "Nutrient niche specificity for glycosaminoglycans is reflected in polysaccharide utilization locus architecture of gut Bacteroides species." *Front. Microbiol.,* 13(1033355).

Parada AE, Needham DM, Fuhrman JA. Every base matters: assessing small subunit rRNA primers for marine microbiomes with mock communities, time series and global field samples. Environ Microbiol. 2016.

Parker, A., & Gottesman, S. (2016). Small RNA Regulation of TolC, the Outer Membrane Component of Bacterial Multidrug Transporters. *Journal of Bacteriology*, *198*(7).

Pasquinelli, A. E., Reinhart, B. J., Slack, F., Martindale, M. Q., Kuroda, M. I., Maller, B., Hayward, D. C., Ball, E. E., Degnan, B., Müller, P., Spring, J., Srinivasan, A., Fishman, M., Finnerty, J., Corbo, J., Levine, M., Leahy, P., Davidson, E., & Ruvkun, G. (2000). Conservation of the sequence and temporal expression of let-7 heterochronic regulatory RNA. *Nature*, *408*(6808).

Patangia, D. V., Anthony Ryan, C., Dempsey, E., Paul Ross, R., & Stanton, C. (2022). Impact of antibiotics on the human microbiome and consequences for host health. In *MicrobiologyOpen*, 11(1).

Peng, Y., & Croce, C. M. (2016). The role of microRNAs in human cancer. In *Signal Transduction and Targeted Therapy*, 1.

Peterson, J., Garges, S., Giovanni, M., McInnes, P., Wang, L., Schloss, J. A., Bonazzi, V., McEwen, J. E., Wetterstrand, K. A., Deal, C., Baker, C. C., Di Francesco, V., Howcroft, T. K., Karp, R. W., Lunsford, R. D., Wellington, C. R., Belachew, T., Wright, M., Giblin, C., … Guyer, M. (2009). The NIH Human Microbiome Project. *Genome Research*, *19*(12).

Petkovic, Marija *et al.* (2020). "Mechanistic Actions of microRNAs in Diabetic Wound Healing." *Cells* , 9(10).

Piquer-Esteban, S., Ruiz-Ruiz, S., Arnau, V., Diaz, W., & Moya, A. (2022). Exploring the universal healthy human gut microbiota around the World. *Computational and Structural Biotechnology Journal*, *20*.

Pither, M. D., Illiano, A., Pagliuca, C., Jacobson, A., Mantova, G., Stornaiuolo, A., Colicchio, R., Vitiello, M., Pinto, G., Silipo, A., Fischbach, M. A., Salvatore, P., Amoresano, A., Molinaro, A., & Di Lorenzo, F. (2022). Bacteroides thetaiotaomicron rough-type lipopolysaccharide: The chemical structure and the immunological activity. *Carbohydrate Polymers*, *297*, 120040.

Pjevac, P., Hausmann, B., Schwarz, J., Kohl, G., Herbold, C. W., Loy, A., & Berry, D. (2021). An Economical and Flexible Dual Barcoding, Two-Step PCR Approach for Highly Multiplexed Amplicon Sequencing. *Frontiers in Microbiology*, *12*.

Plotnikova, O., Baranova, A., & Skoblov, M. (2019). Comprehensive Analysis of Human microRNA–mRNA Interactome. *Frontiers in Genetics*, *10*.

Prezza, G., Ryan, D., Mädler, G., Reichardt, S., Barquist, L., & Westermann, A. J. (2022). Comparative genomics provides structural and functional insights into Bacteroides RNA biology. *Molecular Microbiology*, *117*(1).

Qiu, P., Ishimoto, T., Fu, L., Zhang, J., Zhang, Z., & Liu, Y. (2022). The Gut Microbiota in Inflammatory Bowel Disease. In *Frontiers in Cellular and Infection Microbiology*, 12.

Rangel F, Enes P, Gasco L, Gai F, Hausmann B, Berry D, Oliva-Teles A, Serra CR and Pereira FC (2022) Differential Modulation of the European Sea Bass Gut Microbiota by Distinct Insect Meals. *Front. Microbiol,* 13(831034).

Rinninella E, Raoul P, Cintoni M, Franceschi F, Miggiano GAD, Gasbarrini A, Mele MC. What is the Healthy Gut Microbiota Composition? A Changing Ecosystem across Age, Environment, Diet, and Diseases. Microorganisms. 2019.

Rojas-Feria, M., Romero-García, T., Caballero-Rico, J. Á. F., Ramírez, H. P., Avilés-Recio, M., Castro-Fernandez, M., Porcuna, N. C., Romero-Gómez, M., García, F., Grande, L., & Del Campo, J. A. (2018). Modulation of faecal metagenome in Crohn's disease: Role of microRNAs as biomarkers. *World Journal of Gastroenterology*, *24*(46).

Rosenbaum, M., Knight, R., & Leibel, R. L. (2015). The gut microbiota in human energy homeostasis and obesity. In *Trends in Endocrinology and Metabolism*, 26(9).

Ro, Y. T., Jo, G. H., Jung, S. A., Lee, E. H., Shin, J., & Lee, J. H. (2018). Salmonella-induced miR-155 enhances necroptotic death in macrophage cells via targeting RIP1/3. *Molecular Medicine Reports*, *18*(6).

Rusk, N. (2012). Prokaryotic RNAi. *Nature Methods*, *9*(3).

Sainio, E. L., Pulkki, K., & Young, S. N. (1996). L-Tryptophan: Biochemical, nutritional and pharmacological aspects. In *Amino Acids* (Vol. 10, Issue 1).

Sarshar, M., Scribano, D., Ambrosi, C., Palamara, A. T., & Masotti, A. (2020). Fecal microrna as innovative biomarkers of intestinal diseases and effective players in hostmicrobiome interactions. In *Cancers*, 12(8).

Sberro, H., Fremin, B. J., Zlitni, S., Edfors, F., Greenfield, N., Snyder, M. P., Pavlopoulos, G. A., Kyrpides, N. C., & Bhatt, A. S. (2019). Large-Scale Analyses of Human Microbiomes Reveal Thousands of Small, Novel Genes. *Cell*, *178*(5).

Shabalina, S. A., & Koonin, E. V. (2008). Origins and evolution of eukaryotic RNA interference. In *Trends in Ecology and Evolution*, 23(10).

Sharon, I., Quijada, N. M., Pasolli, E., Fabbrini, M., Vitali, F., Agamennone, V., Dötsch, A., Selberherr, E., Grau, J. H., Meixner, M., Liere, K., Ercolini, D., de Filippo, C., Caderni, G., Brigidi, P., & Turroni, S. (2022). The Core Human Microbiome: Does It Exist and How Can We Find It? A Critical Review of the Concept. *Nutrients*, *14*(14).

Shi, C., Liang, Y., Yang, J., Xia, Y., Chen, H., Han, H., Yang, Y., Wu, W., Gao, R., & Qin, H. (2013). MicroRNA-21 Knockout Improve the Survival Rate in DSS Induced Fatal Colitis through Protecting against Inflammation and Tissue Injury. *PLoS ONE*, *8*(6).

Shukla, G. C., Singh, J., & Barik, S. (2011). MicroRNAs: Processing, maturation, target recognition and regulatory functions. *Molecular and Cellular Pharmacology*, *3*(3).

Singh, U. P., Murphy, A. E., Enos, R. T., Shamran, H. A., Singh, N. P., Guan, H., Hegde, V. L., Fan, D., Price, R. L., Taub, D. D., Mishra, M. K., Nagarkatti, M., & Nagarkatti, P. S. (2014). miR-155 deficiency protects mice from experimental colitis by reducing T helper type 1/type 17 responses. *Immunology*, *143*(3).

Smith, K., McCoy, K. D., & Macpherson, A. J. (2007). Use of axenic animals in studying the adaptation of mammals to their commensal intestinal microbiota. *Seminars in Immunology*, *19*(2).

Sofia, M. A., Ciorba, M. A., Meckel, K., Lim, C. K., Guillemin, G. J., Weber, C. R., Bissonnette, M., & Pekow, J. R. (2018). Tryptophan metabolism through the kynurenine pathway is associated with endoscopic inflammation in ulcerative colitis. *Inflammatory Bowel Diseases*, *24*(7).

Soifer, H. S., Rossi, J. J., & Sætrom, P. (2007). MicroRNAs in disease and potential therapeutic applications. In *Molecular Therapy*, 15(12).

Sommer, F., & Bäckhed, F. (2013). The gut microbiota-masters of host development and physiology. In *Nature Reviews Microbiology*, 11(4).

Tahmasebi, S., Khoutorsky, A., Mathews, M. B., & Sonenberg, N. (2018). Translation deregulation in human disease. In *Nature Reviews Molecular Cell Biology*, 19(12).

Teng, Y., Ren, Y., Sayed, M., Hu, X., Lei, C., Kumar, A., Hutchins, E., Mu, J., Deng, Z., Luo, C., Sundaram, K., Zhang, L., Hsieh, M., Reiman, R., Haribabu, B., Yan, J., Jala, V. R., Miller, D. M., Van Keuren-Jensen, K., … Zhang, H. G. (2018). Plant-Derived Exosomal MicroRNAs Shape the Gut Microbiota. *Cell Host and Microbe*, *24*(5).

Thorlacius-Ussing, G., Schnack Nielsen, B., Andersen, V., Holmstrøm, K., & Pedersen, A. E. (2017). Expression and Localization of miR-21 and miR-126 in Mucosal Tissue from Patients with Inflammatory Bowel Disease. *Inflammatory Bowel Diseases*, *23*(5).

Treviño-Quintanilla, L., Freyre-González, J., & Martínez-Flores, I. (2013). Anti-Sigma Factors in E. coli: Common Regulatory Mechanisms Controlling Sigma Factors Availability. *Current Genomics*, *14*(6).

Truesdell, S. S., Mortensen, R. D., Seo, M., Schroeder, J. C., Lee, J. H., Letonqueze, O., & Vasudevan, S. V. (2012). MicroRNA-mediated mRNA translation activation in quiescent cells and oocytes involves recruitment of a nuclear microRNP. *Scientific Reports*, *2*.

Turchinovich, A., Weiz, L., & Burwinkel, B. (2012). Extracellular miRNAs: The mystery of their origin and function. *Trends in Biochemical Sciences*, *37*(11).

Turchinovich, A., Weiz, L., Langheinz, A., & Burwinkel, B. (2011). Characterization of extracellular circulating microRNA. *Nucleic Acids Research*, *39*(16).

Turnbaugh, P. J., & Gordon, J. I. (2009). The core gut microbiome, energy balance and obesity. *Journal of Physiology*, *587*(17).

Turnbaugh, P. J., Hamady, M., Yatsunenko, T., Cantarel, B. L., Duncan, A., Ley, R. E., Sogin, M. L., Jones, W. J., Roe, B. A., Affourtit, J. P., Egholm, M., Henrissat, B., Heath, A. C., Knight, R., & Gordon, J. I. (2009). A core gut microbiome in obese and lean twins. *Nature*, *457*(7228).

Turnbaugh, P. J., Ley, R. E., Hamady, M., Fraser-liggett, C., Knight, R., & Gordon, J. I. (2007). The human microbiome project: exploring the microbial part of ourselves in a changing world. *Nature*, *449*(7164).

Valadi, H., Ekström, K., Bossios, A., Sjöstrand, M., Lee, J. J., & Lötvall, J. O. (2007). Exosome-mediated transfer of mRNAs and microRNAs is a novel mechanism of genetic exchange between cells. *Nature Cell Biology*, *9*(6).

Valles-Colomer, M., Blanco-Míguez, A., Manghi, P., Asnicar, F., Dubois, L., Golzato, D., Armanini, F., Cumbo, F., Huang, K. D., Manara, S., Masetti, G., Pinto, F., Piperni, E., Punčochář, M., Ricci, L., Zolfo, M., Farrant, O., Goncalves, A., Selma-Royo, M., … Segata, N. (2023). The person-to-person transmission landscape of the gut and oral microbiomes. *Nature*, *614*(7946).

Van Niel, G., Mallegol, J., Bevilacqua, C., Candalh, C., Brugière, S., Tomaskovic-Crook, E., Heath, J. K., Cerf-Bensussan, N., & Heyman, M. (2003). Intestinal epithelial exosomes carry MHC class II/peptides able to inform the immune system in mice. *Gut*, *52*(12).

Venegas, D. P., De La Fuente, M. K., Landskron, G., González, M. J., Quera, R., Dijkstra, G., Harmsen, H. J. M., Faber, K. N., & Hermoso, M. A. (2019). Short chain fatty acids (SCFAs)mediated gut epithelial and immune regulation and its relevance for inflammatory bowel diseases. In *Frontiers in Immunology*, 10(MAR).

Viennois, E., Zhao, Y., Han, M. K., Xiao, B., Zhang, M., Prasad, M., Wang, L., & Merlin, D. (2017). Serum miRNA signature diagnoses and discriminates murine colitis subtypes and predicts ulcerative colitis in humans. *Scientific Reports*, *7*(1).

Vuong, C., Kocianova, S., Voyich, J. M., Yao, Y., Fischer, E. R., DeLeo, F. R., & Otto, M. (2004). A crucial role for exopolysaccharide modification in bacterial biofilm formation, immune evasion, and virulence. *Journal of Biological Chemistry*, *279*(52).

Wang, Z. K., Yang, Y. S., Chen, Y., Yuan, J., Sun, G., & Peng, L. H. (2014). Intestinal microbiota pathogenesis and fecal microbiota transplantation for inflammatory bowel disease. In *World Journal of Gastroenterology*, 20(40).

Weber, J. A., Baxter, D. H., Zhang, S., Huang, D. Y., Huang, K. H., Lee, M. J., Galas, D. J., & Wang, K. (2010). The microRNA spectrum in 12 body fluids. *Clinical Chemistry*, *56*(11).

Wu, F., Zikusoka, M., Trindade, A., Dassopoulos, T., Harris, M. L., Bayless, T. M., Brant, S. R., Chakravarti, S., & Kwon, J. H. (2008). MicroRNAs Are Differentially Expressed in Ulcerative Colitis and Alter Expression of Macrophage Inflammatory Peptide-2α. *Gastroenterology*, *135*(5).

Wu, N., Mah, C., Koentgen, S., Zhang, L., Grimm, M. C., El-Omar, E., & Hold, G. L. (2021). Inflammatory bowel disease and the gut microbiota. *Proceedings of the Nutrition Society*, *80*(4).

Xu J., Bjursell M. K., Himrod J., Deng S., Carmichael L. K., Chiang H. C., *et al*.. (2003). A genomic view of the human-*Bacteroides thetaiotaomicron* symbiosis New York, NY. *Science* 299.

Yatsunenko, T., Rey, F. E., Manary, M. J., Trehan, I., Dominguez-Bello, M. G., Contreras, M., Magris, M., Hidalgo, G., Baldassano, R. N., Anokhin, A. P., Heath, A. C., Warner, B., Reeder, J., Kuczynski, J., Caporaso, J. G., Lozupone, C. A., Lauber, C., Clemente, J. C., Knights, D., … Gordon, J. I. (2012). Human gut microbiome viewed across age and geography. In *Nature*, 486(7402).

Zhang, L., Shen, J., Cheng, J., & Fan, X. (2015). MicroRNA-21 regulates intestinal epithelial tight junction permeability. *Cell Biochemistry and Function*, *33*(4).

Zlotorynski, E. (2019). Insights into the kinetics of microRNA biogenesis and turnover. *Nature Reviews Molecular Cell Biology*, *20*(9).

Zocco, M. A., Ainora, M. E., Gasbarrini, G., & Gasbarrini, A. (2007). Bacteroides thetaiotaomicron in the gut: Molecular aspects of their interaction. In *Digestive and Liver Disease*, 39(8).